OPTIMIZATION OF DUAL-FUEL ENGINE UTILIZING FLEXIBLE VALVE TRAIN TECHNOLOGY

Dissertation

zur

Erlangung des akademischen Grades

Doktor-Ingenieur (Dr.-Ing.)

der Fakultät für Maschinenbau und Schiffstechnik

der Universität Rostock

vorgelegt von

M.Sc. Mina Abaskharon

geboren am 09.01.1988 in Ägypten

Lehrstuhl für Kolbenmaschinen und Verbrennungsmotoren

Universität Rostock

2023

https://doi.org/10.18453/rosdok_id00004258

Erstgutachter:	Prof. Dr.-Ing. Bert Buchholz Lehrstuhl für Kolbenmaschinen und Verbrennungsmotoren Universität Rostock
Zweitgutachter:	Prof. Dr.-Ing. habil. Karsten Müller Lehrstuhl für Technische Thermodynamik Universität Rostock
Tag der Einreichung:	25.10.2022
Tag der Verteidigung:	17.02.2023

Acknowledgement

This Ph.D. thesis has been achieved in the Piston Machines and Internal Combustion Engines Department, Faculty of Mechanical Engineering and Marine Technology, Rostock University.

Firstly, I wish to express my deepest thanks and gratitude to my supervisor ***Professor Dr.-Ing. Bert Buchholz***, the head of the department for his continuous support and guidance during my study from the first day until writing these lines. I'm extremely grateful for his assistance and advice to achieve this thesis as it is now.

My sincere gratitude and thanks also for the ***LEDF Team, Dipl.-Ing. Karsten Schleef, Dr.-Ing. Björn Henke and M.Sc. Sebastian Cepelak*** for their efforts and help in all phases of this work.

Also, my deep thanks and appreciations for ***Dr.-Ing. Karl Wilhelm Najar, M.Sc. Alexander Dottei and Dr.-Ing. Sascha Andree*** for their invaluable assistance in the software and simulation side.

Further, a special thanks for ***Dipl.-Ing. Benjamin Stengel*** for his continuous help from the first day, especially in the registration phase and after that during my study.

Many thanks to ***all the members*** of the laboratory for their help and assistance in the experimental tests.

And finally, my faithful thanks and gratitude to ***my family*** for their support, patience, and encouragement through the years of this study.

Rostock, August 2022 Mina Abaskharon

Kurzfassung

Das Ziel dieser Forschungsarbeit ist es, die Leistung eines Dual-Fuel-Schiffsmotors durch den Einsatz eines flexiblen Ventiltriebs zu optimieren. Zu diesem Ansatz wird ein Simulationsmodell entwickelt, um die Motorleistung und Emissionen unter Berücksichtigung der flexiblen Ventilsteuerungsfähigkeit vorherzusagen. Zunächst wird in MATLAB ein mathematisches Modell für die Strategie des flexiblen Ventiltriebs einschließlich seiner beiden Teilmechanismen (FCT und Multisegment-Nockenwelle) entwickelt. Das Ziel dieses Modells ist es, alle Ventilsteuerzeiten für die Einlass- und Auslassventile mit unterschiedlichen Nockenprofilen vorherzusagen. Außerdem vermeidet es die Ventilsteuerpositionen, an denen eine Kollision mit dem Kolben möglich ist. Anschließend wird in AVL CRUISE-M ein phänomenologisches Verbrennungsmodell basierend auf dem fraktalen Verbrennungsprinzip entwickelt. Das Verbrennungsmodell kann die Ventilsteuerzeiten mit unterschiedlichen Tuningmustern importieren, um deren Einfluss auf Motorleistung und Emissionen zu untersuchen. Die Simulationsergebnisse wurden mit den experimentellen Daten verglichen und zeigten eine gute Übereinstimmung in Bezug auf die Parameter im Zylinder und die Emissionsparameter. Es kann berichtet werden, dass die Verwendung des FCT die Anwendung des Miller-Zyklus-Effekts ermöglicht, der die Klopfintensität insbesondere bei hohen Lasten reduziert und für eine stabilere Verbrennung sorgt. Andererseits führte eine Erhöhung des FCT-Winkels zu einer längeren Überlappungszeit, was sich negativ auf die Abgasemissionen auswirkte. Das vorzeitige Öffnen des Einlassventils ist mit einer geringeren Klopfintensität verbunden, aber es wurde ein erhöhter Methanschlupf in den Abgasemissionen festgestellt. Die Abstimmung des Schließpunkts des Auslassventils zeigte im Vergleich zur Öffnung des Einlassventils einen geringeren Einfluss auf die Motorleistung. Dabei werden im Allgemeinen der Methanschlupf und die

Klopfintensität durch das extreme Vorverlegen des Auslassventilschließens negativ beeinflusst. In den meisten Fällen wurde ein Kompromiss zwischen Methanschlupf und Stickoxiden festgestellt, sodass ein Kompromisspunkt angewendet werden muss. In Bezug auf die Ventilüberschneidungszeit zeigten die Ergebnisse, dass sowohl der Betrag als auch die Position der Ventilüberschneidung einen signifikanten Einfluss auf die Motorleistung haben, da sie einige Vorteile während des Spülvorgangs haben. Eine bessere Leistung wurde festgestellt, wenn der Schwerpunkt der Überlappung sich in der Nähe des oberen Totpunkts befand.

Abstract

The aim of this research is to optimize the performance of a dual-fuel marine engine by a flexible valve train approach. From this perspective, a simulation model is developed to predict the engine performance and emissions taking into consideration the flexible valve timing capability.

Firstly, a mathematical model for the flexible valve train strategy including its two sub-mechanisms (Flexible Camshaft Technology (FCT) and Multi-segment Camshaft) is developed in MATLAB. The goal of this model is to predict all the available valve timing positions for the intake and exhaust valves with different cam profiles. It also avoids valve timing positions where a collision with the piston is possible.

After that, a phenomenological combustion model based on the fractal combustion principle is developed in AVL CRUISE-M. The combustion model includes many sub-models to represent the different phenomena during the combustion process. Additionally, it allows the valve timing positions to be imported in order to investigate their influence on engine performance and emissions.

Simulation results were compared with the experimental data, and they demonstrated a good agreement in terms of in-cylinder and emission parameters.

It can be reported that using the FCT allows to apply different levels of Miller cycle effect, which reduces the knocking intensity especially at high engine loads and provides more stable combustion. On the other hand, the higher values of the FCT angle increased the valve overlap period which had a negative effect on the exhaust emissions.

Advancing the intake cam opening point is associated with lower knock intensity but more methane slip was detected in the exhaust emissions. Tuning the exhaust valve closing point showed a lesser influence on the engine performance in comparison with the intake valve opening. Generally, methane slip and knock intensity are affected negatively by extreme advancing of exhaust valve closing. A trade-off between methane slip and nitrogen oxides was noticed in the most cases, so a compromise point has to be carefully chosen.

In terms of the valve overlap period, results showed that both the value and the position of the valve overlap has a significant influence on engine performance since it has some benefits during exhaust scavenging process. The engine performance was improved when the overlap position was near to top dead center.

Contents

Acknowledgement ..... **I**

Kurzfassung ..... **III**

Abstract ..... **V**

Nomenclature ..... **IX**

Abbreviations ..... **X**

1 Introduction **1**

- 1.1 Motivation and Problem Overview 1
- 1.2 Objectives of the Study 3
- 1.3 Thesis Layout 4

2 State of the Art **5**

- 2.1 Recent Combustion Technologies 5
- 2.2 Valve Train for Heavy-Duty and Marine Engines 12
- 2.3 Cam Profile Characteristics 15
- 2.4 Valve Timing Approaches 17
  - 2.4.1 Valve Overlap and Scavenging 17
  - 2.4.2 Miller Cycle 19
- 2.5 Combustion Modelling Approaches 24
  - 2.5.1 Thermodynamic Models (Zero-dimensional) 25
  - 2.5.2 Phenomenological Models (Quasi-dimensional) 26
  - 2.5.3 Computational Fluid Dynamic Models (CFD Multi-dimensional) 31
- 2.6 Summary 32

3 Engine Test Bench **35**

- 3.1 Dual-Fuel Research Engine 35
- 3.2 Flexible Valve Train Strategy 38
  - 3.2.1 Flexible Camshaft Technology (FCT) 38
  - 3.2.2 Multi-segment Camshaft 42
- 3.3 Summary 43

4 Model Description and Formulation **45**

- 4.1 Model Structure 45
- 4.2 Flexible Valve Train Model 46
- 4.3 Engine Simulation Model 51
  - 4.3.1 Combustion Model 52

4.3.2 Ignition Delay Model ... 55
4.3.3 Heat Transfer Model ... 56
4.3.4 NO_x Formation Model ... 56
4.3.5 Methane Slip Formation Model ... 57
4.4 Simulation Setup ... 58
4.5 Summary ... 59
5 Model Validation and Results Analysis ... 61
5.1 Models Validation ... 61
5.1.1 Flexible Valve Train Model ... 61
5.1.2 Combustion Model ... 62
5.1.3 Emissions and Ignition Delay Models ... 63
5.2 Results Analysis and Discussion ... 64
5.2.1 Effect of FCT on Engine Performance and Emissions ... 64
5.2.2 Effect of Intake Valve Timing on Engine Performance and Emissions ... 67
5.2.3 Effect of Exhaust Valve Timing on Engine Performance and Emissions ... 71
5.2.4 Effect of Valve Overlap Position on Engine Performance and Emissions ... 75
6 Conclusion and Outlook ... 81
6.1 Conclusion ... 81
6.2 Outlook ... 82
7 References ... 85

Nomenclature

Symbol	Unit	Description
A_L	(m^2)	*Laminar Flame Surface Area*
A_T	(m^2)	*Turbulent Flame Surface Area*
D_3	(-)	*Fractal Dimension*
F_p	(-)	*Mass Fraction of Unburned Charge*
L_{max}	(m)	*Maximum Length Scale*
L_{min}	(m)	*Minimum Length Scale*
P_{cyl}	(bar)	*Cylinder Pressure*
R_e	(-)	*Reynolds Number*
S_L	(m/s)	*Laminar Flame Speed*
S_T	(m/s)	*Turbulent Flame Speed*
T_{cyl}	(K)	*Cylinder Temperature*
T_{gas}	(K)	*Gas Temperature*
T_w	(K)	*Wall Temperature*
$\dot{m}$	(g/s)	*Mass Flow*
m_b	(g)	*Burned Mass*
$m_{crevice}$	(g)	*Crevice Mass*
θ_{ign}	$(\,^\circ)$	*Crank Angle at the Ignition Onset*
ρ_u	(g/m^3)	*Unburned Charge Density*
τ_{ID}	(ms)	*Ignition Delay*
$\Delta\theta$	$(\,^\circ)$	*Combustion Duration*
η_{th}	(%)	*Thermal Efficiency*
D	(m)	*Bore*
K	(m^2/s^2)	*Turbulent Kinetic Energy*
P	(m^2/s^3)	*Turbulent Kinetic Energy Production Rate*
ε	(m^2/s^3)	*Turbulent Dissipation Rate*
θ	$(\,^\circ)$	*Crank Angle*

Abbreviations

Abbreviation	Description
ATDC	*After Top Dead Center*
BDC	*Bottom Dead Center*
BSFC	*Break Specific Fuel Consumption*
$BSNO_x$	*Brake Specific Nitrogen Oxides*
BTDC	*Before Top Dead Center*
CA	*Crank Angle*
CDC	*Conventional Diesel Combustion*
CFD	*Computational Fluid Dynamics*
CH_4	*Methane*
CN	*Cetane Number*
CO	*Carbon Monoxide*
CO_2	*Carbon Dioxide*
CoC	*Center of Combustion*
CoV	*Coefficient of Variation*
CR	*Compression Ratio*
EGR	*Exhaust Gas Recirculation*
EVC	*Exhaust Valve Close*
EVO	*Exhaust Valve Open*
EZM	*Extended Zeldovich Mechanism*
FCT	*Flexible Camshaft Technology*
FTIR	*Fourier Transformation Infrared Spectroscopy*
GHGs	*Greenhouse Gases*
HCCI	*Homogeneous Charge Compression Ignition*
HRF	*High Reactivity Fuel*
LRF	*Low Reactivity Fuel*
LTC	*Low Temperature Combustion*
N_2O	*Nitrous Oxide*
NG	*Natural Gas*

Abbreviation	Description
NO_x	*Nitrogen Oxides*
NVO	*Negative Valve Overlap*
PCCI	*Premixed Charge Compression Ignition*
PFI	*Port Fuel Injection*
Pilot-DF	*Pilot Dual-Fuel*
PM	*Particulate Matter*
R&D	*Research and Development*
RCCI	*Reactivity Controlled Compression Ignition*
ROHR	*Rate of Heat Release*
RPM	*Revolution per Minute*
SCR	*Selective Catalytic Reduction*
SOI	*Start of Injection*
TDC	*Top Dead Center*
UHC	*Unburned Hydrocarbon*

1 Introduction

1.1 Motivation and Problem Overview

Internal combustion engines have been considered the main prime mover for several decades since they are used in several applications such as transport and power generation. They have been preferred due to their wide speed and load ranges parallel with the fuel flexibility as they deal with various fuels including gasoline, diesel, natural gas, propane, and biogas. Since the high population growth and the increased industrial activities, the emitted pollutants from internal combustion engines have got more attention as the global target now is to reduce the harmful emissions such as nitrogen oxides (NO_x), particulate matter (PM), and greenhouse gases (GHGs). These pollutants affect the environment in different ways. For example, the NO_x emissions cause photochemical smog and are responsible for acid rain, while PM consists mainly of soot and is considered extremely harmful for human health and the environment. Transport sector is a major source of the emissions and pollutants as it is responsible for more than 25% of the GHGs in the European union and contributes significantly in the climate change and global warming issues [1]. Greenhouse gases increase the temperature of the earth by trapping the absorbed energy and slowing its dissipation back to space. High earth temperature on the long term has a negative effect on the life characteristics especially on the biodiversity, the wildlife, and the water resources. Generally, GHGs could be classified into two categories depending on the atmospheric lifetime:

- Long-lived climate pollutants like carbon dioxide (CO_2) and nitrous oxide (N_2O)
- Short-lived climate pollutants like methane (CH_4)

The atmospheric lifetime of CO_2 is very long, and it is expected to remain in the atmosphere for over 1000 years. Nitrous oxide is the second long-lived greenhouse gas with an atmospheric lifetime of about 120 years, while methane has an atmospheric lifetime of about 12 years and affects the climate for the next few decades [2]. As every gas has a different impact level, it was necessary to develop a single equivalent factor to make the comparison possible between the different greenhouse gases. The most used equivalence factor is the global warming potential (GWP), which reflects the climate effect by a one ton of emissions relative to the same mass of CO_2 over a specified time period, usually 20 or 100 years as shown in Figure 1.1. Greenhouse gases with higher GWP absorb more energy and have a stronger trapping effect than those with lower GWP [3, 4].

The major sources of CO_2 are the burning of fossil fuels, solid wastes and as a result of some chemical reactions like those in the cement manufacturing, while N_2O is emitted mainly during the agricultural and fertilizer applications and some industrial activities.

Methane is the main component of natural gas (NG) and is considered the most important greenhouse gas directly after CO_2. Nowadays, NG is more preferred and used widely in many applications as it has lower carbon to hydrogen ratio in comparison with the other fuels. The combustion products of NG have lower NO_X emission at the same time with almost zero smoke and PM. As a result of the enlarged usage of NG in the internal combustion engines, the emitted unburned methane or "methane slip" from the exhaust is considered a major source of the methane in the atmosphere. The other sources of methane are the livestock, the agriculture activities, and the fossil fuel production processes [4].

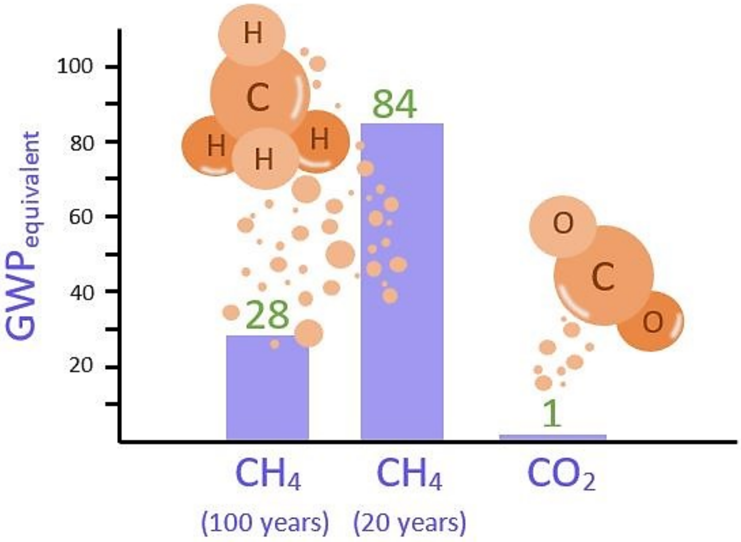

Figure 1.1: GWP for methane after 20 and 100 years [5].

From this point of view and with the dramatic rising of energy demand, many countries have promoted more restrictive emissions legislations for cars, trucks, and ships in order to protect the public health and minimize the pollution levels to control the global warming issue. To fulfill this target, a lot of development approaches have been introduced in the last few years to optimize conventional combustion engines like diesel and gasoline. However, they still cannot face these challenges effectively and are not able to meet stronger emission regulations in the future. So new combustion technologies have become mandatory nowadays as the R&D community have intended to go further beyond the conventional combustion strategies to manufacture a more environment friendly engines.

1.2 Objectives of the Study

Dual-fuel technology represents a promising solution towards lower emissions and highly efficient engines as it combines the features of diesel and gasoline engines together. However, it still requires more optimization due to the combustion control complexity and the relatively high amount of unburned hydrocarbon (UHC) in the exhaust emissions. The load range is also considered another limitation for the dual-fuel engines as they are more efficient at low and medium loads. Several techniques have been developed to overcome these challenges such as different injection strategies, exhaust gas recirculation (EGR), and fuel additives. Also, valve timing is not far away as it plays an essential role during the combustion process by regulating charge and exhaust flow. Many variable valve actuation approaches have been proposed in the automotive sector aiming to optimize the engines' performance with lower emissions and the results have proved promising success. Some approaches include tuning the valves either on the intake side, on the exhaust side, or both of them. Particularly in the dual-fuel engines, tuning the intake valve timing allows different levels of Miller cycle by changing the effective compression ratio. As a result, the thermodynamic state in the cylinder is significantly influenced and combustion parameters such as maximum temperature, maximum pressure, and rate of heat release can be controlled. Additionally, flexible valve timing allows to adopt the overlap period which affects the unburned hydrocarbon, the exhaust scavenging efficiency, and can be used as internal EGR. Consequently, the emissions formation is significantly optimized and strong knocking at the high loads can be avoided. In terms of the exhaust valve, it can be adjusted to control the back pressure on the piston and the exhaust flow as both affect engine performance and emissions. Furthermore, using variable valve timing in the dual-fuel engines paves the road to employ various fuels with different reactivity grades which enables more fuel-flexible engines. From this point of view, the target of this study is to develop a simulation model to optimize the performance and emissions of a dual-fuel engine through a flexible valve train strategy. The model includes two sections, the first one aims to simulate the flexible valve train mechanism with all the available valve timings and cam profiles. The second one is the engine model, which predicts the combustion behavior, the heat release rate, and the exhaust emissions in the dual-fuel engine. By combining the two parts together, the effect of the flexible valve train on the engine can be investigated. Also, the model figures out the appropriate valve timing for the different operating conditions to achieve ultra-low emissions with high combustion efficiency.

1.3 Thesis Layout

The thesis includes 6 chapters, **Chapter 1** is a general introduction about global warming issue and greenhouse gases. Additionally, it discusses how the internal combustion engines contribute to this aspect. The purpose of the current study is introduced also in this chapter.

Chapter 2 presents the state of the art for the new combustion technologies which are relative to the dual-fuel combustion indicating the difference between them, and their advantages and disadvantages in comparison with the conventional combustion concepts. The cutting-edge strategies and principles for the valve train mechanisms and Miller cycle in the heavy-duty engines are included also. Furthermore, the chapter gives an overview for the applied approaches in the combustion modelling and simulation.

Chapter 3 introduces an overview for the engine test bed and the used instrumentations in the experimental tests. Also, it includes a detailed description of the flexible valve train mechanism in the engine, describing its components and how it works.

In **Chapter 4**, the whole model structure and components are presented. The chapter demonstrates a detailed description for the valve train model including the different cam profiles and the valve timing combinations. Moreover, the engine model involving the integrated sub-models and the interface between them are introduced.

Chapter 5 contains the model validation against experimental data. It also includes results and discussion for the effect of the flexible valve train strategy on the dual-fuel engine emissions and efficiency. The Influence of different parameters such as intake valve timing, exhaust valve timing, and valve overlap is considered.

And finally, **chapter 6** outlines the summary and the conclusion of the thesis with suggestions and recommendations for the future development concerned with the same scope.

2 State of the Art

In this section, the literature concerned with the new combustion technologies such as HCCI, PCCI, and RCCI are presented and investigated. The characteristics of each one of them are reviewed and discussed. The chapter tries to answer the question of why we need these new combustion technologies, and which benefits they could introduce in terms of the exhaust emissions and engine performance. After that, the essential concepts for the valve timing mechanisms in the heavy-duty engines are introduced. Different valve timing strategies such as Miller cycle and negative valve overlap are considered also. Since the study employs the simulation and modelling principle to investigate the dual-fuel engine performance, the chapter provides a comparison for the different modelling approaches in this aspect. The features of them are presented and discussed aiming to figure out how suitable are each of them for the different purposes.

2.1 Recent Combustion Technologies

As already referred in the introduction, the strictive emission regulations force the engine manufacturers to develop new combustion technologies. Figure 2.1 shows some of these technologies illustrating their operation range.

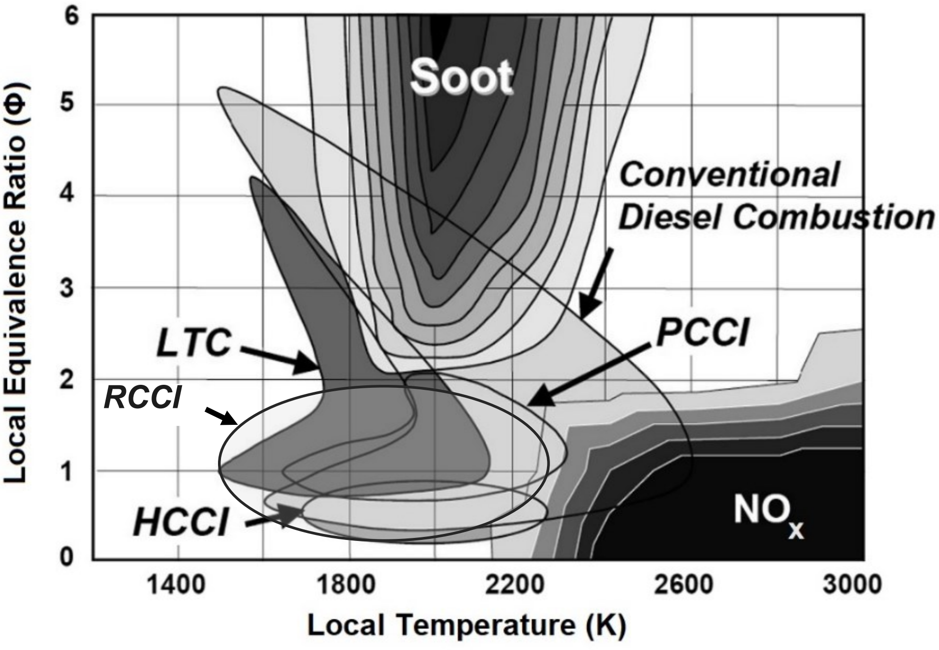

Figure 2.1: New combustion strategies classification map. Conventional Diesel Combustion (CDC), Premixed Charge Compression Ignition (PCCI), Low Temperature Combustion (LTC), Reactivity Controlled Compression Ignition (RCCI), Homogenous Charge Compression Ignition (HCCI). Adapted from [6].

In heavy-duty applications, diesel engines have been preferred due to their higher thermal efficiency (η_{th}) and torque in comparison with gasoline engines. But from environmental view, CDC has some drawbacks and is considered one of the main pollution sources as it produces high amount of NO_x and PM due to the high temperature combustion characteristics [7]. To reduce the pollutants from diesel engines, researchers have developed many techniques like exhaust gases aftertreatment and common rail injection systems, but they still cannot minimize PM and NO_x simultaneously due to the trade-off between them. Furthermore, most of the exhaust aftertreatment systems such as diesel particulate filter and selective catalytic reduction (SCR) increase the fuel consumption beside to the high maintenance costs [8, 9]. As viewed in Figure 2.1, the new combustion technologies deal with lower combustion temperature and leaner mixture to reduce NO_x and PM simultaneously as possible. However, these technologies still face some challenges such as controlling the combustion phase and the high amount of UHC due to the lower combustion temperature. Also, they need more development due to their limited load and speed range beside to the control complexities in the multi-cylinder engines [6, 10]. Some characteristics are common between these combustion technologies while everyone has its own advantages and is preferred in specific applications, the main features for each are as follows:

LTC: Low Temperature Combustion is an umbrella term that includes all the new combustion technologies which deal with lower combustion temperature and leaner equivalence ratio than the conventional combustion. The most common features of LTC are the early fuel injection in order to promote the mixture homogeneity, the lower heat losses, and the using of EGR as an assistant approach to control the combustion temperature and minimize NO_x formation [9, 11]. All the LTC technologies are very effective in NO_x reduction due to the high activation energy of the NO_x formation reactions [12].

HCCI: Homogenous Charge Compression Ignition is a promising hybrid combustion concept which combines the advantages of Otto and Diesel engines together. In HCCI, the fuel is injected with the incoming air into the cylinder during the intake stroke and then the mixture is compressed and auto-ignited when the temperature reaches the self-ignition temperature. There is no sparkplug or injection event to initiate the combustion. The physiochemical properties of the fuel beside to the temporal and spatial histories of the mixture temperature strongly determine the ignition timing. So, a significant limitation of HCCI is the poor combustion control, that is why various ignition control techniques are used in HCCI like variable valve actuation, internal and external EGR, variable inlet temperature, and compression ratio control. These techniques are used solely or conjunctively with each other to control the mixture properties at the end of the compression stroke and achieve the desired ignition timing. The Short combustion duration in HCCI is another limitation at high loads, while the lack of the necessary pressure and temperature at low load is considered an obstacle. As a result, HCCI has a narrow operating range around middle loads. The positive side is that HCCI produces lower soot due to the mixture homogeneity and the absence of local-rich combustion [9, 11].

PCCI: Premixed Charge Compression Ignition is a form of HCCI but with better combustion control as it lies between the full HCCI and the full CDC. In PCCI the mixture is less premixed than that in HCCI and tends more to stratification rather than homogeneity. PCCI depends on the fuel direct injection during the compression stroke to obtain different levels of fuel stratification and sometimes multiple injections are used for this purpose. Hence, PCCI has better combustion control than HCCI, but still suffer from some combustion instability und high UHC emissions due to the lower combustion temperature [9, 11].

RCCI: Reactivity Controlled Compression Ignition uses the stratification of two different reactivity fuels to ignite the mixture. The low reactivity fuel (LRF) like gasoline, alcohol fuel, or natural gas is introduced to the cylinder via port fuel injection (PFI), while the high reactivity fuel (HRF) like diesel or biodiesel is injected directly during the compression stroke using single or multiple injections. This process of in-cylinder fuel blending develops fuel reactivity gradients in the combustion chamber. Combustion initiation depends totally on the chemical kinetics between the two fuels and can be controlled by changing the mass ratio between them. In comparison with PCCI and HCCI, RCCI provides more efficient control on the combustion process [6, 11].

Pilot-DF: Pilot Dual-Fuel combustion is considered an advanced form of RCCI. In pilot-DF engines the LRF is injected in the intake port with the incoming air during the intake stroke, while the HRF is injected directly close to the TDC at high pressure as an igniter to initiate the combustion. Hence, combustion is controlled by tuning the pilot injection timing. In this type of engines, NG is the most employed LRF due to its worldwide availability and low price. In terms of fuel properties, NG is considered a low carbon fuel and has higher heating value in comparison with the other fuel types. Also, it has higher octane number than the other fuels, which is suitable for engines with high compression ratios (CR). Dual-Fuel engines provide higher thermal efficiency and lower NO_x emissions, however they suffer from high methane slip in the exhaust in some operating conditions [6, 11, 13]. Figure 2.2 shows the combustion approaches for the CDC, HCCI, PCCI, RCCI, and pilot-DF technologies according to the fuel injection pattern. Sometimes they could be categorized as single fuel combustion technologies (HCCI and PCCI) and double fuel combustion technologies (RCCI and pilot-DF).

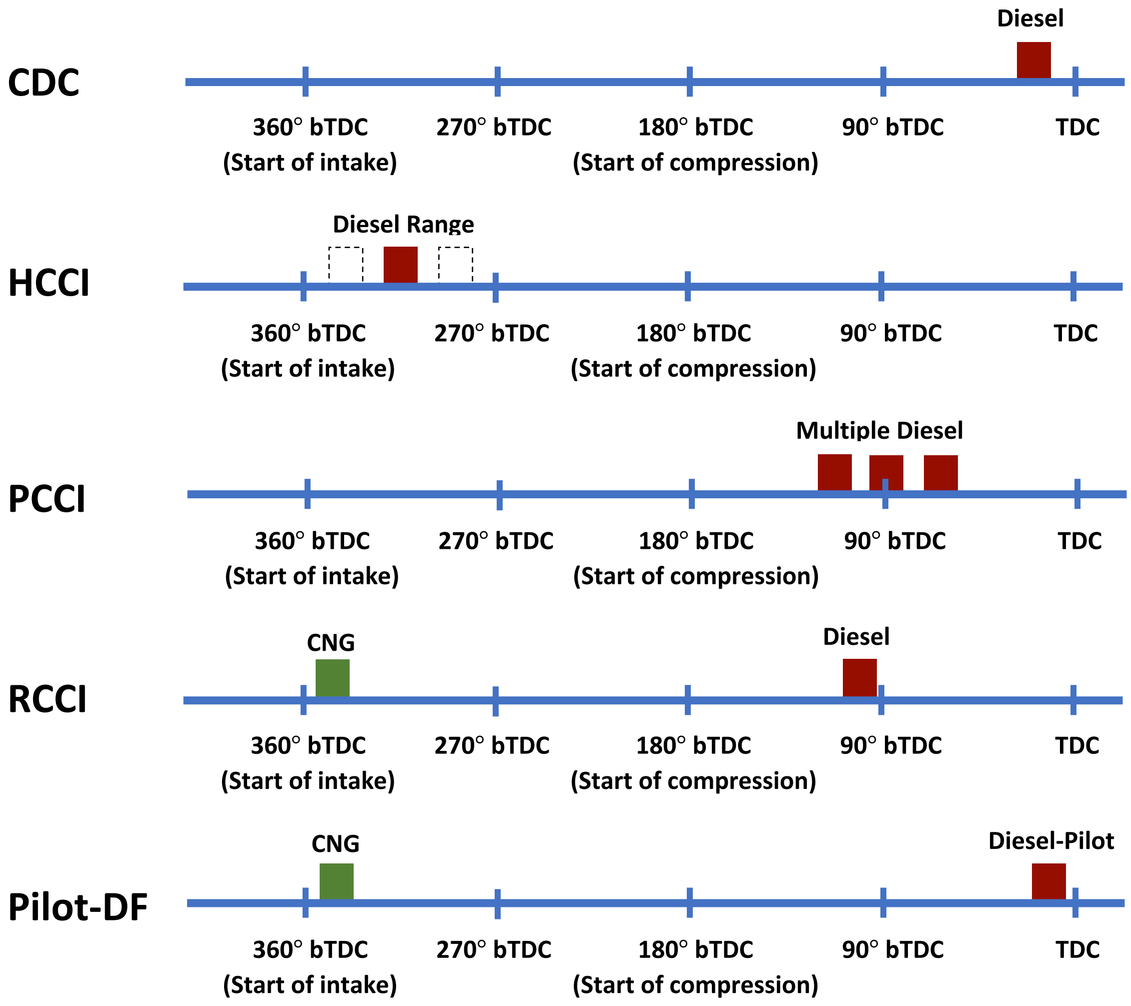
Diesel
CDC
360° bTDC (Start of intake)
270° bTDC
180° bTDC (Start of compression)
90° bTDC
TDC
Diesel Range
HCCI
Multiple Diesel
PCCI
CNG
Diesel
RCCI
CNG
Diesel-Pilot
Pilot-DF

Figure 2.2: Fuel supply pattern for different combustion technologies. Adapted from[6].

In [6], a comparison between the previously mentioned technologies was introduced. The combustion characteristics, exhaust emissions, and thermal efficiency were studied on a heavy-duty single-cylinder diesel engine. Generally, results showed that HCCI, PCCI, RCCI, and pilot-DF can reduce the PM and NO_x emissions simultaneously and meet the Euro-VI emission regulations without aftertreatment systems. The double-fuel technologies (RCCI and pilot-DF) have better and easier control on combustion initiation phase either by changing the diesel to NG ratio, or by adjusting the diesel injection timing, or by using the both methods together.

Coefficient of variation for the indicated mean effective pressure (CoV_{IMEP}) was measured also, as it reflects a sign of the combustion stability and it was over 4% for the HCCI and PCCI, while it was under than 3% for the RCCI and pilot-DF. The carbon monoxide (CO) and UHC emission levels were extremely higher in both HCCI and PCCI than those of RCCI and pilot-DF. Thermal efficiency was deteriorated in HCCI and PCCI due to the unstable combustion and the high heat losses, however it was higher with RCCI and pilot-DF as they have better combustion controllability.

In RCCI, engine design parameters like compression ratio and piston bowl geometry play an effective role in combustion behavior. The selected fuels also determine the mixing and evaporation quality, which affects the rest of the combustion process. That is why RCCI is considered more flexible than the other combustion technologies and has a wider range of engine loads (4.6-14.6 bar) with near zero levels of NO_x and soot emissions. Comparing to CDC, RCCI has lower heat losses which increased the gross indicated thermal efficiency by about 16.4% [14].

The optimized RCCI operation usually needs the assistance of EGR especially at high engine loads to control the pressure rise rate. Furthermore, NO_x and soot emissions are lower with the use of EGR due to the dilution effect which reduces the combustion temperature. On the other side, most of the studies found that UHC and CO are increased by using EGR as a result of the low combustion temperature and the absence of the sufficient oxygen, which is required for the oxidation process [15, 16]. The two-fuel strategy in RCCI requires two fuel tanks in the oriented vehicles and ships, which occupies more space than usual. To save this space, a single fuel strategy is considered in RCCI by adding some additives and cetane improvers to the LRF to alter its reactivity as shown in Figure 2.3.

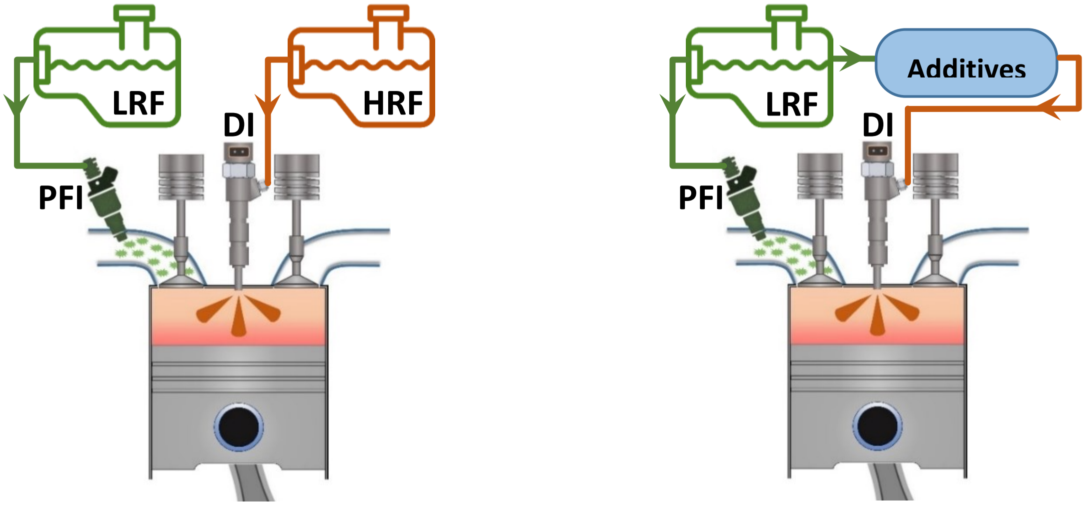

Figure 2.3: Double and single fuel strategies in RCCI.

Consequently, a reactivity difference utilizing one fuel type is possible, and then the LRF mixed with additives is injected directly into the cylinder playing the role of the HRF [15].

Using a single-cylinder light-duty diesel engine, RCCI combustion with two fuel combinations of (methanol/diesel) and (gasoline/diesel) are compared in [17]. Results concluded that with methanol/diesel combination, a significant increase of HRF (diesel) is required compared to the gasoline/diesel pair to achieve the similar combustion phasing. That was due to the charge cooling effect from methanol and its high-octane number. And as a result, higher NO_x emissions were observed with the case of methanol/diesel. Also, with methanol/diesel combination, it was possible to keep a load until ~12 bar IMEP without need of EGR, while with the gasoline/diesel combination, EGR was a mandatory over ~7 bar IMEP.

Injection strategy of HRF strongly affects the combustion characteristics especially in RCCI and pilot-DF engines, because many tunable parameters can be adjusted like fuel mass fraction, injection time, and injection pattern (single, double, or tribble pulses). Since diesel fuel is commonly used as an igniter in the pilot-DF engines, cetane number plays an important role in the combustion process and affects the peak heat-release rate in the ignition phase of the pilot fuel. The effect of diesel cetane number (CN) in pilot-DF engine was investigated in [13] and results showed that diesel fuel with CN = 54.7 has shorter ignition delay and combustion duration than a diesel fuel with CN = 43.3, also a noticeable reduction of UHC and CO was observed with the higher CN.

The effect of pilot diesel quantity and injection timing on the combustion performance in a natural gas/diesel dual-fuel engine was proposed by [18]. Results indicated that the peak cylinder pressure, maximum pressure rise rate, and NO_x emissions increased with the increase of pilot diesel quantity. The reason is that the higher pilot quantity represents a larger ignition source and provides more energy for the combustion initiation which increases the heat release rate and the combustion temperature. Also, with advancing the pilot injection timing, the peak cylinder pressure and maximum pressure rise rate were higher and appeared earlier. As reported in [19], increasing the pilot injection pressure in pilot-DF engine improved the combustion characteristics and had higher thermal efficiency with a positive effect on the emissions except for NO_x. Results also showed that retarding the NG injection timing can enhance flame propagation and improve combustion efficiency specially under low and part engine loads, while under high engine loads a negative impact was observed by retarding the NG injection timing.

The effect of natural gas substitution ratio on performance and emissions of dual-fuel engine was experimentally investigated in [20]. Tests were carried out at 2000 rpm on a single-cylinder, four-stroke, and naturally aspirated diesel engine, which was modified for dual-fuel operation. The NG was inducted to the cylinder through the intake valve with the charge air, while diesel fuel was injected at 26° BTDC as an igniter and the injection timing kept constant. Results indicated that, for all examined cases, dual-fuel operation mode has longer ignition delay and lower peak cylinder pressure than that of the diesel operation. Additionally for 40% and 80% engine loads, the cylinder pressure under dual-fuel mode was reduced with the increasing of NG ratio, especially during the compression stroke and the initial periods of combustion phase. That was due to the higher specific heat capacity of NG than that of air, which reduces the mean cylinder temperature and pressure during the compression stroke. In terms of exhaust emissions, the levels of NO_x emissions under dual-fuel mode were lower than that of the diesel mode. UHC and CO are generally higher with the dual-fuel operation, and both showed higher values with the increase of the natural gas percentage.

As stated in [7], many authors reported that pilot-DF engines have higher amount of CO and UHC in the exhaust emissions. Both are considered a sign of incomplete combustion and they increased in the exhaust with the higher NG mass ratios in the mixture. That was due to the flame quenching and the trapping of the natural gas-air mixture in the crevice volumes. At the expansion stroke, the trapped mixture releases from the crevice volumes but it cannot be completely oxidized because of the low temperature in comparison with the CDC, and with the increasing of the NG ratio this effect is enhanced. UHC in pilot-DF engines can be improved by avoiding the too lean mixture and by adjusting the proper valve timing to prevent charge escaping during valve overlap. There is always a trade-off relationship between NO_x on one side, and UHC and CO on the other side. As the higher temperature boosts the NO_x formation, it is not sufficient to oxidize CO and UHC. Carbon dioxide (CO_2) is a sign of complete combustion as hydrocarbon fuels are firstly oxidized to CO during the combustion process and then in the presence of sufficient oxygen, CO is oxidized to CO_2. That is why CO_2 formation depends strongly on the oxygen concentration and the cylinder temperature.

The performance of a large diesel engine running on dual-fuel operation mode was investigated in [21]. Results showed that CO_2 emissions under dual-fuel mode were lower than those compared to the single diesel mode for all the engine speeds from 1100 rpm to 2000 rpm, while UHC and CO were higher with the dual-fuel mode.

The investigation of the soot emissions for a dual-fuel engine in [22] showed that, for all the examined conditions under dual-fuel mode, soot emissions were significantly lower than those compared to normal diesel mode. Also, with the increasing of engine load, the soot emissions from normal diesel mode increased obviously. However, under dual-fuel mode, a reduction of soot emissions was observed with increasing the engine load. In a dual-fuel mode, most of the diesel fuel is replaced by natural gas, so the premixed combustion is more dominant than the diffusion one. Therefore, less soot emissions were detected with the dual-fuel mode. Furthermore, in the dual-fuel mode, the addition of the NG prolongs the ignition delay which provides more time for better homogeneity than that in the diesel mode. The fuel characteristics for diesel and NG also play an important role in soot formation, as NG does not contain a C-C bond and is free of sulfur. So, it has a lower tendency to produce soot than that with diesel fuel.

The torque and power of a dual-fuel engine were investigated in [21, 23] and results indicated that the maximum torque and power under dual-fuel mode was slightly lower than that of the normal diesel operation. This power loss is due to the lower volumetric efficiency with the dual-fuel mode as the addition of the NG reduces the intake air amount in comparison with the full diesel mode.

2.2 Valve Train for Heavy-Duty and Marine Engines

Nowadays, engines have become more sophisticated and used in many applications with different demands. Unlike the two-stroke engines, four-stroke engines have intake and exhaust valves to control the gas exchange process, which improves engine’s dynamics and response. Valve train mechanism plays a vital role in comparison with the other engine sub-systems since it aims to keep the appropriate valve timing synchronically with the piston position. Additionally, some mechanisms use variable valve timing to meet the engine requirements at different operating conditions. Friction losses from the valve train mechanism represents around 7.5% : 21% from the total engine friction losses as it is driven from the crankshaft either with timing belts, chains, or gears [24].

As shown in Figure 2.4, many mechanisms have been developed in order to fulfil the needs of modern engines. They can be classified according to many criteria, but the main one is the camshaft position either in the cylinder block or in the cylinder head. Although all the modern engines have valves placed in the cylinder head, the term “Overhead Valve (OHV)” is used to describe the pushrod mechanism with the cam shaft installed in the cylinder block.

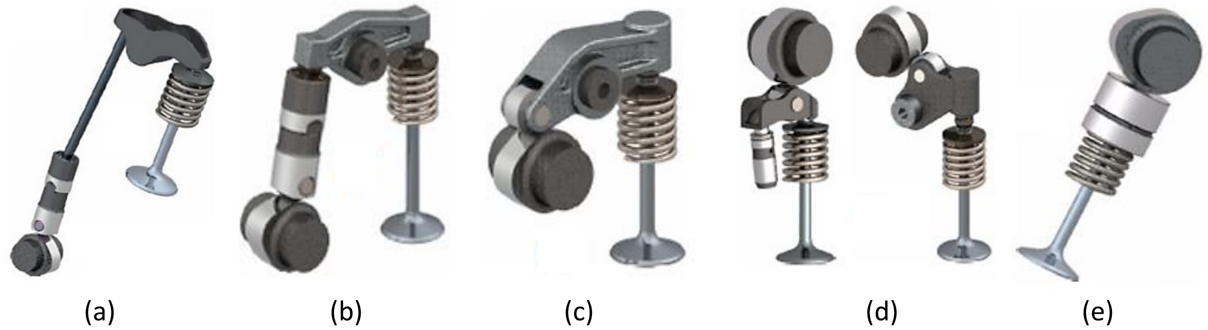

Figure 2.4: Different valve train mechanisms. cylinder block camshaft (a), center pivot OHC with follower (b), center pivot OHC (c), end pivot OHC (d), direct acting OHC (e). Adapted from [25].

On the other hand, the valve train configuration where the camshaft installed in the cylinder head is mentioned as "Overhead Camshaft (OHC)". Every configuration is preferred for specific applications due to its own characteristics. The pushrod mechanism is the basic design and is considered suitable for the low and medium speed engines, while the OHC is preferred in the high-speed engines due to its simplicity as it has less components which means less inertia with low friction. In the marine sector, engines have high capacity and most of them are undersquare (bore < stroke) as this design provides higher torque at lower rpm in comparison with the oversquare engines (bore > stroke). Therefore, using an OHC is not preferred because the distance between the crankshaft and camshaft will be extremely long. Hence, many gears are required to drive the camshaft as using the timing belts and chains are avoided due to the high strength and lifetime considerations. From this point of view, most of the low and medium-speed marine engines use the conventional valve train mechanism as demonstrated in Figure 2.5. In this design the camshaft is driven by gears and the cam displacement is transferred to the valves through pushrods and rocker arms.

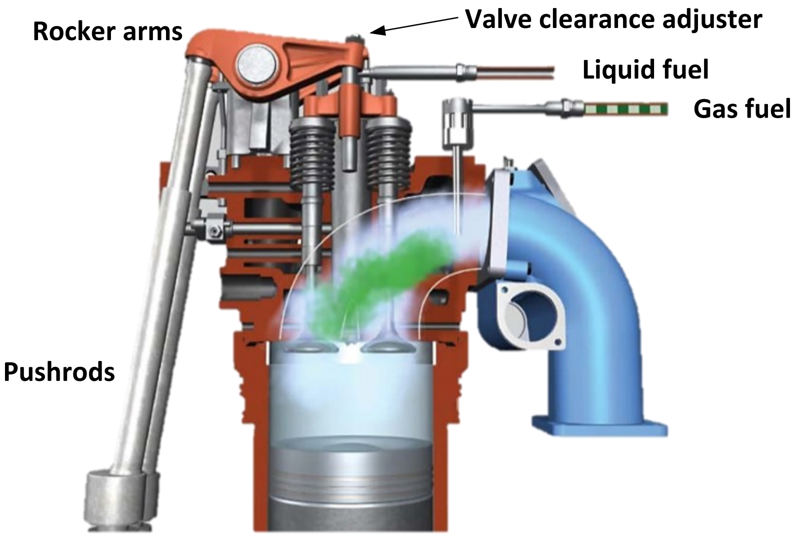

Figure 2.5: Valve train mechanism in dual-fuel engine (Wärtsilä). Adapted from [26].

This mechanism is widely used in heavy-duty and marine engines since it is very simple. Additionally, in the case of V-engines, it allows to use one camshaft instead of two overhead camshafts to drive the two banks. In contrast, it has some drawbacks such as the limited number of valves per cylinder and the less control over the valve timing.

To assure precision valve timing for different operating conditions, valve clearance is considered between the valve tip and the rocker arm to accommodate valve expansion due to the high temperature. Also, it assists to keep a continuous contact through the elements of the mechanism. Many valve clearance strategies are applied nowadays depending on the engine characteristics. In the automotive sector, the most dominant type is the hydraulic lifter which depends on oil under pressure to compensate any expansion in the mechanism. This type is maintenance-free and does not need any external adjusting. On the other hand, many marine engines use the typical screw and locknut adjustment method as it considered more suitable for the low-speed engines and provides more flexibility. Several development phases have been achieved in this aspect. One of them is a valve train mechanism with a hydraulic adjuster from MAN engines. The mechanism is designed for the heavy-duty engines as the hydraulic adjuster replaces the adjusting screw and nut as shown in Figure 2.6. Applying the hydraulic adjuster eliminates the regular checking and adjustment which saves time and cost.

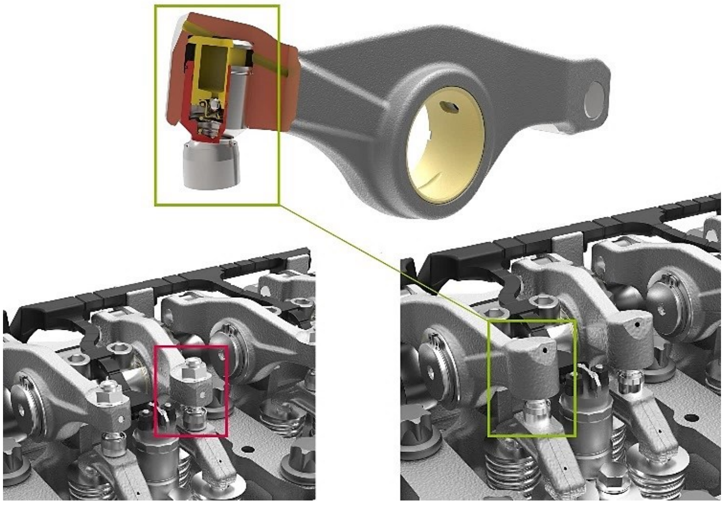

Figure 2.6: Valve train with hydraulic lifter (MAN engines) [27].

In terms of cylinder head design, it is slightly different in the large engines than those in the automotive sector as the latter have one entire cylinder head for all cylinders. But in heavy-duty and marine engines, it consists of many sections connected together and every cylinder has its own cylinder head as indicated in Figure 2.7. By employing this design, no mechanical or thermal stresses will be transferred to the whole cylinder head like that in the conventional engines. Hence, less cracks possibility. Furthermore, it assures easy and low-cost maintenance since the damaged section can be replaced individually.

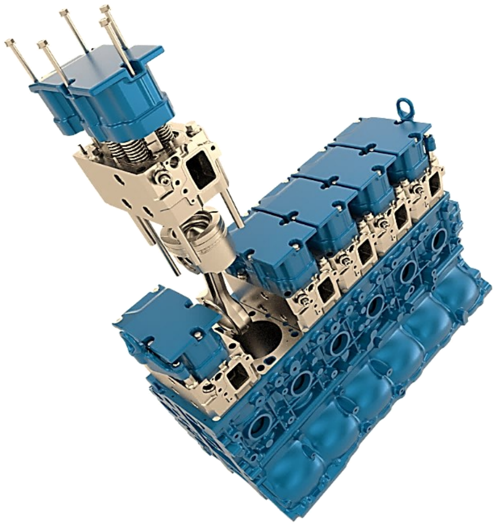

Figure 2.7: Six-cylinder marine engine with separated cylinder head (Model: Baudouin 6F21) [28].

2.3 Cam Profile Characteristics

During the gas exchange process, the components of the valve train mechanism determine the behavior of the valves' actuation since high volumetric and scavenging efficiency are required in the most operating conditions. Intake and exhaust cams are the heart of this mechanism, and many criteria are considered in their design to assure smooth operation with low vibration and noise. Further, cam design should enhance continuous contact between the mechanism's parts and avoid valve bounce. The main parts of the cam profile are base circle, opening and closing ramps, opening and closing flanks, and nose as indicated in Figure 2.8.

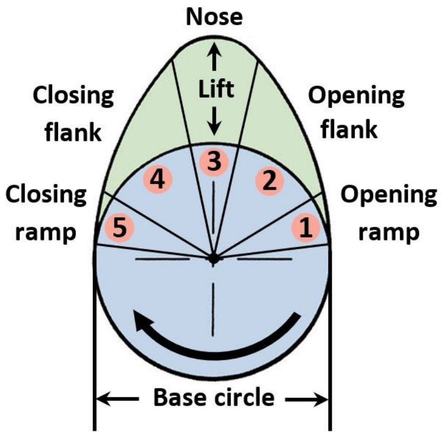

Figure 2.8: Main parts of cam profile. Adapted from [29].

The base circle denotes the duration when the valve is still closed and does not provide any lift. The opening ramp compensates the valve clearance and determines how fast the valve leaves its seat. Similarly, the closing ramp assures that the valve will gently close without collision and avoids high closing velocity which leads to valve bounce. The two flanks are mainly responsible for valve opening and closing, but indeed the function of them is slightly different. While the opening flank drives the mechanism to open the valve, the closing one aims to keep the contact between the mechanism's parts as the valve is closed under the effect of the spring. Cam nose refers to the transition phase between opening and closing when the valve is held opened at the maximum lift. Due to the stiffness in the valve train mechanism, the actual valve motion is a little different than the theoretical one. The effect of cam parts in Figure 2.8 on the theoretical valve lift, velocity, and acceleration is shown in Figure 2.9.

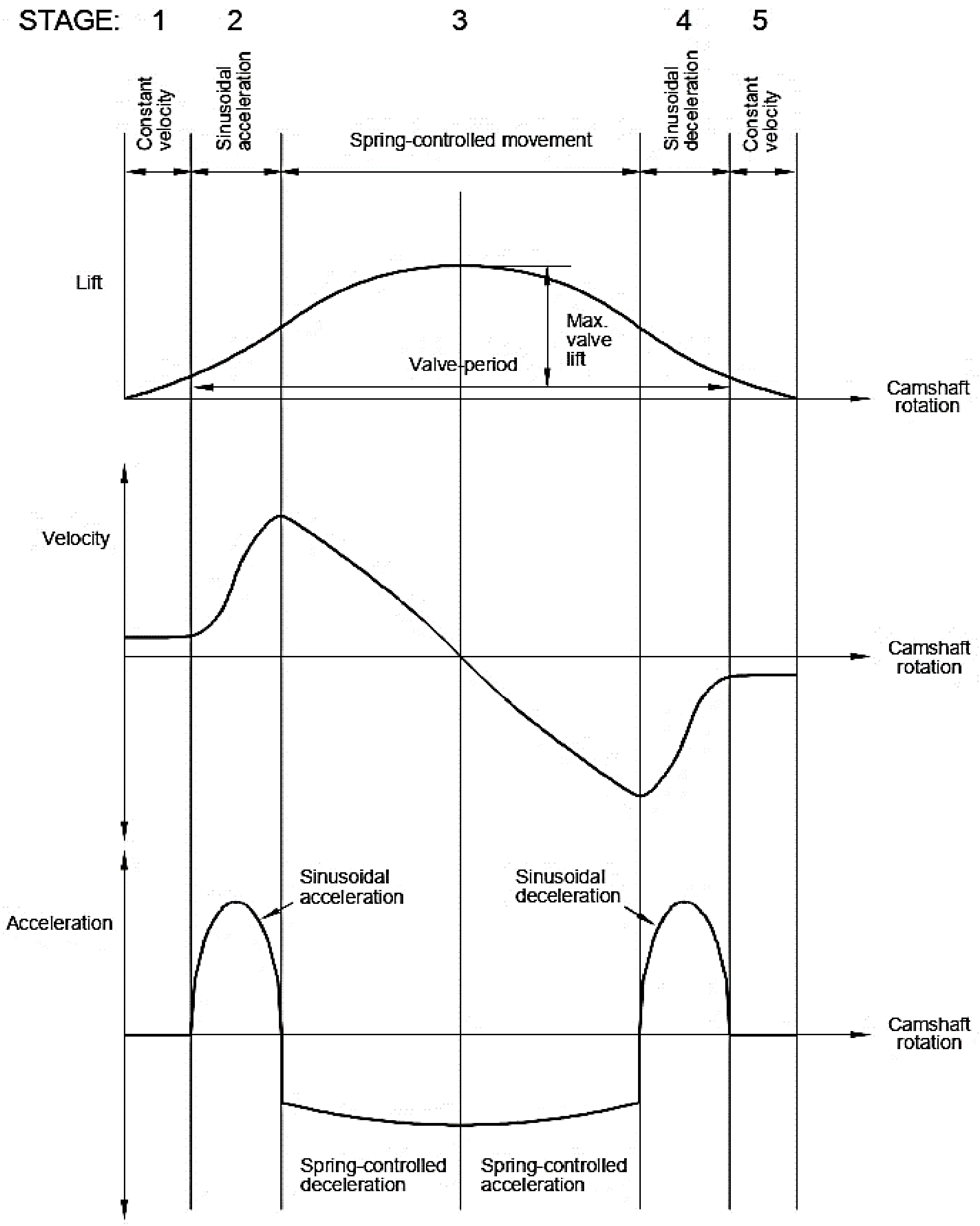
STAGE: 1 2 3 4 5
Constant velocity
Sinusoidal acceleration
Spring-controlled movement
Sinusoidal deceleration
Constant velocity
Lift
Max. valve lift
Valve period
Camshaft rotation
Velocity
Camshaft rotation
Acceleration
Sinusoidal acceleration
Sinusoidal deceleration
Camshaft rotation
Spring-controlled deceleration
Spring-controlled acceleration

Figure 2.9: Stages of theoretical valve motion [30].

At the beginning of the cam rotation, the valve clearance is taken up and then the valve starts to move. In stage (1), the opening ramp is designed to keep a constant valve velocity to control the impact stresses. Directly followed by stage (2), where the opening flank accelerates the valve with sinusoidal acceleration since it is preferred rather than the constant one to minimize the shock loading. As the valve approaches the maximum lift in stage (3), the spring is loaded enough to begin the closing process. Subsequently during stage (4), the cam supports the valve against the spring effect with sinusoidal deceleration also. And finally in stage (5), a constant closing velocity is maintained for the same consideration as the first stage [30, 31].

2.4 Valve Timing Approaches

2.4.1 Valve Overlap and Scavenging

Valve timing is considered one of the critical parameters which significantly affects engine performance, since it controls the charge induction and exhaust scavenging which serves as the engine breathing. Furthermore, in the previously mentioned LTC strategies, variable valve actuation represents a sophisticated solution to overcome the challenges of these strategies. In Otto and Diesel cycles, to assure optimal exhaust gases sweeping at the exhaust stroke, the exhaust valve closes slightly after TDC. Likewise, the same consideration with the intake valve during the intake stroke, as it opens partially before TDC to maintain higher volumetric efficiency. As a result, the intake and exhaust valves are open simultaneously forming the valve overlap period, in which the intake and exhaust ducts are “short-circuited” directly through the cylinder. This condition causes one of two possible effects. The first one is when some fresh charge can escape through the exhaust valve without participating in the combustion as shown in Figure 2.10 (a). Consequently, more UHC exists in the exhaust with higher fuel consumption. The second effect occurs when a small amount of the exhaust gases is pushed through the intake valve causing a reversed flow as shown in Figure 2.10 (b). Therefore, this amount is carried back again to the cylinder in the next intake stroke, which causes a dilution effect and acts as internal EGR by reducing the volumetric efficiency and displacing the fresh charge. The pressure difference between the intake charge and the exhaust gases determines whether the first or the second effect would be the dominant [32]. If the engine has a turbocharger or supercharger, the first effect will be the most common. Generally, the amount of valve overlap is determined depending on the engine design as small valve overlap is preferred to enhance the scavenging process during the exhaust stroke.

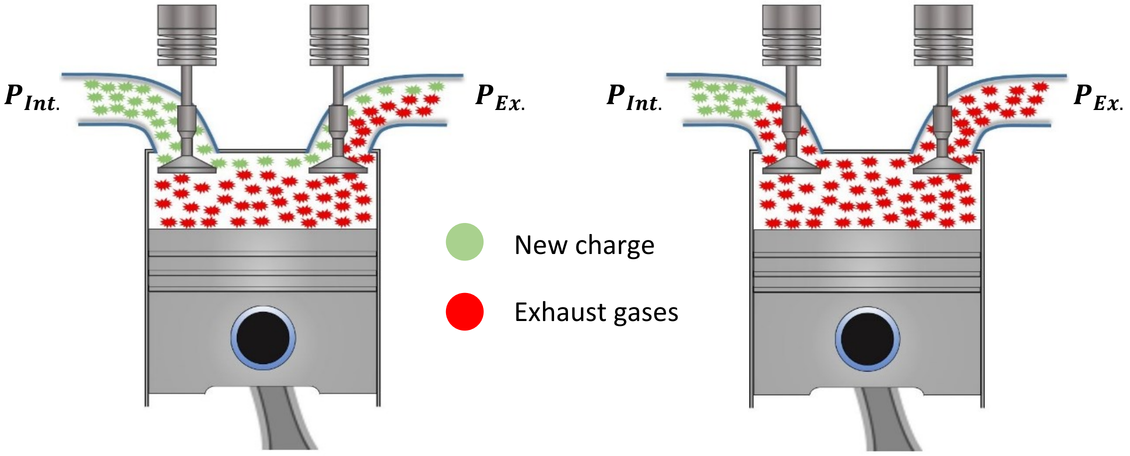

(a)
$P_{Int.} > P_{Ex.}$

(b)
$P_{Int.} < P_{Ex.}$

Figure 2.10: Gases exchange during valve overlap.

On the other hand, in the low and medium speed engines the influence of the valve overlap is more critical, and the previously mentioned effects are promoted. Because those engines have more available time for the gas exchange process, although the valves have the same relative opening and closing angular position.

Parallel with the new LTC strategies' evolution, another valve overlap approach is introduced labeled as "negative valve overlap (NVO)", in which there is no intersection between intake valve opening and exhaust valve closing. This approach combines early exhaust valve closing and late intake valve opening, which results in a crank angle period near to the TDC where the both valves are closed [33]. NVO has got more attention since it can be used as an assistant method for the combustion control in the LTC engines, which allows them to face more challenges and extend their operation range. Practically, moderate NVO values have a positive influence on the combustion in HCCI engines. However, significant levels of NVO increase the thermal stresses in the cylinder and negatively affect combustion stability [34]. Several studies in the literature [35, 36, 37, 38] investigated the potential of the NVO on the HCCI engines. In terms of Pilot-DF engines, the studies concerning NVO are limited. But for example, the authors in [39] studied experimentally the influence of NVO on the performance of a heavy-duty, single-cylinder dual-fuel engine employs diesel and Methanol. The NVO approach was attained by advancing the exhaust valve closing and retarding the intake valve opening as shown in Figure 2.11. Tests were performed at engine speed of 1500 rpm, and with the help of an electro-hydraulic valve actuation mechanism, different range of NVO was applied by sweeping the exhaust valve closing (EVC) event.

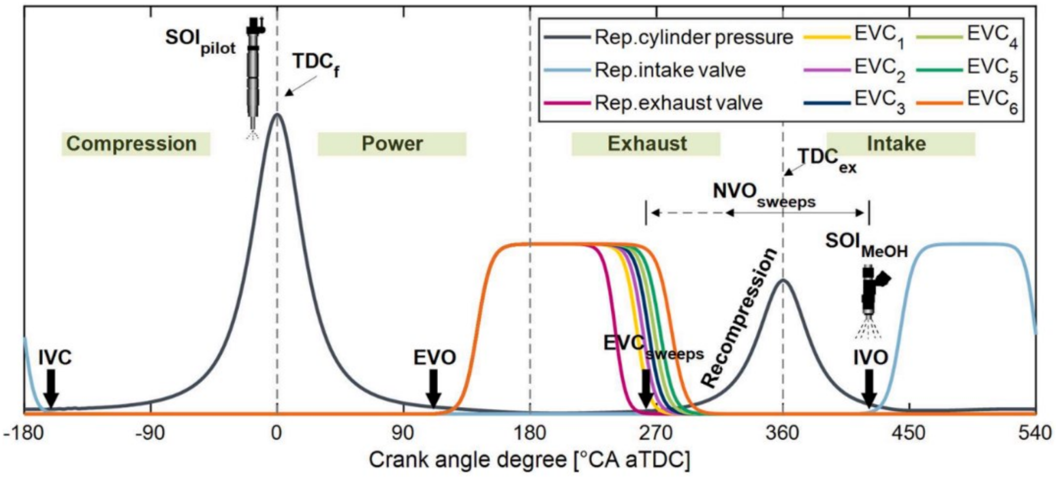

Figure 2.11: Principle of negative valve overlap [39].

The results indicated that the NVO period determines the amount of the trapped exhaust gases in the cylinder, which is directly proportional to the mean mixture temperature. It was observed that the peak heat release rate and peak cylinder pressure increased significantly as the NVO period was prolonged from 120 °CA to 135 °CA. Furthermore, a higher combustion efficiency of 93% was maintained with longer NVO period, in comparison of 33% with the standard valve timing. Combustion stability was positively affected with the NVO operation mode as it showed values lower than 3.5%. Regarding the exhaust emissions, lower UHC and CO, with higher NO_x were observed at the longer NVO operation. The reason behind that is the high temperature resulted from the residual gases, which increased the reactivity of the methanol-air mixture and enhanced the oxidation effect.

2.4.2 Miller Cycle

In comparison with the standard Otto and Diesel cycles, Miller cycle has lower combustion temperature as it has larger expansion ratio than the compression one. Hence, combining Miller cycle with the LTC technologies successfully reduces NO_x emissions and allows better combustion control with the different operating conditions via variable compression ratios. To accomplish Miller timing, the intake valve closing (IVC) can be advanced or retarded with respect to the BDC, which affects the temperature and pressure of the charge at the end of the compression stroke. When the IVC is advanced as shown in Figure 2.12 (b), the air-fuel mixture is exposed to vacuum, which expands the mixture slightly. Retarding the IVC after BDC as shown in Figure 2.12 (c), reduces the back pressure on the piston but can lied to a partial reverse flow through the intake valve. In comparison with the conventional valve timing in Figure 2.12 (a), Miller cycle has lower pumping losses either with early or late IVC.

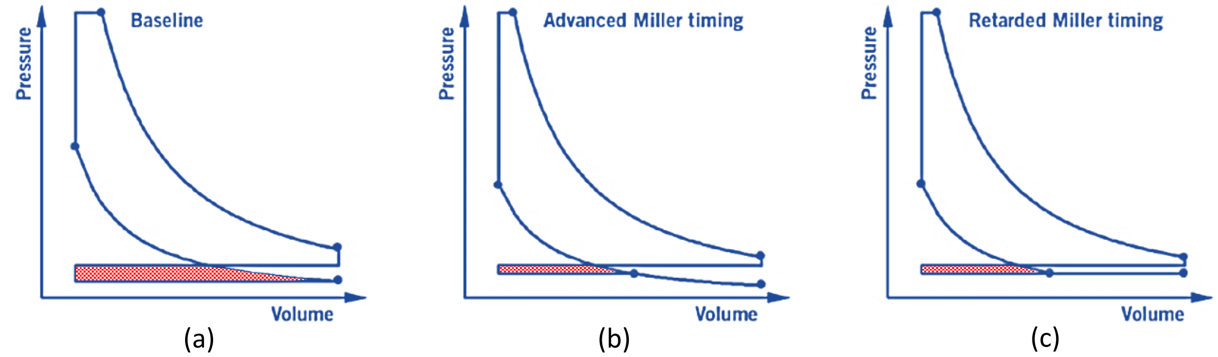
Pressure
Baseline
Volume
(a)
Pressure
Advanced Miller timing
Volume
(b)
Pressure
Retarded Miller timing
Volume
(c)

Figure 2.12: P-V diagram for Miller cycle. Adapted from[40].

Sometimes the retarded Miller cycle in Figure 2.12 (c) is referred as Atkinson cycle. Usually, Miller cycle is associated with using a turbocharger or supercharger to improve the volumetric efficiency and overcome the loss of charge due to early or late IVC [40, 41, 42].

Different types of turbochargers are available since they are used in many engines for various applications. Turbocharger characteristics are determined from the compressor map which indicates the correlation between air flow, pressure ratio, and efficiency as shown in Figure 2.13. The pressure ratio on the vertical axis is calculated by dividing the absolute outlet pressure on the absolute inlet one. The surge limit represents the border of the unstable area after exceeding the maximum pressure, while the choke limit on the right side is defined as the flow rate at maximum compressor speed. The two borders should be avoided as they can cause damage to a turbocharger. The dashed lines across the two borders are the lines of a constant compressor speed.

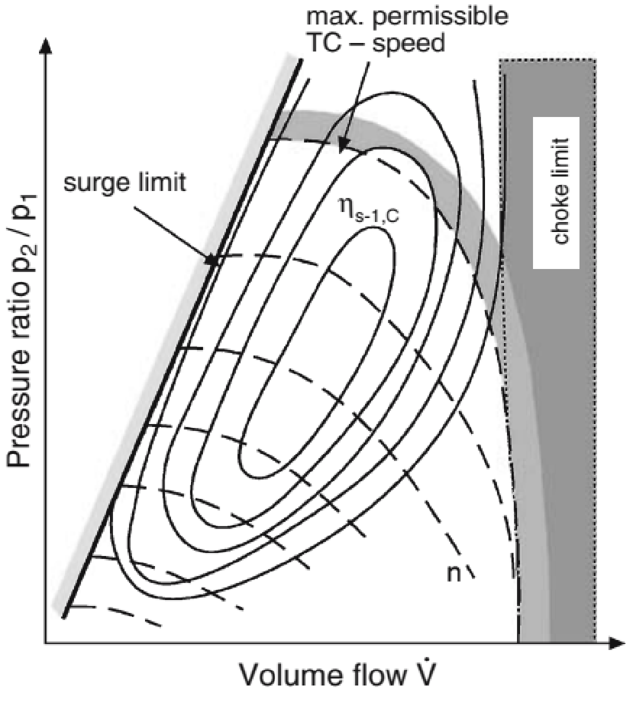
max. permissible
TC – speed
surge limit
$\eta_{s-1,C}$
choke limit
n
Pressure ratio p_2 / p_1
Volume flow $\dot{V}$

Figure 2.13: Compressor map in turbocharger [43].

Since the compressor and the turbine are fixed on the same shaft, the compressor speed is considered the same as the whole turbocharger one. The concentric regions indicate the efficiency contour where the smallest one near the center has the highest efficiency. As the contour become bigger, the efficiency drops until reaches the two borders [43].

When high pressure ratios more than the surge limit are required, the two-stage turbocharger is a promising solution as it is a combination of two turbochargers with different size connected in series. In this type, the exhaust gases coming from the engine drives the turbine of the first stage and then is directed to the turbine of the second one. Two-stage turbochargers are preferred in the large marine engines where the required air pressure cannot be achieved with the single-stage turbocharger. Furthermore, utilizing a two-stage turbocharger allows to apply strong or extreme Miller cycle, which can significantly improve engine performance and reduce NO_x emissions.

In this regard, the authors in [44] examined experimentally the influence of aggressive Miller cycle on the performance of a four-cylinder gasoline engine equipped with a two-stage turbocharger. The engine is prepared with a hydraulic cam phaser to achieve different positions for the intake and exhaust valves as indicated in Figure 2.14. Tests were performed at full and half loads with different combinations of valve timing.

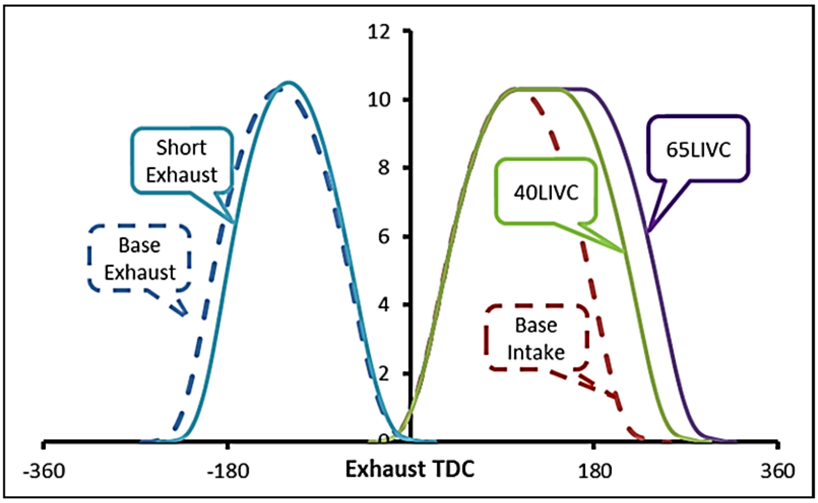

Figure 2.14: The examined positions of intake and exhaust valve [44].

Results showed that the maximum retarding of IVC (65 LIVC) with the short exhaust profile at full load can achieve a CR of 12.5 with the help of the two-stage turbocharger. Under the same conditions, the engine produced a BMEP of 22 bar at 1500, and the BSFC was decreased by 6% in comparison to the base intake valve timing. Additionally, delaying the IVC at part loads provided lower pumping losses which was reflected on the thermal efficiency.

In [45], the influence of Miller timing and intake air cooling were experimentally investigated using a heavy-duty, single-cylinder dual-fuel engine employs diesel and methanol. The engine equipped with a hydraulic variable valve actuation system on the intake camshaft to control the IVC point while the intake valve open (IVO) was fixed as shown in Figure 2.15.

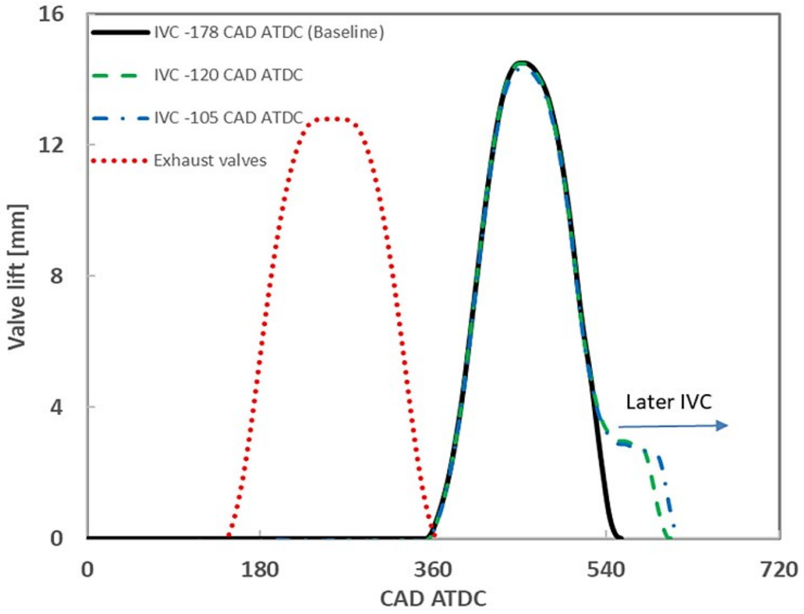

Figure 2.15: Late intake valve closing in Miller cycle [45].

A common rail injection system was used for the diesel fuel, while the methanol was injected via port injection. Tests were carried out at 1200 rpm and 18 bar IMEP with different methanol fraction ratios, while the diesel pilot injection timing was optimized up to the limitations of the maximum pressure rise rate. Results showed that at methanol fraction of 28%, the late IVC led to lower effective compression ratio which reduced the charge temperature and pressure before the combustion. As a result, the ignition and combustion of the premixed fuel was delayed which allowed more advancing of the diesel injection. Also, the reduction in the effective compression ratio resulted in higher average in-cylinder gas temperature during the combustion phase, because of the lower trapped mass with less heat capacity in the cylinder. In terms of intake air temperature, reducing it from 323 K to 305 K decreased the average in-cylinder gas temperature by 50 K during the compression process. Consequently, the ignition delay was prolonged, and the pilot injection was tuned to maintain best combustion characteristics. As a benefit, the lower intake air temperature prevented the autoignition prior to the diesel pilot injection. Furthermore, combining the late IVC with the lower intake air temperature together resulted in a significant reduction of NO_x emissions and increased the net indicated thermal efficiency.

On the other hand, the lower combustion temperature raised the UHC and CO in the exhaust emissions.

Using a two-zone combustion model, the influence of Miller cycle (late IVC) on dual-fuel marine engine was proposed by [46]. The model employs diesel pilot injection as an igniter with 2% energy ratio of the total heat release, while the rest of combustion comes from NG. To calculate the emissions and the thermodynamic processes during combustion, the cylinder was divided to a burned and unburned zone. A Wiebe function was used to describe the heat release rate, and Tabaczynski correlation from [47] was implemented for ignition delay prediction. The NO_x formation was calculated using the extended Zeldovich mechanism including the three-step NO formation reactions. After comparing the model results with the experimental data, it was observed that the earlier IVC requires more intake air pressure to assure enough charge substitution with higher volumetric efficiency. Furthermore, advancing the IVC point from 558 °CA to 490 °CA reduced the combustion temperature at TDC by 136 K, and increased the BSFC from 172 g/kWh to 180 g/kWh. Concerning the emissions, NO_x formation was affected positively also with the same IVC advancing as it was reduced from 19 kg/h to 2 kg/h.

Considering the novel LTC combustion strategies, RCCI engine in combination with Miller cycle was investigated by a multi-zone combustion model in [48]. The used engine was a six-cylinder heavy-duty engine equipped with an electrically actuated variable valve system, enabling early and late IVC. The model includes a detailed chemical kinetics reaction consisting of 354 reactions among 65 species to predict the combustion behavior and the emissions formation. Model results were validated against experimental data from diesel engine that was modified for RCCI operation using diesel and NG. Results showed that early IVC can be used to control the peak in-cylinder pressure and temperature which allows extending the engine load to higher loads without exceeding the engine design limits. Specifically, advancing the IVC from 883 °CA to 865 °CA (considering 720 °CA as ignition TDC) allowed to increase the IMEP from 21 bar to 23 bar, while the indicated efficiency was reduced by 2% and the total UHC increased 3 times in the exhaust. Retarding the IVC event after 750 °CA significantly increased the intake air temperature due the exhaust back flow, while the UHC emissions were reduced by 30%.

Diesel engines are not far away from Miller cycle, as many academic literatures discuss the utilization of Miller cycle to optimize Diesel engine performance. For example, the authors in [49] experimentally investigated the effect of Miller cycle in combination with EGR on the performance of a four-stroke, six-cylinder, turbocharged marine diesel engine in order to meet the IMO Tier III regulations. Since employing Miller cycle and EGR together reduces the amount of the fresh charge, the using of a turbocharger was a mandatory to maintain the sufficient outpower. Different camshafts were redesigned to allow various intake valve closing for Miller cycle as shown in Figure 2.16, while the EGR system was tuned to get different substitution ratios.

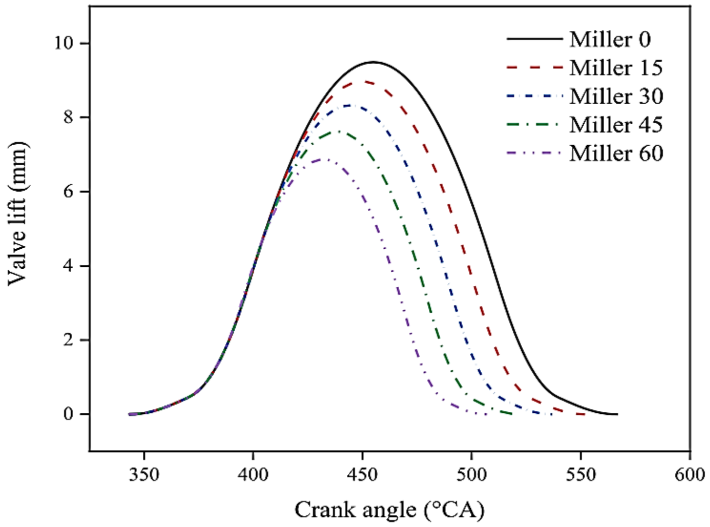

Figure 2.16: Intake valve lift curves for Miller timing [49].

Results indicated that combining Miller cycle with EGR together delayed the ignition timing and decreased the peak heat release rate during the main combustion phase. Generally, the use of medium EGR rates with medium Miller timing can not only meet the NO_x emissions of IMO Tier III, but also improves the BSFC and COV_{IMEP}. Under high load conditions and with different EGR rates from 0% to 25%, the valve lift curve of Miller 30 had more brake thermal efficiency than all the other positions. On the other hand, increasing the EGR rates negatively affected the brake thermal efficiency with all Miller positions because of the dilution effect.

2.5 Combustion Modelling Approaches

Internal combustion engines are considered sophisticated systems, in which many parameters affect their performance. Experimentally testing of them is an effective method in the R&D community but it consumes much time and costs, especially when it comes to the large engines which include many sub-systems. Hence, modelling and simulation approach is preferred as it can predict the engine performance efficiently with a significant reduction in time and cost. In addition, modelling and simulation methodology has more flexibility and higher degree of freedom than the experimental tests, as it is possible to modify and reset all the parameters and the boundary conditions in the model to investigate their effects. Hence, a clear insight and deeper understanding of the thermodynamic processes in the engine is provided. Modelling of internal combustion engines is continuously growing and has become essential nowadays during the engine's development phase. Figure 2.17 summarizes the main features of the combustion modelling approaches which will be discussed in this section.

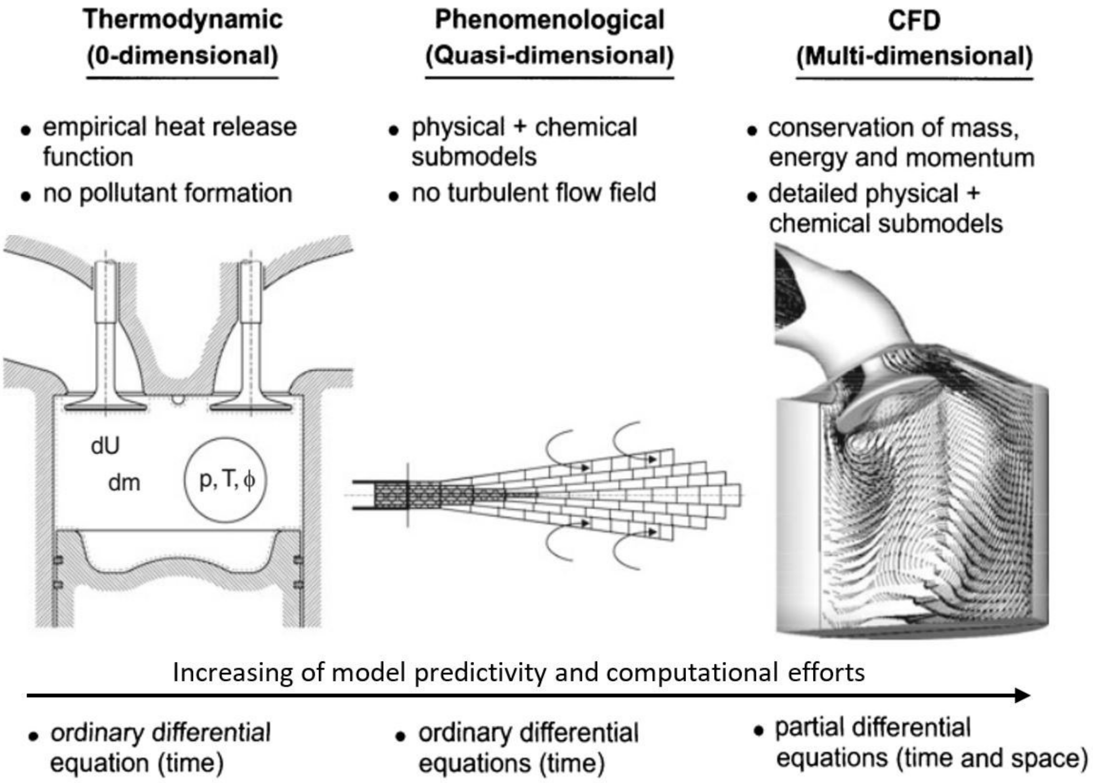
Thermodynamic
(0-dimensional)
Phenomenological
(Quasi-dimensional)
CFD
(Multi-dimensional)
• empirical heat release function
• no pollutant formation
• physical + chemical submodels
• no turbulent flow field
• conservation of mass, energy and momentum
• detailed physical + chemical submodels
dU
dm
p, T, ϕ
Increasing of model predictivity and computational efforts
• ordinary differential equation (time)
• ordinary differential equations (time)
• partial differential equations (time and space)

Figure 2.17: General classification for combustion modelling approaches. Adapted from [50, 51].

2.5.1 Thermodynamic Models (Zero-dimensional)

Thermodynamic models are the simplest strategy as they have only the time-dependance of variables and do not consider the spatial variation for the composition. They assume that all the contents are ideally mixed at any time in the combustion chamber, hence they are computationally efficient. Such models are used only when simple and fast simulation is required, because they depend on the calibration of some empirical correlations without any physical definition. Furthermore, in thermodynamic models the combustion chamber is treated as one homogenous zone. Sometimes to reduce the model shortage and improve its predictability, the combustion chamber can be divided into two or more zones but it stills do not present a local insight for the composition in the cylinder and cannot be used for the simulation of pollutants formation [50].

2.5.2 Phenomenological Models (Quasi-dimensional)

Phenomenological combustion models represent a meeting point between the simple thermodynamic models and the complicated CFD ones, so they are very widespread and more preferred in the R&D community. They combine between the high predictive quality and the low calculation time without the need of high computational resources. Indeed, they are more complex than the thermodynamic ones as they consider a spatial resolution and have the prediction ability of the heat release rates and pollutants formation. In these models the combustion chamber is divided into two or more zones, in which the temperature and composition are different. Furthermore, they include various physical or chemical formulations to describe the thermodynamic processes occurring during the combustion depending on the target of the simulation [50].

A quasi-dimensional multi-zone combustion model was developed in [52] to predict the combustion process and the pollutants formation in a dual-fuel engine. In this model the cylinder was divided into five zones as shown in Figure 2.18. The first two zones are burned and unburned zone for the diesel pilot combustion. After that, a flame propagation zone toward the gaseous fuel-air mixture was implemented. And finally, reaction and unburned zones for the combustion of the gaseous fuel were considered. The heat release rate of the diesel pilot fuel was described by a superposed Wiebe function, while the combustion rate of the gaseous fuel was treated as a function of its concentration.

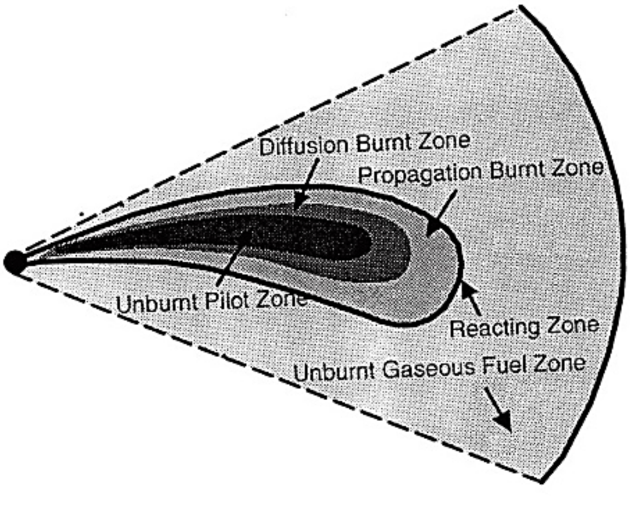

Figure 2.18: Schematically structure of the five-zone model [52].

To describe the pre-ignition and the combustion in the reaction zone, a detailed chemical reaction scheme consists of 138 elementary reaction steps and 32 chemical species was employed. Pilot fuel injection characteristics like spray angle, break-up, and penetration were described based on the correlation suggested by Hiroyasu [53]. Results showed a good agreement with the experimental data, and it was observed that the higher quantity of pilot fuel increased the maximum cylinder pressure but may lead also to an earlier knock onset. Additionally, heat release rate and combustion temperature increased significantly with the higher methane admission. When the temperature increased over 1300 K in the reaction zone, the CO concentration in the exhaust emission was reduced.

Phenomenological models can be developed through either open codes or software. For example in [54], the 1-D commercial software GT-Power was used to develop a two-zone combustion model for a large marine dual-fuel engine in order to investigate its performance and emissions. The engine was Wärtsilä 9L50DF, which is a four-stroke engine and has nine cylinders placed in-line. Also, its equipped with a wastegate turbocharger and intercooler. The model consists of different blocks connected together as shown in Figure 2.19. Each one of them represents a specific engine component with the ability to change its boundary conditions and specifications.

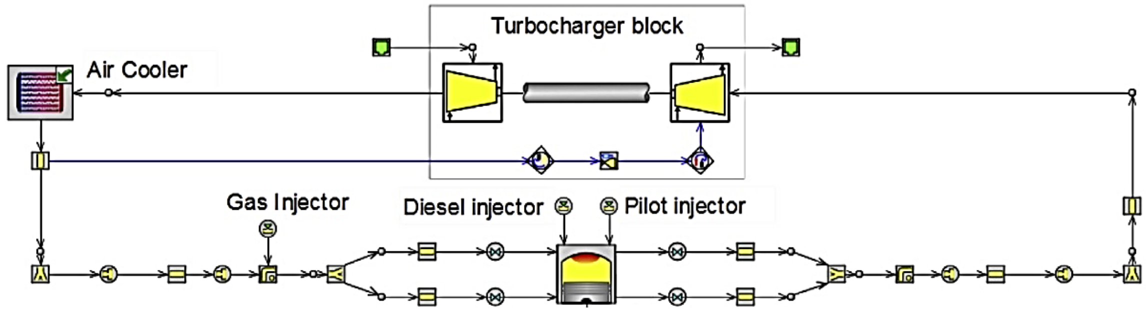

Figure 2.19: One section of engine model in GT-Power environment. Adapted from[54].

The model employs Woschni formula, Sitkei model, and Zeldovich mechanism to describe the cylinder wall heat transfer, ignition delay, and NO_x formation respectively. The cumulative heat release rate was simulated using the sum of multi-Wiebe function which involves three different Wiebe curves. The first one belongs to the premixed combustion of approximately half of the pilot fuel, while the second one for the rest diffusive combustion of the pilot fuel, and the last one for the burning of the gaseous fuel. In this model the valve timing was set according to Miller concept while the fuels used were marine gas oil (MGO) as pilot fuel and NG as gaseous fuel. After running the simulation in both dual-fuel mode and full diesel mode, different model results like maximum cylinder pressure, heat release rate, brake mean effective pressure, and NO_x emissions were compared to the experimental data. It was concluded that the developed model can be used efficiently to represent the engine behavior in the steady state mode. Results showed that the peak heat release rate of the dual-fuel mode is slightly higher than that at the full diesel mode. However, lower maximum cylinder pressure in the dual-fuel mode was observed, which was due to the waste gate valve opening. In terms of engine efficiency, it was observed that the dual-fuel mode is more efficient at the high loads with values up to 47% at 100% load. Considering the exhaust emissions, $BSNO_x$ was lower in the case of dual-fuel mode and matched the IMO Tier III regulation, while only IMO Tier II was satisfied at the diesel mode. The CO_2 emissions in the dual-fuel mode were also lower than those of the diesel mode with an average of 25%, because of the lower carbon to hydrogen ratio of the NG compared to the MGO.

Another phenomenological combustion model for a heavy-duty dual-fuel engine was developed by [55]. Experimental results were obtained from a 15-liter dual-fuel, four-stroke engine equipped with a turbocharger and produces 405 kW at 2000 rpm. The model aims to present an advanced analysis tool for the combustion phenomena and the rate of heat release in the dual-fuel engines. In order to improve the charge mixing characteristics and minimize the soot emissions, the model employed an advanced pilot fuel injection (about 60° BTDC) as ignition source. NG was used as the main heat release source by port fuel injection with substitution rates between 30% and 65%. To describe the heat release rate of the dual-fuel combustion, the authors proposed a four-stage heat release mechanism as shown in Figure 2.20, in which the combustion process is divided into four stages representing the combustion of the diesel fuel and NG.

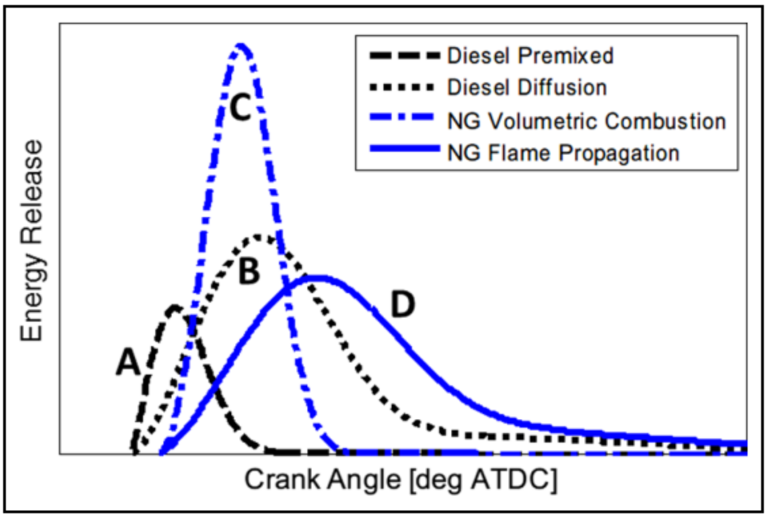

Figure 2.20: Schematic description of the four-stage heat release mechanism [55].

A triple-Wiebe function was used to analyze the heat release rate of each stage according to equation (2.1).

$$\frac{m_{fb}}{m_{ft}} = \sum_{i=p,m,t} f_i \left\{1 - exp\left[-6.9\left(\frac{\theta - \theta_{ign}}{\Delta\theta_i}\right)\right]^{m_i+1}\right\} \qquad (2.1)$$

Where $i = p$, $i = m$, and $i = t$ indicate the phases of premixed combustion, main combustion, and tail combustion respectively. θ is the crank angle in degrees, θ_{ign} is the crank angle at the ignition onset, $\Delta\theta_i$ is the combustion duration, and m_i is the shape tuning factor.

Ignition delay for pilot fuel combustion was described using Assanis correlation as the following:

$$\tau_{ID} = 2.4\ \phi_{pD}^{-0.2}\ .\ P_{Cyl.}^{-1.02}\ .\ exp\ (\frac{E_a}{R_u\ T_{Cyl.}}) \qquad (2.2)$$

Where ϕ_{pD} is the pseudo-diesel equivalence ratio, $\bar{P}$ is the cylinder pressure at start of injection (SOI), $\bar{T}$ is the temperature at SOI, E_a is the activation energy, and R_u is the universal gas constant. From the results, it was observed that the triple-Wiebe function has the ability to represent dual-fuel combustion. In terms of pilot injection timing, advancing the pilot injection improved the charge mixing, reduced the rich pockets of diesel fuel, and had a positive effect on the NO_x emissions due to the lower combustion temperature.

Combustion complexity in dual-fuel engines drove the authors in [56] to propose a simulation model for a duel-fuel engine using the phenomenological approach. The engine has a capacity of 2-liter with four cylinders and was modified to enable natural gas port injection while the diesel fuel was used as pilot injection. To calculate the pilot injection characteristics, a transient diesel jet sub-model according to [57] was implemented while the ignition delay was predicted with a developed 3-Arrhenius approach as in [58]. Additionally, the heat release rate was represented using two Wiebe functions. The first one for the diesel auto-ignition phase and the second one for the NG flame propagation phase. This description of the heat release rate allows deeper analysis for every combustion phase individually. Model results were validated with experimental tests, and they showed a very good agreement so the model can be used for combustion analysis with different operating conditions. The authors concluded that both the combustion phases have a strong dependency on the ignition delay.

Pilot injection conditions like fuel quantity and injection timing significantly affect the performance and emissions of dual-fuel engines. In order to investigate the effect of these two parameters, a comprehensive two-zone phenomenological model for a high-speed dual-fuel engine was proposed in [59]. In this study, experimental investigations were performed on a modified Lister LV1 engine, which is a single-cylinder, naturally aspirated diesel engine and was modified to operate under dual-fuel mode using NG. As shown in Figure 2.21, the model assumes that the conical pilot spray is the burned zone. The boundary of this spray constitutes the flame front and separates between the two zones. Based on experimental data reported a flame thickness of approximately 0.2 mm under normal engine conditions in [60], it was assumed that the flame front has a negligible thickness.

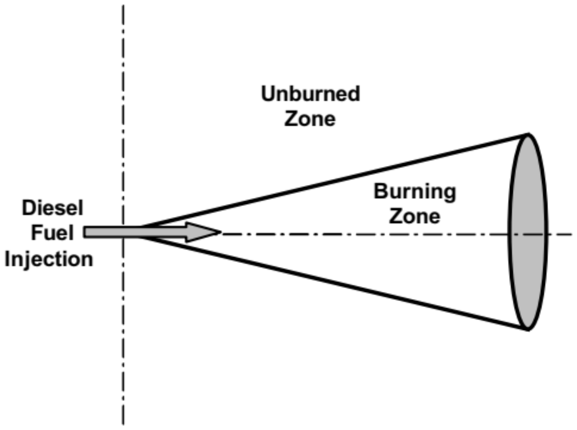

Figure 2.21: Definition of burned and unburned zone [59].

The model considers that the combustion occurs in the burned zone, which consists of unburned evaporated diesel fuel, unburned gaseous fuel, air that has not yet participated in the combustion, and combustion products. The unburned zone has the rest of the gas-air mixture, which is reduced synchronically with the flame propagation. Further, the heat transfer between the two zones was neglected. Spray characteristics and heat release rate from diesel fuel were calculated using the developed Hiroyasu model in [61], while the combustion of the gaseous fuel was described using an Arrhenius premixed reaction rate. Consequently, the total heat release rate is the sum of them. An extended Zeldovich mechanism was implemented for the estimation of NO_x formation while the CO was calculated using the kinetics of the main formation and oxidation reactions. Model results were validated by experimental tests, and they showed a good coincidence in terms of engine performance and emissions. Results indicated an improvement in BSFC with the increasing of the pilot fuel quantity when the injection timing was fixed. This improvement was due to the higher heat release rate from the larger pilot fuel quantity especially during diffusion combustion phase of the pilot fuel. Also, advancing the pilot injection timing led to a slight improvement in BSFC in comparison with the normal injection timing. This improvement was more noticeable at high engine loads due to the sharper increase in the heat release rate. The NO_x concentration in the exhaust showed a negative effect with increasing the pilot fuel quantity, as the combustion temperature inside the cylinder increased significantly. Furthermore, a reduction in the CO level was observed with increasing the pilot fuel amount while advancing the pilot injection timing increased the CO emissions.

A more comprehensive quasi-dimensional combustion model for dual-fuel engine was presented by [62], in which diesel fuel was used for pilot injection and methane for gas combustion. In this model a modified multi-zone combustion sub-model based on the packet approach in [61] was implemented to describe the pilot fuel combustion. Different physical processes relevant to spray such as injection, liquid spray breakup, charge entrainment, droplets evaporation, and combustion were included. Furthermore, a K-ε turbulence model was extended to represent the effect of the diesel pilot injection on the turbulence level, while the ignition delay effect was calculated using special table. The gaseous combustion phase was predicted using a modified fractal combustion model based on the flame propagation theory from [63]. The fractal combustion model assumes that the thin flame front is highly wrinkled due to the turbulent effect which results in higher burning rate and larger flame front surface with respect to the laminar one. This principle gives the possibility to relate the turbulent flame speed to the laminar one depending on the turbulent intensity. Experimental tests were performed on a high speed 2-liter diesel engine which was modified to operate on the dual-fuel mode. Simulation results were in a good fit with the experimental data and the model can be used for further investigations. Results showed that the spray parameters strongly affect the ignition delay and the initial stage of the combustion, while the flame propagation characteristics have dependency on the turbulence level.

2.5.3 Computational Fluid Dynamic Models (CFD Multi-dimensional)

Multi-dimensional CFD models are considered the most sophisticated approach in combustion engines' simulation. Although they lie out of the focus in this study, but they worth to be mentioned. CFD models based on the locally resolved solutions of mass, energy, and momentum conservation of small cells connected together forming a numerical mesh. Also, they include various detailed physically and chemically sub-models in order to describe the thermodynamic phenomena inside the cylinder. High spatial and temporal resolution are considered in CFD, which provide a micro-scale insight in the engine. In contrast, these models are more consuming in terms of computational resources and time [50].

By utilizing the CFD approach, the effect of different fuel ratios on performance and emissions of dual-fuel engine was investigated in [64]. The experimental tests were achieved on a four-stroke turbocharged diesel engine, which employs diesel fuel and NG for pilot injection and gaseous mixture respectively. The CFD model includes a structured dynamic mesh for the cylinder which was obtained using ANSYS-ICEM CFD meshing tool, while KIVA-3V software was used as a flow solver. The entire grid size has 104,000 cells while the cylinder and bowl volume discretizations were nearly 58,000 and 5000 cells respectively. The computational domain also includes the intake and exhaust ducts as the open valve periods were considered. To predict the initial spray break-up, the Kelvin-Helmholtz wave model was implemented and the Rayleigh-Taylor model was used in conjunction to describe the secondary break-up of the droplets. The delay period of the diesel fuel was represented by Stringer correlation [65] and the diesel combustion was described using a classical one step kinetic mechanism of fuel oxidation combined with eddy dissipation approach [66]. The NG combustion was predicted using a two-step mechanism. By comparing the numerical and experimental results together, a qualitative agreement was found in terms of cylinder pressure and emissions and the model was used for further investigations. Results indicated that increasing the methane content in the mixture caused higher flame speed and faster pressure rise rate. Concerning the exhaust emissions, a progressive reduction for NO was observed with increasing the NG substitution rate, while the CO formation was negatively affected.

2.6 Summary

From the discussed literature in this chapter, it can be concluded that the new combustion technologies (HCCI, PCCI, RCCI and pilot-DF) have a promising future in terms of exhaust emissions reduction. They can achieve low NO_x and PM emissions parallel with high thermal efficiency in comparison with the conventional diesel combustion. Indeed, the double fuel technologies (RCCI and pilot-DF) have better combustion control since two fuels are included but they still need more development. Therefore, many combustion control approaches are used in conjunction with these technologies aiming to improve the combustion control. Variable valve actuation is considered an effective technique in this aspect as it allows to control the combustion characteristics. It can be achieved by tuning intake valve timing, exhaust valve timing, or both of them together. Miller cycle is a concept which deals with an early intake valve closing in order to obtain variable compression ratios. As a result, engine performance and emissions can be optimized at the different operating conditions. Additionally, it enables to control the valve overlap period which significantly affects the unburned hydrocarbon amount in the exhaust emissions. Improper valve overlap leads to poor combustion with high fuel consumption, since too much overlap will cause that the fresh charge escape from the exhaust port. Or in some cases, the exhaust gases are pushed through the intake port. Typically, Miller cycle is combined with a pressurized charge air to assure high volumetric efficiency. In order to investigate the effect of valve timing on engine performance and emissions, the modelling and simulation approach is preferred since it allows more flexible investigations in comparison with the experimental tests. In this regard, phenomenological modeling represents a flexible methodology as many sub-models can be integrated depending on the target of the simulation.

3 Engine Test Bench

The aim of this chapter is to introduce a detailed description of the dual-fuel engine test bed with the included sub-systems. Also, the different instrumentations and devices for the measuring and controlling purposes are presented. And finally, the flexible valve train strategy with all its component is outlined and discussed since it represents the heart of this study.

3.1 Dual-Fuel Research Engine

The engine test bench consists of a medium-speed, dual-fuel marine engine equipped with auxiliary systems and several monitoring units, which allow executing various experimental tests and able to validate simulation results. Concerning the flexibility considerations, the engine represents only one cylinder from the full engine of MaK M34DF [67]. With the cooperation of Caterpillar, it was assembled in the Department of Piston Machines and Internal Combustion Engines, Faculty of Mechanical Engineering and Marine Technology, Rostock University. The main engine specifications are outlined in Table 3.1. To simulate the engine load effect, the engine is coupled to a 1.2 MW 4-quadrant dynamometer, which can act as a prime mover or power absorber.

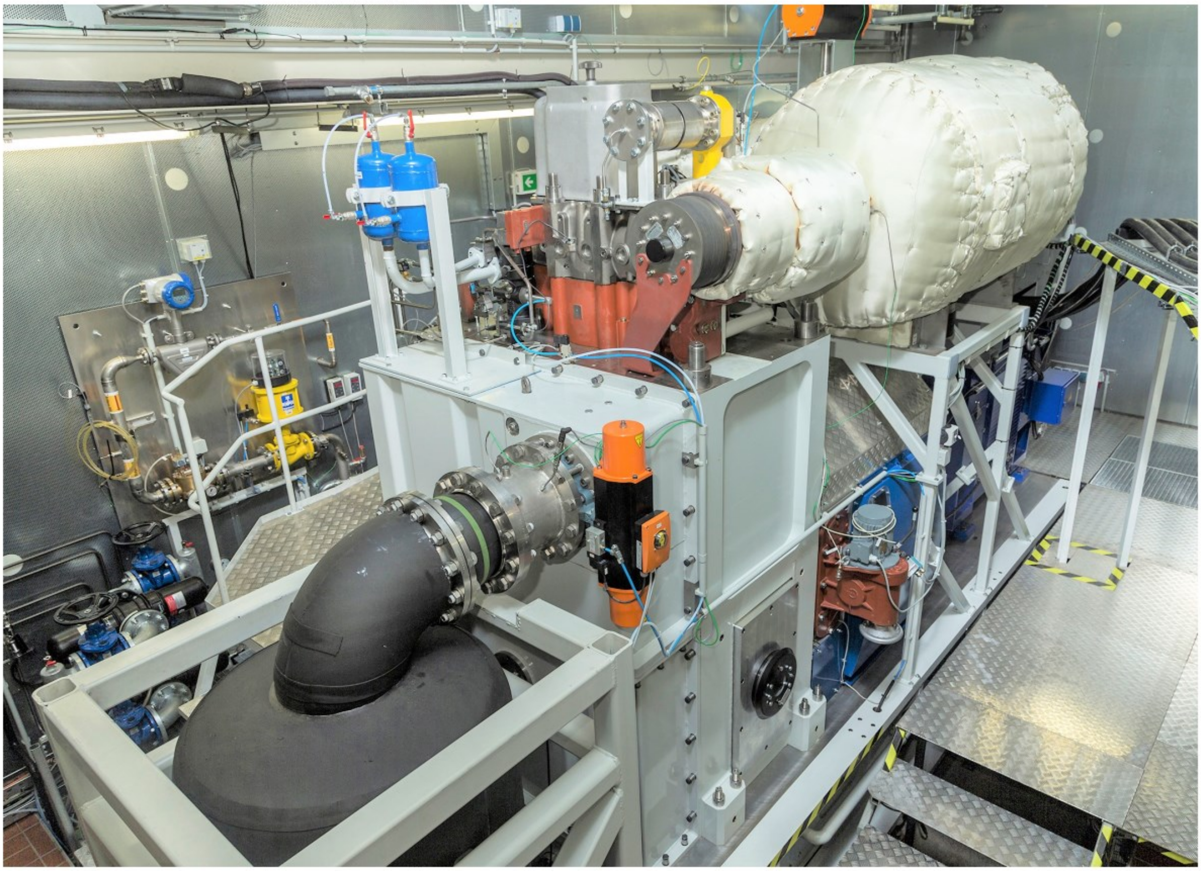

Figure 3.1: Dual-fuel research engine at Rostock University.

Table 3.1: Specifications of dual-fuel research engine

Specification	Unit	Value
Number of cylinders	**-**	**1**
Stroke	**mm**	**460**
Bore	**mm**	**340**
Compression ratio	**-**	**12.75**
Speed	**RPM**	**720**
Indicated power	**kW**	**550**

The dynamometer is speed-controlled, while the engine torque is adjusted by modifying the fuel quantity and the other combustion parameters to keep the desired engine load. A schematic diagram for the engine setup including the necessary sub-systems and the main circuits is shown in Figure 3.2.

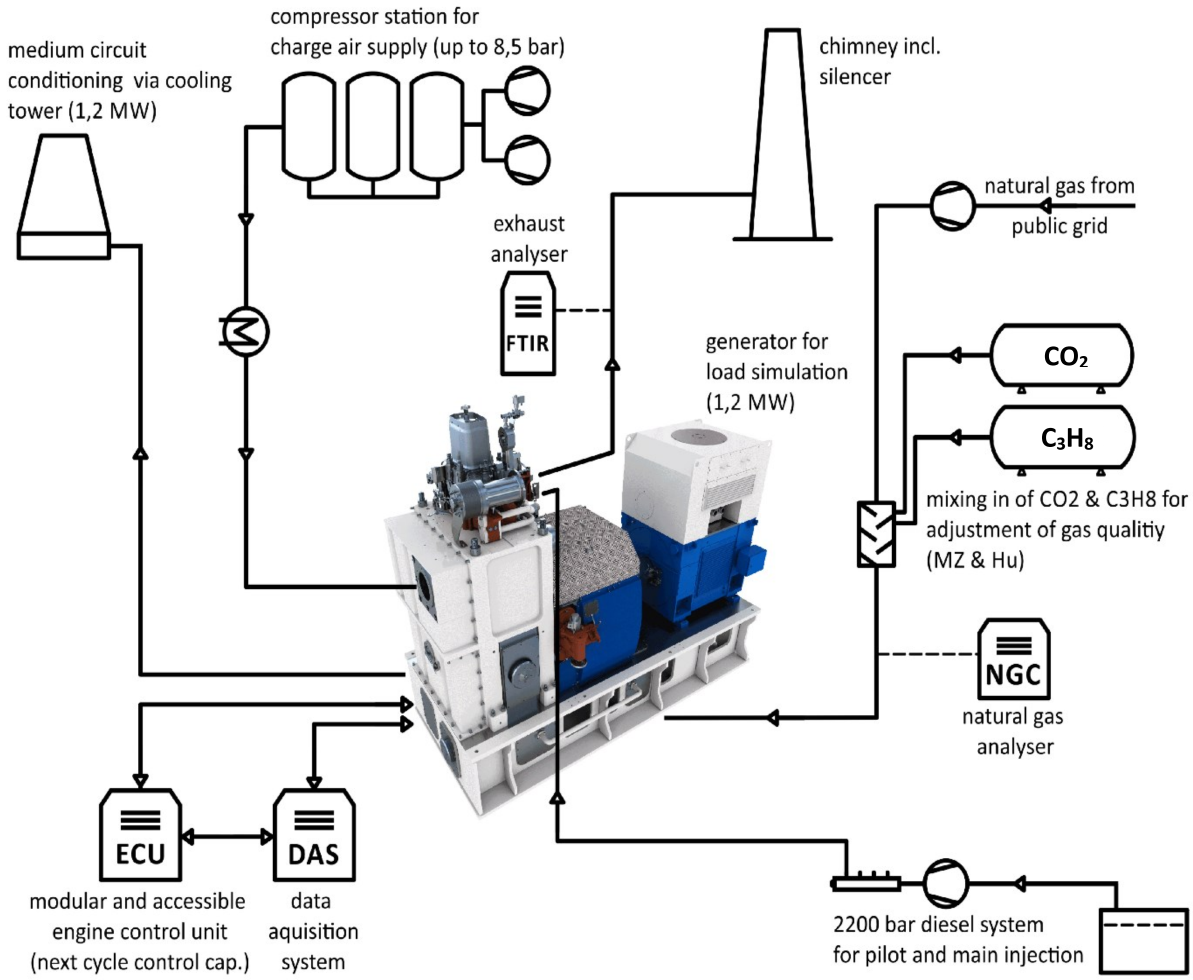
compressor station for
charge air supply (up to 8,5 bar)
medium circuit
conditioning via cooling
tower (1,2 MW)
chimney incl.
silencer
natural gas from
public grid
exhaust
analyser
FTIR
generator for
load simulation
(1,2 MW)
CO₂
C₃H₈
mixing in of CO2 & C3H8 for
adjustment of gas qualitiy
(MZ & Hu)
NGC
natural gas
analyser
ECU
DAS
modular and accessible
engine control unit
(next cycle control cap.)
data
aquisition
system
2200 bar diesel system
for pilot and main injection

Figure 3.2: Schematic diagram for dual-fuel engine setup with the main sub-systems.

- **Diesel Injection System**

The engine is equipped with a common rail injection system, which is controlled via a programmable control unit. Hence, the different injection parameters such as injection timing, rail pressure, injection quantity, and multiple pilot injection can be tuned. The system can be used either in the form of pilot injection to provide an ignition pulse in the case of dual-fuel operation, or as a conventional diesel injection for the pure diesel operation mode with a maximum rail pressure of 2200 bar.

- **Natural Gas Supply System**

The natural gas is supplied to the engine from the city public network, passing through a mixing station, which has two tanks for CO_2 and C_3H_8. The mixing station is used to regulate the gas pressure. Furthermore, it allows to adjust the gas quality in order to maintain stable gas properties over a specific range of experiments as the substitution ratio of CO_2 and C_3H_8 can be modified to compensate any change in the methane content or the calorific value. The properties of the outlet gas are monitored with a gas chromatograph, and then the gas is fed to the engine through a solenoid valve (SOGAV 105) mounted on the intake duct. This valve employs the PWM technique so the gas admission can be controlled effectively. Concerning optimal mixing characteristics and stable gas admission, the gas pressure is continuously regulated to be more than the intake air pressure by 1.6 bar [68].

- **Intake Air and Exhaust Gas**

To control the intake air properties, two air compressors are connected to the engine with a flowrate capability up to 5400 kg/h and maximum pressure of 8.5 bar. The air temperature is regulated through heaters included in the circuit, while the air pressure is controlled using two pressure control valves mounted before the engine in the intake path. On the other side, the exhaust gas pressure is controlled through two flap valves with different sizes installed in the exhaust system. The large one is used for the main control while the small one for the fine tuning. Furthermore, the intake and exhaust pressures are correlated, as they are regulated according to a specific map to simulate the effect of a turbocharger. For exhaust emissions measurement, an AVL SESAM i60 FT exhaust gases analyzer was used, which is able to measure more than 20 gas components simultaneously. The measuring principle of this analyzer is based on the Fourier Transformation Infrared Spectroscopy (FTIR) and it has a measuring frequency of 1 Hz [69].

An AVL Smoke Meter 415s was employed for smoke detection, as it depends on the filter paper blackening method to determine the soot concentration in a sample of exhaust gases [70]. To measure the particle size distribution, a TSI particle sizer spectrometer model 3090 was used since it measures particle size from 5.6 to 560 nm.

- **Combustion Chamber**

For combustion chamber analysis, an AVL IndiSet system was utilized, which collects pressure signals from different sensors based on the crank angle position, as the latter is measured with encoder. To ensure a reliable engine operation with synchronized control, a maximum resolution of 0.1 °CA was selected for the measurement of cylinder pressure, injector activation, and NG valve while a resolution of 1 °CA for the other variables was considered.

- **Data Acquisition and Measurement Interface**

The signals from different measuring devices and sensors are collected and processed through NI hardware with a recording frequency of 1 Hz. With the help of NI SCM console, the control devices are connected to the computers in the control room. For the test bench management, a graphical user interface based on the LabView environment is developed which allows reliable and real time control for all parameters.

3.2 Flexible Valve Train Strategy

The innovative flexible valve train strategy represents a core point for this study, as it is utilized to optimize the performance and emissions of the dual-fuel engine. Mainly, it can be divided into two sub-mechanisms, the first one is the Flexible Camshaft Technology (FCT) and the second one is the Multi-segment Camshaft. In this section a detailed description for both of them will be presented, including all components and the theory of operation.

3.2.1 Flexible Camshaft Technology (FCT)

The flexible camshaft technology aims to control both the intake and exhaust valves together in an opposite manner as it advances the opening and closing points for the intake valve, while retards them for the exhaust valve. By using the FCT, it is possible to adjust the valve timing during the engine operation, which allows to adopt the optimal valve timing for different operation conditions over the entire load range. Additionally, FCT enables to apply different levels of Miller cycle effect as will be discussed later. The main components of the FCT are the valve drive and the actuator as shown in Figure 3.3.

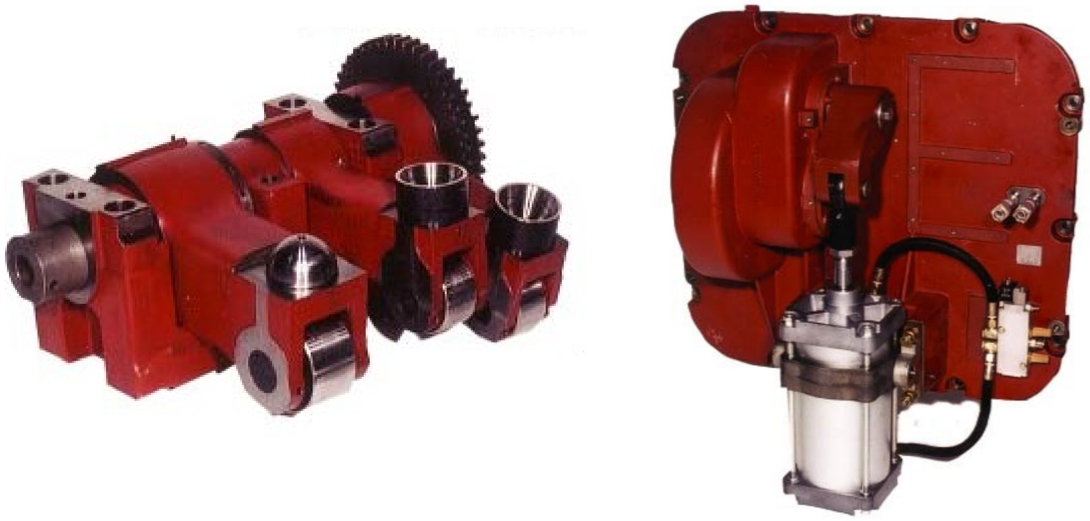

(a) (b)

Figure 3.3: Valve drive (a), and actuator (b) of the FCT system [71].

The valve drive represents the heart of the mechanism as it consists of three operating levers connected from one side to three eccentric cams, which are fitted together on a control shaft as described schematically in Figure 3.4. The other side of the levers are in contact with the cams through rollers and transfer the displacement from the cams to the pushrods.

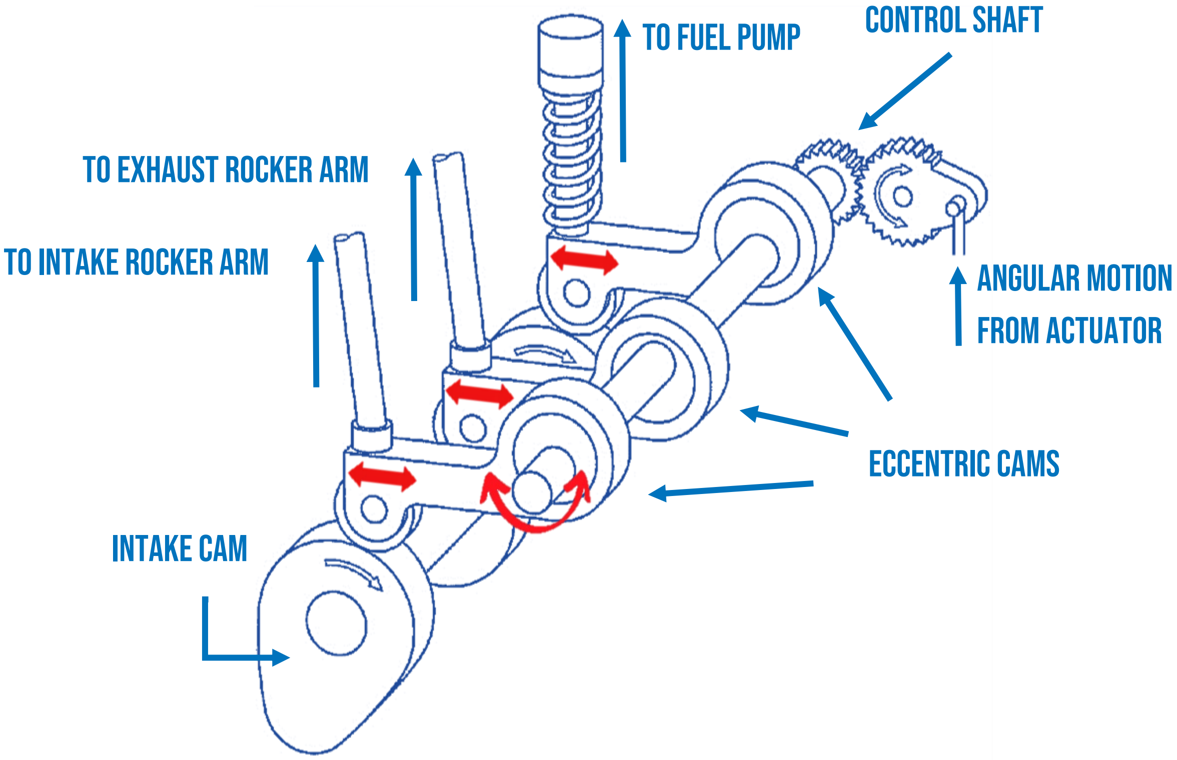
TO FUEL PUMP
CONTROL SHAFT
TO EXHAUST ROCKER ARM
TO INTAKE ROCKER ARM
ANGULAR MOTION
FROM ACTUATOR
ECCENTRIC CAMS
INTAKE CAM

Figure 3.4: Schematic diagram for the valve drive in FCT mechanism. Adapted from [72].

When the control shaft is rotated for some degrees, the levers are moved forward and backward which changes the tilt angle of the pushrods. Consequently, the opening and closing points of the valves are advanced or retarded depending on the rotation direction. As seen from the previous Figure, the angular position of the eccentric cams for the intake and exhaust valves is inversed. So, when one valve is advanced the other is retarded. The third cam which actuates the fuel pump is not used in the current research engine since the engine has its own common rail injection system.

In the basic design of the FCT mechanism, the control shaft was driven by the hydraulic actuator in Figure 3.3 (b) which allowed only two positions within a resolution of 180°. After that and during the current research project, the mechanism was developed by replacing the hydraulic actuator with an electric motor and encoder as shown in Figure 3.5. The motor unit consists of a three-phase electric motor combined with a worm gear to provide a slow output speed of 0.97 rpm. As a result, the control shaft has more resolution with precision control and can achieve multiple positions within the range.

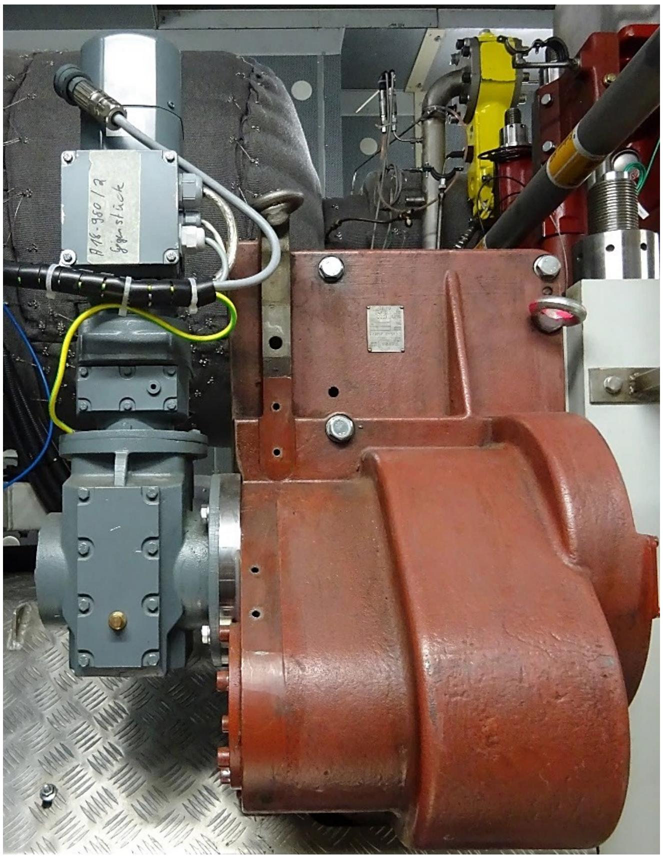

Figure 3.5: Electric motor for FCT control.

The main characteristics of the FCT mechanism including the two configurations are summarized in Table 3.2. In this study, the second configuration is considered to achieve different Miller cycle levels. Also, the angular position of the control shaft will be used as an indicator for the Miller cycle effect and will be mentioned as "FCT = angle°".

Table 3.2: Specifications of FCT mechanism

FCT characteristics	Old configuration	Current configuration
Control	**Hydraulic actuator**	**Electric motor & encoder**
Control shaft range	**0°:180°**	**0°:180°**
Control shaft angle resolution	**180°**	**1°**
Control shaft positions	**2 positions (0° or 180°)**	**Multi-positions (0°:180°)**
Max. effect on intake valve	**Advancing by 10 °CA**	**Advancing by 10 °CA**
Max. effect on exhaust valve	**Retarding by 10 °CA**	**Retarding by 10 °CA**
Valves movement resolution	**10 °CA**	**1 °CA**

Figure 3.6 shows the effect of the FCT mechanism on the valves' position considering only the minimum and maximum values of the FCT control shaft. On the left (a), the FCT = 0° which refers to the standard valves' position without any influence of the FCT mechanism (no Miller cycle effect). The opposite is on the right (b), as the FCT = 180° which indicates the maximum Miller cycle effect.

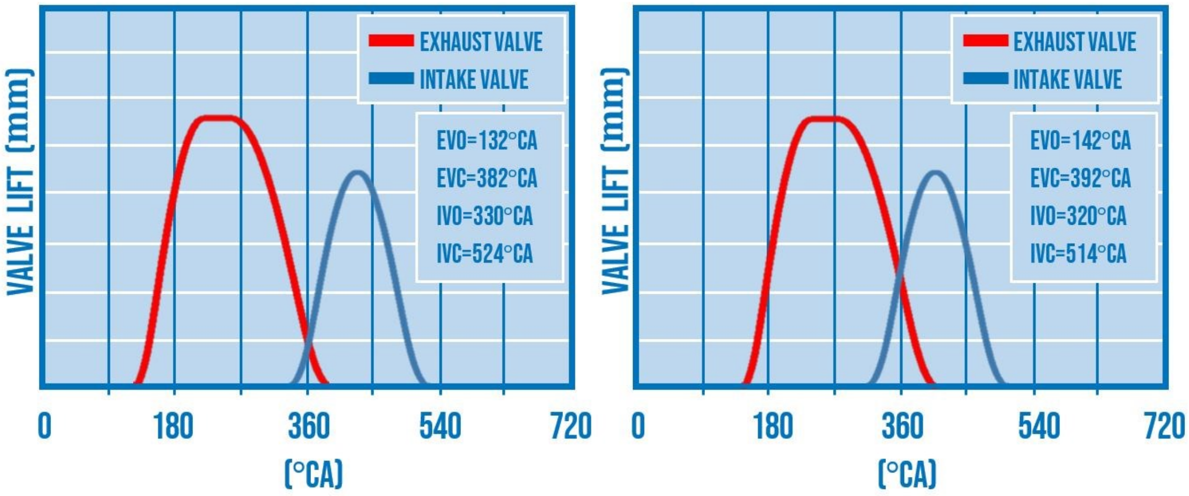

(a)
FCT=0°

(b)
FCT=180°

Figure 3.6: Effect of FCT control shaft on valves' position using the standard cams.

The influence of the FCT control shaft within the full range (0°:180°) on the valve timing is indicated in the following Figure. The FCT mechanism deals only with the opening and closing positions of the valves as it has the same shifting effect (10° CA) for any cam profile depending on the cam design.

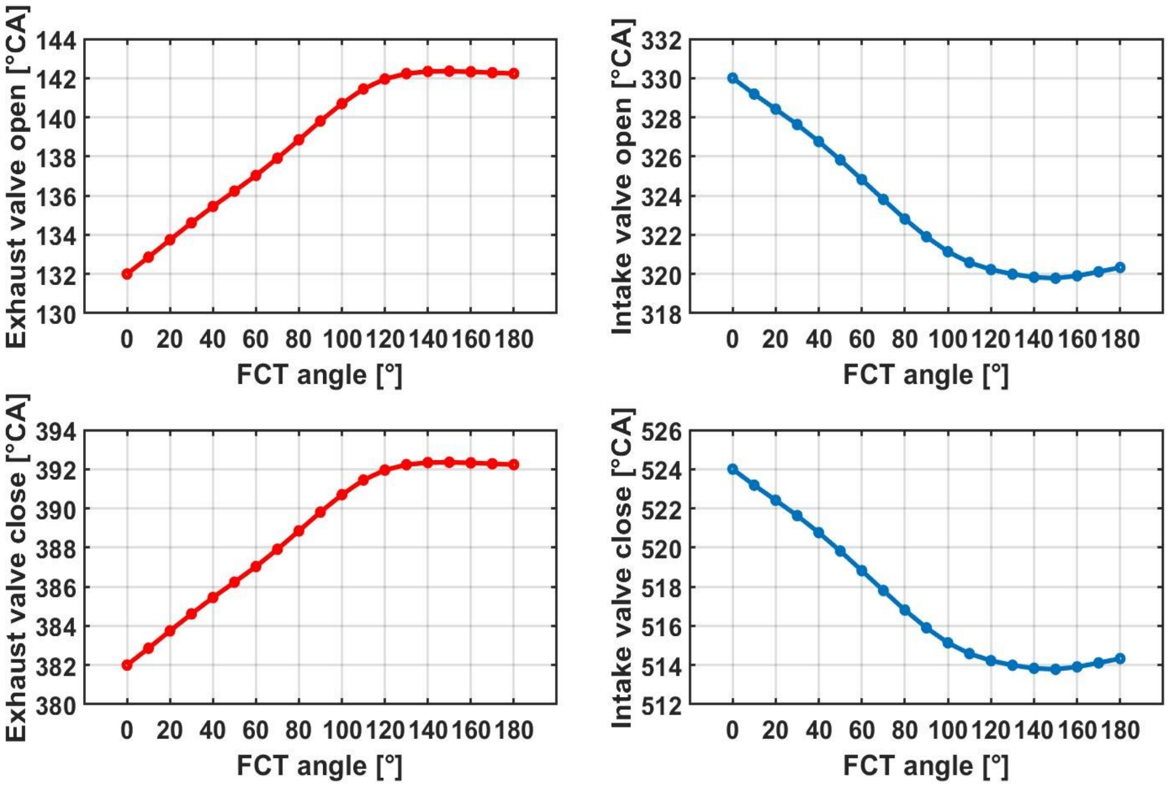

Figure 3.7: Valve timing with the full range of FCT using the standard cams.

3.2.2 Multi-segment Camshaft

The mutli-segment camshaft consists of three cam segments connected together on the same shaft.

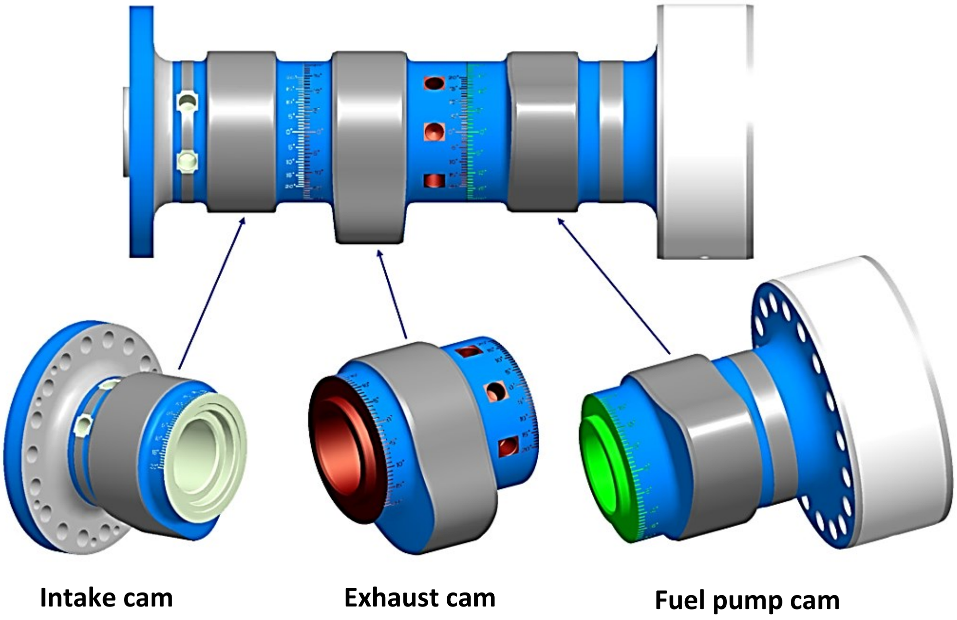

Figure 3.8: Multi-segment Camshaft [73].

The angular position of every cam can be adopted independently of the other, which allows to tune the valve timing as desired.

Also, it enables to investigate different cam profiles without changing the entire camshaft. As shown in the previous Figure, every segment has a scale to adjust the required phase angle whether advancing or retarding. Unlike the FCT, it is not possible to modify the cams' position during the engine operation as it requires some assembly and disassembly procedures, so it has to be adjusted before the engine starts. By combining the two sub-mechanisms together (FCT and Multi-segment Camshaft), different valve timing and cam profiles can be investigated. The experimental tests' procedures depend on selecting the required cam phase angle through the Multi-segment Camshaft before starting the engine, and then the FCT is used during the engine operation to control the two valves together. In this study, the cam phase angle using the Multi-segment Camshaft will be mentioned as "Cam phase angle = value °CA", where the positive value refers to cam retarding, the negative value means cam advancing, and the zero value means the neutral cam position without advancing or regarding.

3.3 Summary

A single-cylinder dual-fuel marine engine was constructed and assembled at the Department of Piston Machines and Internal Combustion Engines, Faculty of Mechanical Engineering and Marine Technology, Rostock University. The engine is coupled to a 4-quadrant dynamometer to simulate the load effect. The natural gas is mixed with the induced air through a PWM valve located on the intake runner. Then, the mixture is ignited using a pilot diesel injection from common rail injection system. The ignition parameters such as injection timing, rail pressure, and injection quantity are tunable which provide flexible tests as required. In order to attain flexible valve timing, the engine is equipped with flexible valve train strategy which includes two sub-mechanisms. The first one is the Flexible Camshaft Technology (FCT) which controls both the intake and exhaust valves together. To assure precision valve timing, the FCT mechanism was upgraded with an electric motor and encoder, instead of the hydraulic control in its first configuration. The second sub-mechanism is the Multi-segment Camshaft, which allows separable cam tuning. By combing the two sub-mechanisms together, a wide range of valve timing are obtained.

4 Model Description and Formulation

Since this study employs the modelling and simulation approach, this chapter introduces a comprehensive description for the whole model including all the components. Firstly, the flexible valve train model with the different cam profiles is presented. Also, a detailed flowchart indicating the processes' sequence is involved. Then, the resulted test points where the simulation was performed are discussed and previewed. After that, the engine model which predicts the combustion characteristics is demonstrated including all the sub-models. And finally, the simulation setup with the operating conditions are introduced.

4.1 Model Structure

As shown in Figure 4.1, the simulation framework includes the flexible valve train model, which was developed using MATLAB to simulate all the possible valve timing with the different cam profiles.

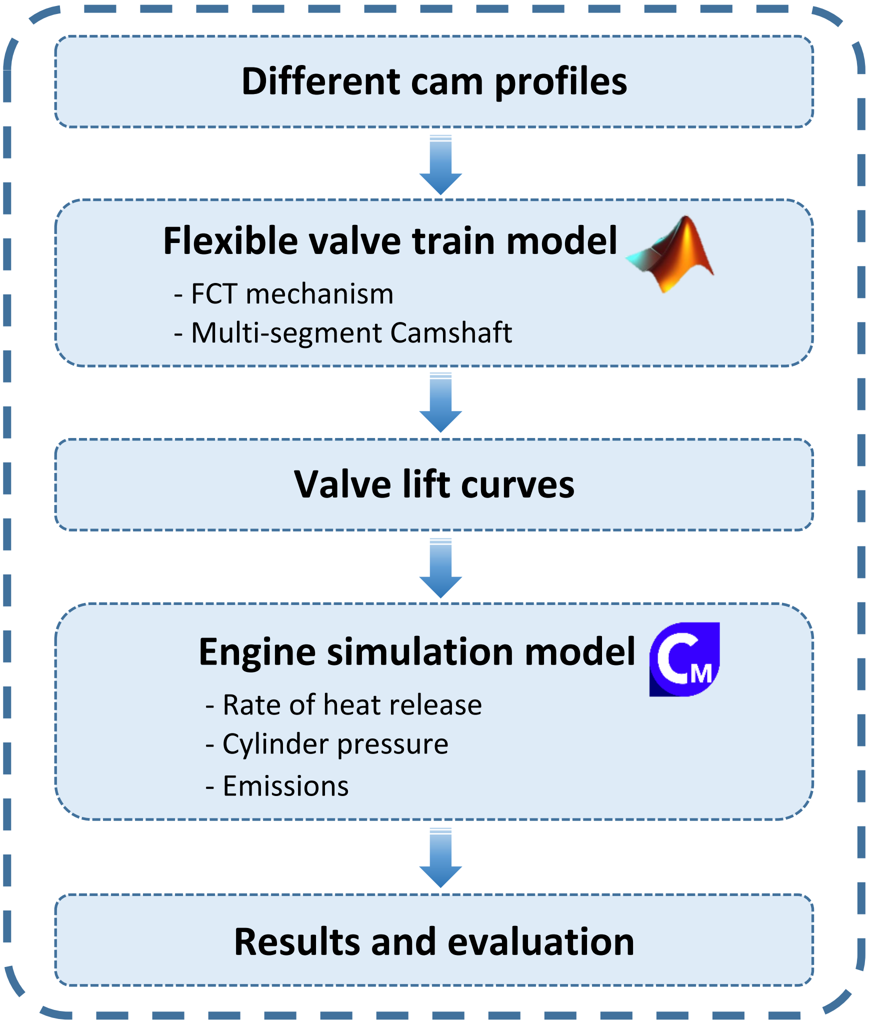
Different cam profiles
Flexible valve train model
- FCT mechanism
- Multi-segment Camshaft
Valve lift curves
Engine simulation model
- Rate of heat release
- Cylinder pressure
- Emissions
Results and evaluation

Figure 4.1: Full model structure using MATLAB and AVL CRUISE-M.

The resulting valve lift curves were exported to the engine model, which was established through AVL CRUISE-M platform. The engine model depends on the phenomenological approach and calculates many characteristics in terms of engine performance and emissions. Finally, the influence of the valve timing and the cam profiles were evaluated.

4.2 Flexible Valve Train Model

The valve train model predicts the behavior of the flexible valve train strategy by calculating the mechanism geometry. The model considers the effect of the two sub-mechanisms (FCT and cam phasing by Multi-segment Camshaft) beside to the possibility of using different cam profiles. Finally, the model generates the valve lift curves according to the input conditions and tests them against piston collision as shown in the following Figure.

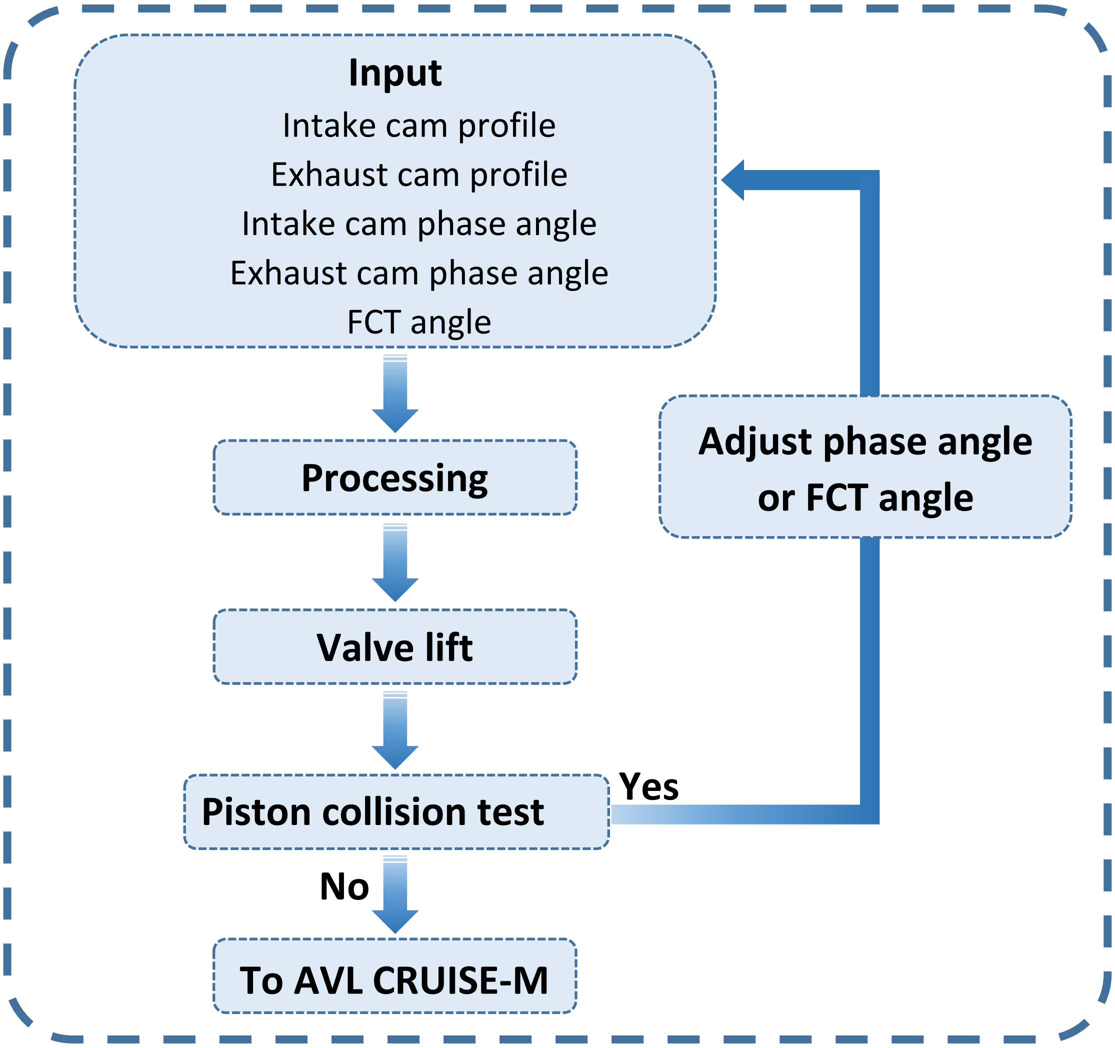
Input
Intake cam profile
Exhaust cam profile
Intake cam phase angle
Exhaust cam phase angle
FCT angle
Processing
Adjust phase angle or FCT angle
Valve lift
Piston collision test
Yes
No
To AVL CRUISE-M

Figure 4.2: Flowchart of flexible valve train model in MATLAB.

In this study, seven cam profiles were tested as illustrated in Figure 4.3. Two of them are the standard intake and exhaust cams (abbreviated as "Std."), which are specified for this engine.

The other five cams are for the research purpose and are divided as two intake cams and three exhaust cams.

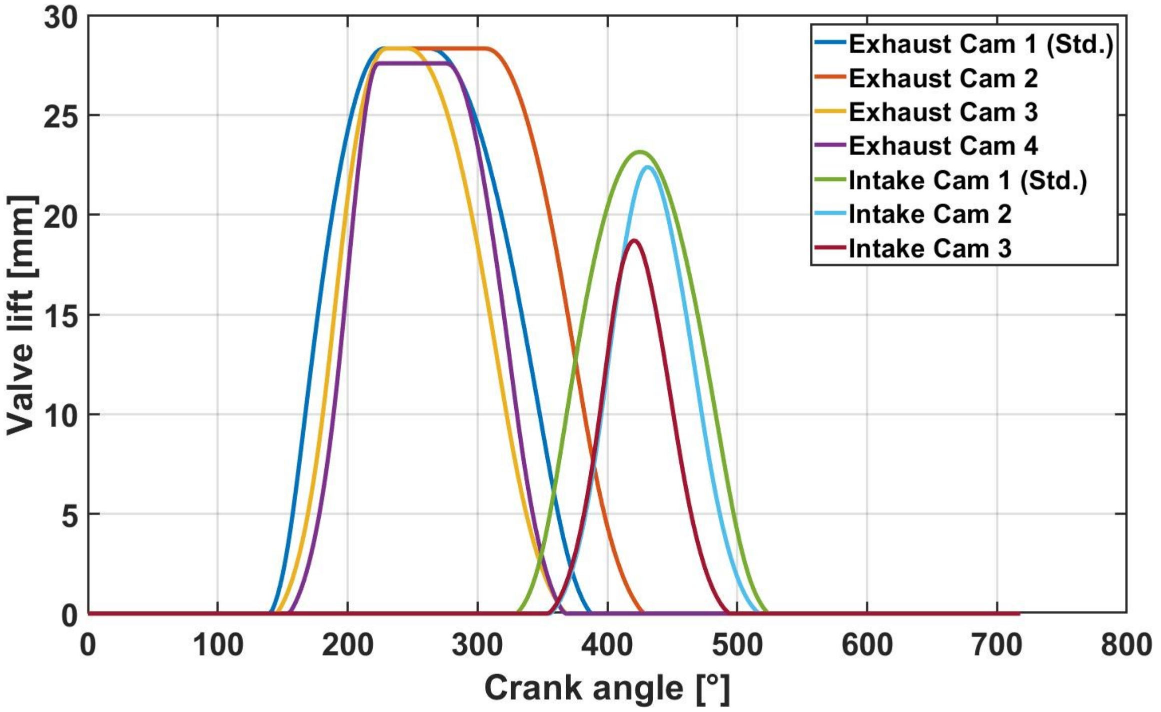

Figure 4.3: Cam profiles for flexible valve train model.

Combining those seven cams together, twelve cam pairs are available as shown in Figure 4.4, where cam pair (1) represents the standard cams for the engine.

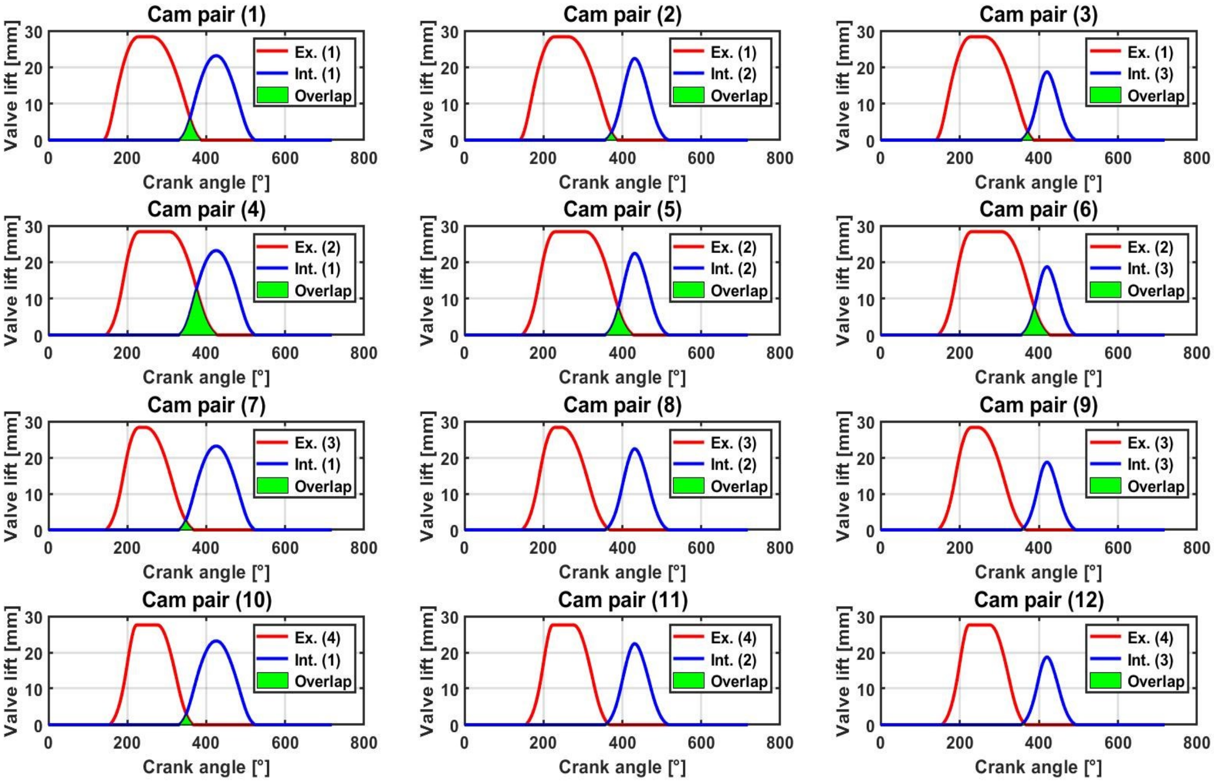

Figure 4.4: Twelve cam pairs under investigation.

The extreme tuning of valve timing using the FCT and the cam phasing possibility may cause collision between the valves and the piston in some positions depending on the cam profile. So, every cam pair from the previous Figure was firstly checked against piston collision at various valve timing positions. The safe distance before the collision was set to 7 mm vertically between the piston and the valves according to the manufacturer's recommendations. Any valve timing position exceeds the safe distance was considered as positive collision possibility and was avoided. Cam pairs (1, 2, 3, 7, 8, 9, 10, 11, 12) did not exceed the safe distance at any valve timing position. Hence, every pair of them was tested on wide range at 250 valve timing positions including 5 intake cam phase angles, 5 exhaust cam phase angles, and 10 FCT positions. Only cam pairs (4, 5, 6) have exceeded the safe distance in some valve timing positions as the exhaust cam Ex.(2) represents the widest cam profile in comparison with the other pairs. Figure 4.5 shows an example for the collision check with cam pair (4) when the exhaust cam was retarded by 10 °CA. It can be seen that the vertical distance between the piston and the exhaust valve is less than 7 mm.

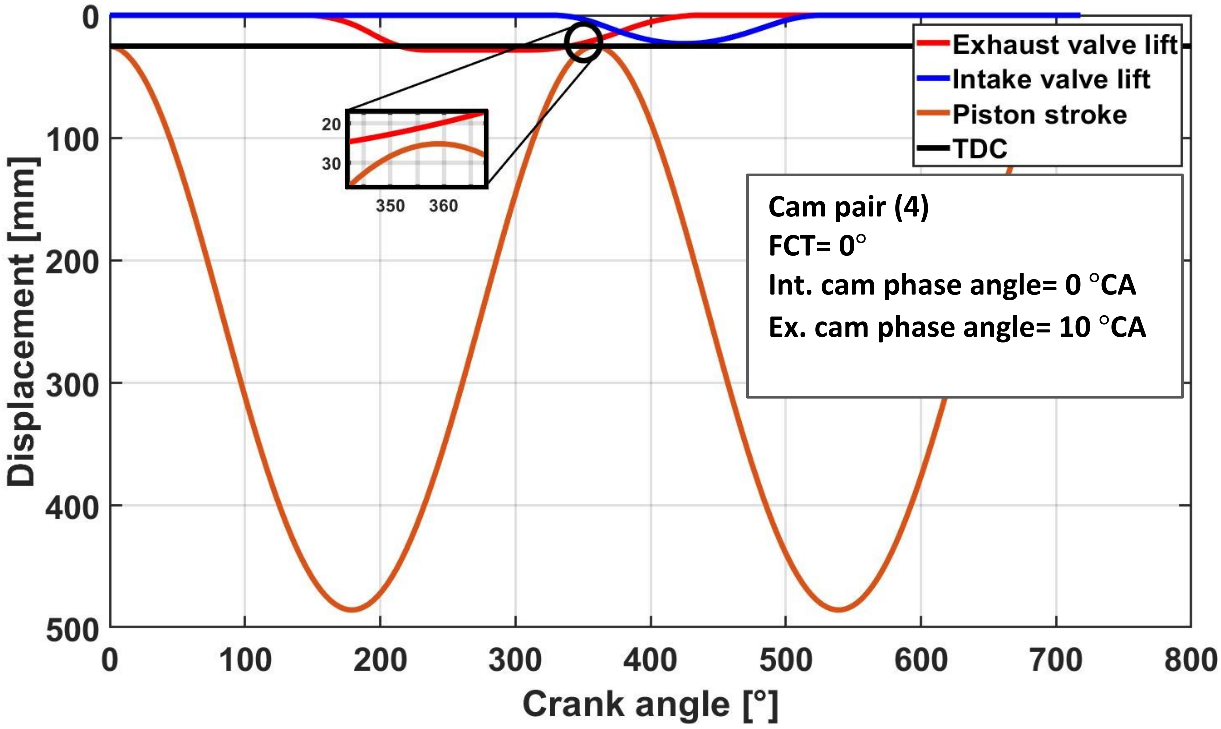

Figure 4.5: Collision check between piston and valves.

After excluding the unsafe positions, cam pairs (4, 5, 6) were tested at only 100 valve timing positions including 5 intake cam phase angles, 2 exhaust cam phase angles, and 10 FCT positions. All the valid valve timing positions which were exported to the engine model in AVL CRUISE-M are shown in Table 4.1.

Table 4.1: Safe valve timing positions

Cam pair	Intake cam phase angle [°CA]		Exhaust cam phase angle [°CA]		FCT [°]		Total positions
	Range	Step	Range	Step	Range	Step	
1	-20: 20	10	-20: 20	10	0: 180	20	250
2	-20: 20	10	-20: 20	10	0: 180	20	250
3	-20: 20	10	-20: 20	10	0: 180	20	250
4	-20: 20	10	-20: -10	10	0: 180	20	100
5	-20: 20	10	-20: -10	10	0: 180	20	100
6	-20: 20	10	-20: -10	10	0: 180	20	100
7	-20: 20	10	-20: 20	10	0: 180	20	250
8	-20: 20	10	-20: 20	10	0: 180	20	250
9	-20: 20	10	-20: 20	10	0: 180	20	250
10	-20: 20	10	-20: 20	10	0: 180	20	250
11	-20: 20	10	-20: 20	10	0: 180	20	250
12	-20: 20	10	-20: 20	10	0: 180	20	250

The engine model investigates the engine performance and emissions with all the valve timings for every cam pair in Table 4.1 depending on combinations between the three parameters (intake cam phase angle, exhaust cam phase angle, and FCT angle). The combinations pattern was formed for every cam pair by testing the first intake cam phase angle with all exhaust cam phase angles and FCT positions. Then, the process is repeated with the second and third intake cam phase angle until the last one. Figures 4.6 and 4.7 show the test points, in which the engine performance and emissions were evaluated with cam pair (1, 2, 3, 7, 8, 9, 10, 11, 12) and cam pair (4, 5, 6) respectively. The red point in the base of Figure 4.6 represents the neutral position where the three parameters equal zero. In Figure 4.7 there is no neutral point as the exhaust cam had to be advanced to avoid piston collision.

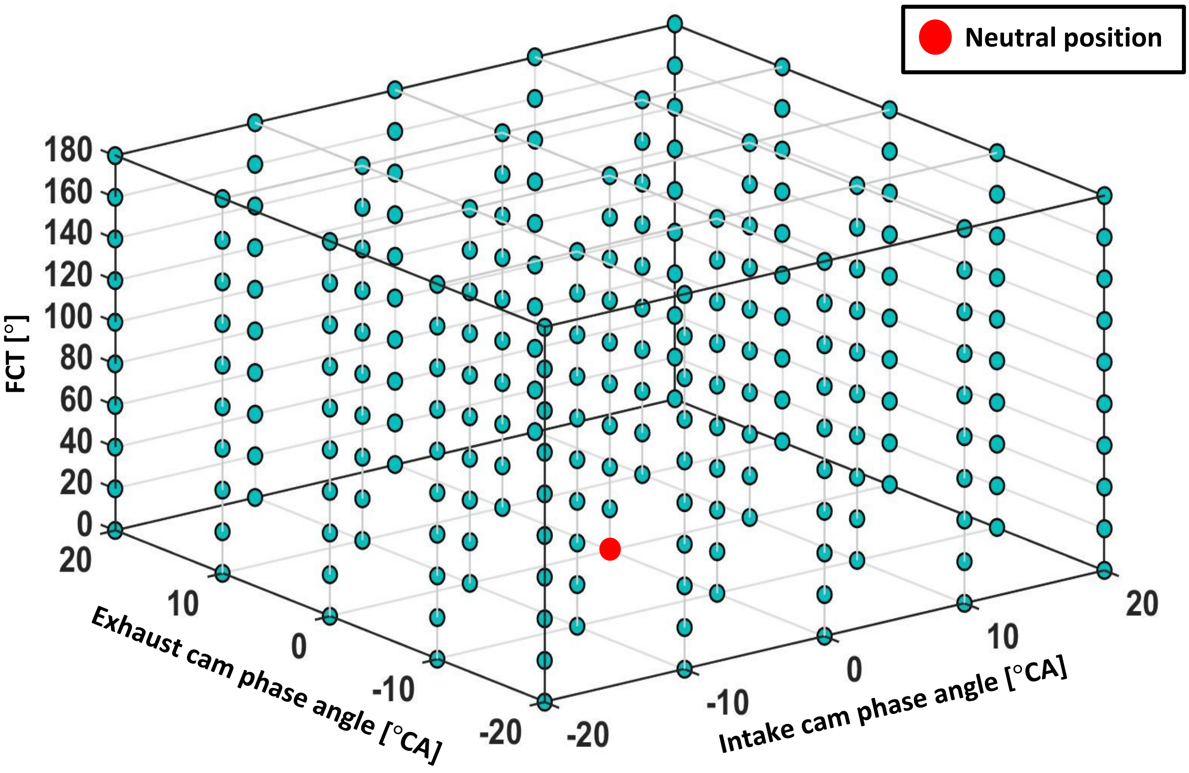

Figure 4.6: Test matrix for cam pair (1, 2, 3, 7, 8, 9, 10, 11, 12).

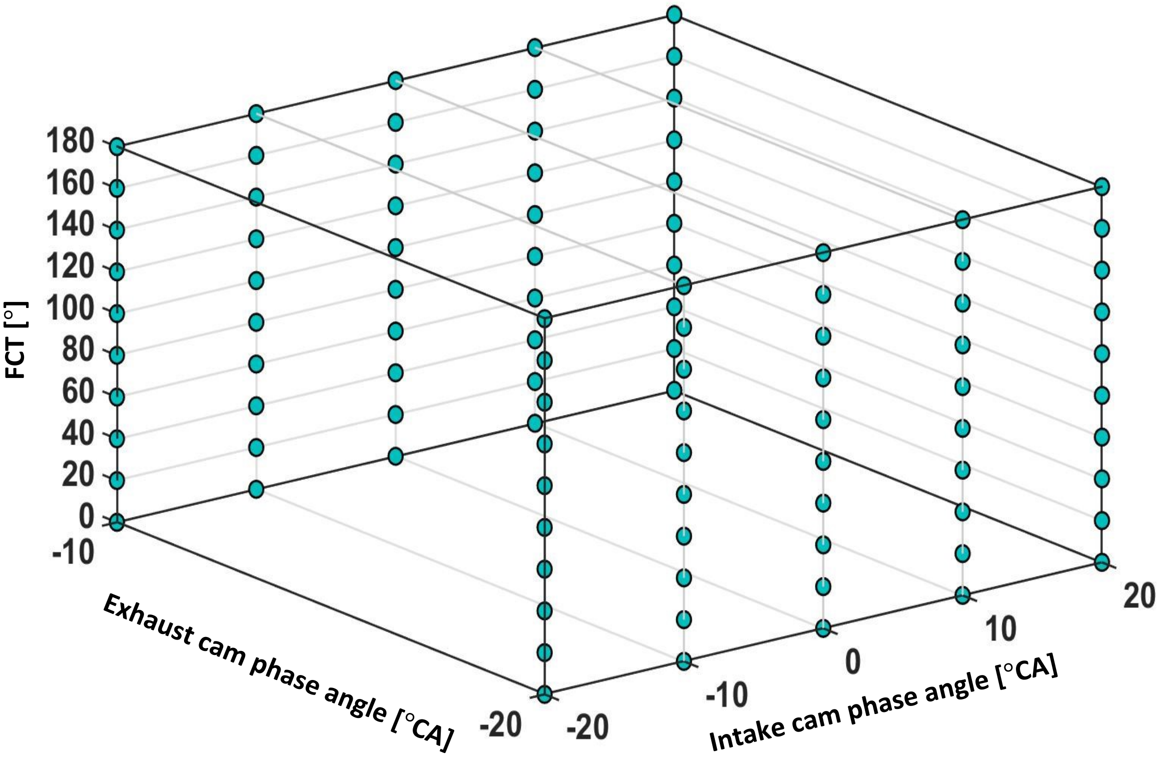

Figure 4.7: Test matrix for cam pair (4, 5, 6).

4.3 Engine Simulation Model

The engine model plays a major role in this study as it was used to evaluate the engine performance and emissions with the flexible valve train strategy. The model was established using the real time simulation platform AVL CRUISE-M, which supports the model-based development for engines and powertrains. The structure of the model depends on connecting predefined blocks, which are provided in the software toolbox. Most of them are used to configure all the relevant engine components (intake manifold, runners, valves, combustion chamber, etc.) and the other blocks aim to control and monitor the simulation process. Each block contains different parameters and boundary conditions to define it in terms of the geometric properties and the thermodynamic state. Similar to the engine test bench, one cylinder is considered in this model with the entire thermodynamic cycle (four strokes). The model was developed depending on the phenomenological approach, in which many sub-models were implemented to simulate the thermodynamic processes in the cylinder such as the combustion and the emissions' formation. Figure 4.8 shows the full model including all the blocks and connections.

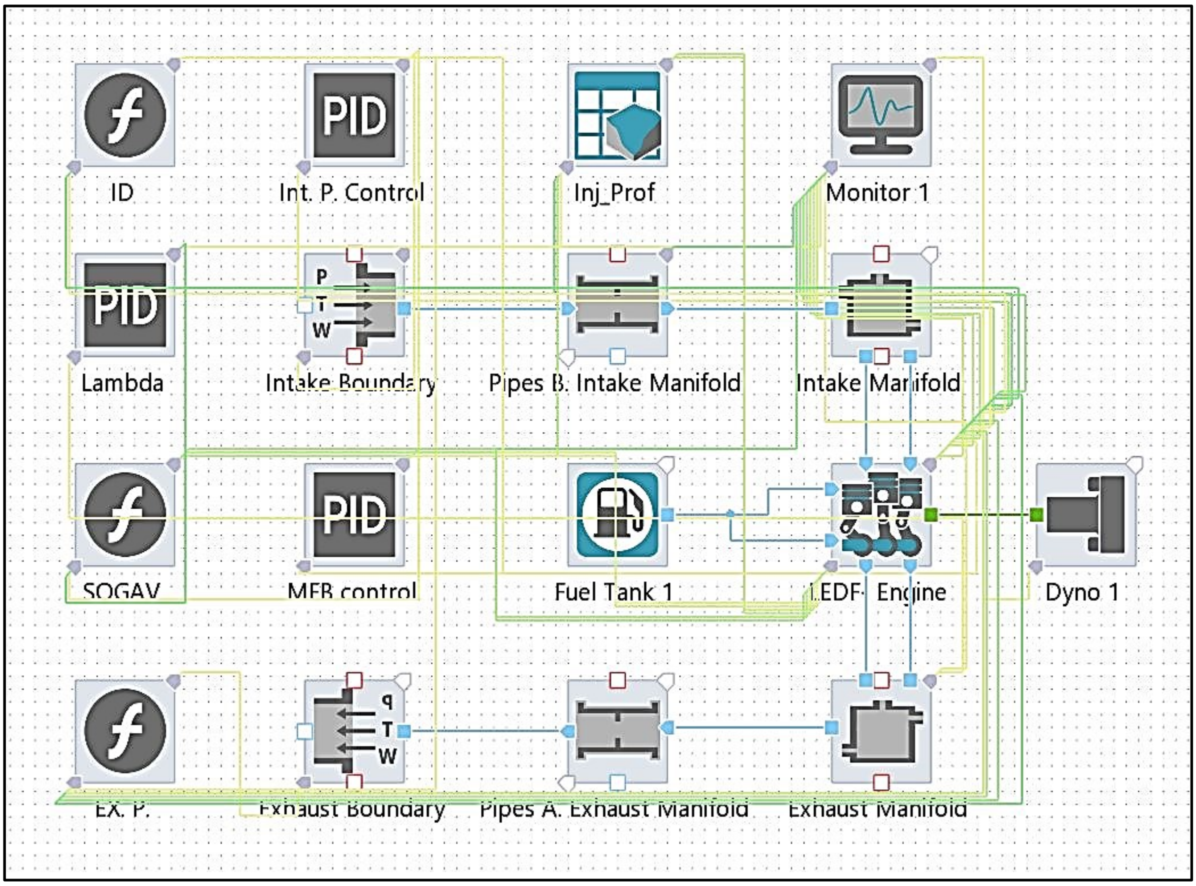
ID
Int. P. Control
Inj_Prof
Monitor 1
Lambda
Intake Boundary
Pipes B. Intake Manifold
Intake Manifold
SOGAV
MFB control
Fuel Tank 1
LEDF- Engine
Dyno 1
EX. P.
Exhaust Boundary
Pipes A. Exhaust Manifold
Exhaust Manifold
PID
P
T
W
q

Figure 4.8: Engine model in AVL CRUISE-M.

4.3.1 Combustion Model

The dual-fuel engine in this study depends on the diesel pilot injection to ignite a mixture of air and natural gas as the latter is the main fuel. The relative amount of the natural gas represents 95% from the total energy supplied during the combustion, while the diesel fuel participates with only around 5% to initiate the ignition. From this perspective, all the combustion process in this model is considered a premixed combustion and the diesel fuel was took into account in the fuel composition. To simulate the combustion process, a quasi-dimensional two-zone combustion model depending on the fractal combustion principle was implemented as shown in Figure 4.9.

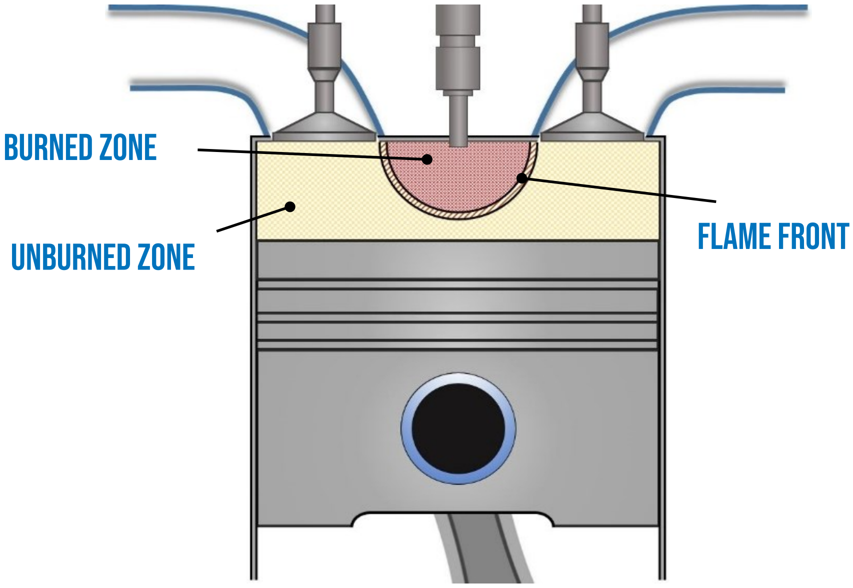

Figure 4.9: Two-zone combustion model.

Fractal combustion principle is a predictive combustion modelling approach, which predicts the mixture burning rate depending on the turbulent flame propagation considering the effect of the combustion chamber shape, the cylinder composition, and the turbulent level. In this principle, the flame front is treated as a very thin spherical layer separating between burned and unburned zone. Then during the flame propagation, the laminar flame surface (A_L) is highly wrinkled due to turbulent eddies of different length scales. As a result, the burning rate is enhanced, and the overall area of the flame front is increased leading to a turbulent flame surface (A_T) as shown in Figure 4.10. The increase in the flame surface (A_T/A_L) represents the wrinkling factor and is primary responsible for the increase in the turbulent flame speed (S_T) with respect to the laminar one (S_L) [74, 75]. This principle is successfully approved to predict the combustion rate in many academic literature [76, 77, 78].

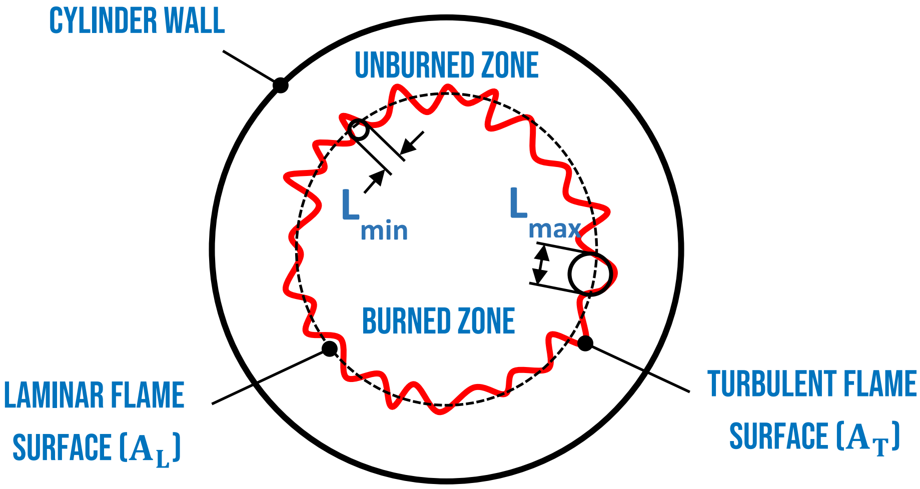
CYLINDER WALL
UNBURNED ZONE
L_{min}
L_{max}
BURNED ZONE
LAMINAR FLAME SURFACE (A_L)
TURBULENT FLAME SURFACE (A_T)

Figure 4.10: Schematic of the flame surfaces in the fractal model.

According to Damköhler [79], the mass burning rate can be expressed as:

$$\frac{dm_b}{dt} = \rho_u \, A_T \, S_L = \rho_u \left(\frac{A_T}{A_L}\right) A_L \, S_L \tag{4.1}$$

Where:

$$\left(\frac{S_T}{S_L}\right) = \left(\frac{A_T}{A_L}\right) \tag{4.2}$$

m_b is the mass of burned charge, ρ_u is the density of unburned charge, and t represents the time.

The wrinkling factor (A_T/A_L) can be represented by the maximum and minimum flame wrinkling scale (L_{max}) and (L_{min}) respectively. To characterize the wrinkled factor, the fractal principle is applied, which is a mathematical method to describe the irregular geometries with repeated similarity on all scales [74]. Under the above assumption:

$$\left(\frac{A_T}{A_L}\right) = \left(\frac{L_{max}}{L_{min}}\right)^{D_3-2} \tag{4.3}$$

Where (D_3) is the fractal dimension which characterizes the roughness of the flame wrinkling and basically depends on the turbulent intensity and the laminar flame speed. According to [63], its defined as the following:

$$D_3 = \frac{2.35u' + 2.05S_L}{u' + S_L} \tag{4.4}$$

Where u' is the turbulence intensity. Substituting Eq. (4.3) in Eq. (4.1) gives the mass burning rate as:

$$\frac{dm_b}{dt} = \rho_u \left(\frac{L_{max}}{L_{min}}\right)^{D_3-2} A_L S_L \tag{4.5}$$

The minimum flame wrinkling scale (L_{min}) is assumed to be equal to the Kolmogorov length scale (L_k), while (L_{max}) is equal to the integral length scale (L_I).

Based on the fractal principle mentioned above, the computation of (L_{min}), (L_{max}), and (D_3) depends on the turbulent flow inside the cylinder.

In this combustion model, the in-cylinder turbulence is characterized by the two-equation modified *K*-*k* model [80], which is a simplified form of the *K*-ε approach. The *K*-*k* model is widely used for turbulence predicting, for example in [78, 81] and is described as the following:

The kinetic energy of the mean flow K:

$$\frac{dK}{dt} = \frac{1}{2}\,\dot{m}_{in}\,u_{in}^2 + \left(\frac{\dot{\rho}_u}{\rho_u}\right)K - \left(\frac{K}{m}\right)\dot{m}_{ex} - P \tag{4.6}$$

The kinetic energy of the turbulent flow k:

$$\frac{dk}{dt} = P + \left(\frac{\dot{\rho}_u}{\rho_u}\right)k - \left(\frac{k}{m}\right)\dot{m}_{ex} - m\varepsilon \tag{4.7}$$

Where:

$$K = \frac{1}{2}m\,U_f^2 \tag{4.8}$$

$$k = \frac{3}{2}m\,u'^2 \tag{4.9}$$

$$\varepsilon = \frac{u'^3}{L_I} \tag{4.10}$$

$$P = c_P\,\frac{K}{L_I}u' \tag{4.11}$$

$$c_P = 0.3307\;c_t\,\sqrt{\frac{3}{2}} \tag{4.12}$$

$$L_I = c_l\,\frac{V_{cyl}}{A_{cyl}} \tag{4.13}$$

$$L_k = \frac{L_I}{Re^{\,3/4}} \tag{4.14}$$

$\dot{m}_{in}$ and $\dot{m}_{ex}$ are the mas flow rates into and out of the cylinder, u_{in} is the velocity of the charge entering the cylinder, $\dot{\rho}_u$ is the change rate of the unburned charge density, ρ_u is the unburned charge density, *m* is the mass of the charge, *P* is the turbulence production rate, ε is the rate of the kinetic energy dissipation for unit mass, U_f is the mean velocity of the charge, u' is the turbulence intensity, L_I is the integral length scale, L_k is the Kolmogorov length scale, and R_e represents Reynolds number. The two factors c_t and c_l represent the turbulent production constant and the turbulent length scale respectively, which are used together for the calibration purpose. The boundary conditions for the model are summarized in Table 4.2.

Table 4.2: The main boundary conditions for the combustion model

Component	Parameter	Value	Unit
Intake boundary	**Pressure**	**Controlled from PID**	**bar**
	Temperature	**40**	℃
Intake pipes	**Length**	**110**	**cm**
	Diameter	**26**	**cm**
Intake manifold	**Length**	**150**	**cm**
	Diameter	**84**	**cm**
Engine	**Speed**	**720**	**rpm**
	No of cylinders	**1**	**-**
	Bore	**34**	**cm**
	Stroke	**46**	**cm**
	Compression ratio	**12.75**	**-**
	Connecting rod length	**95**	**cm**
	Turbulent production const.	**1.9**	**-**
	Turbulent length scale	**1.16**	**-**
	Ignition timing	**Controlled from PID**	**°CA**
	Fuel rate	**Controlled from PID**	**g/s**
Cylinder head	**Number of intake valves**	**2**	**-**
	Number of exhaust valves	**2**	**-**
	Intake valve diameter	**10**	**cm**
	Exhaust valve diameter	**10**	**cm**
	Intake valve lift	**Variable**	**cm**
	Intake valve timing	**Variable**	**°CA**
	Exhaust valve lift	**Variable**	**cm**
	Exhaust valve timing	**Variable**	**°CA**
Fuel	**NG substitution ratio**	**95**	**%**
	Diesel substitution ratio	**5**	**%**
Exhaust manifold	**Length**	**130**	**cm**
	Diameter	**92**	**cm**
Exhaust pipes	**Length**	**105**	**cm**
	Diameter	**40**	**cm**
Exhaust boundary	**Pressure**	**Depends on Int. Press.**	**bar**
	Temperature	**490**	℃

4.3.2 Ignition Delay Model

Ignition delay in dual-fuel engines is a critical characteristic and has a relevant effect on the combustion process as it includes interaction between two fuels. The ignition delay was estimated according to the correlation from [82, 83], which was developed depending on chemical reaction kinetics with CHEMKIN mechanism.

This correlation considers the diesel substitution ratio and the air-fuel ratio of the NG mixture. Additionally, the in-cylinder temperature and pressure are taken into account also. The formula is presented as the following:

$$\tau_{ID} = C_1 \cdot \lambda^{-1}_{NG.\ mixture} \cdot P^{-1.19}_{Cyl.} \cdot W^{-0.65}_{Diesel} \cdot e^{\frac{C_2}{T_{Cyl.}}} \tag{4.15}$$

Where τ_{ID} is the ignition delay, λ is the AFR_{Actual} to $AFR_{Stoich.}$, $P_{Cyl.}$ is the cylinder pressure, W_{Diesel} is the mass fraction of diesel fuel, and $T_{Cyl.}$ is the cylinder temperature.

The correlation is not integrated in the software and was implemented in the engine model by a user defined function, which transfers the input and output signals to the other engine components through the data bus channels.

4.3.3 Heat Transfer Model

To assure accurate prediction for the combustion process in the cylinder, it was a mandatory to calculate the heating loss through the cylinder wall. So, the Newton heat transfer model was applied as the following:

$$Q_w = M_{HT} \cdot A_{trans.} \cdot \alpha \cdot (T_{gas} - T_w) \tag{4.16}$$

Where Q_w is the cylinder wall heat loss, M_{HT} is heat transfer multiplier, $A_{trans.}$ is the heat transfer surface area, α is the heat transfer coefficient, T_{gas} is the gas temperature, and T_w is the cylinder wall temperature. The heat transfer coefficient (α) was estimated using the modified “Woschni 90” heat transfer model [84], as it considers the effect of IMEP in comparison with the model of “Woschni 78”. The model formula is expressed as:

$$\alpha = 130\ D^{-0.2} \cdot P^{0.8}_{Cyl} \cdot T^{-0.53}_{Cyl} \cdot \left\{c_1 \cdot c_m \left[1 + 2\left(\frac{V^2_{TDC}}{V}\right)\right].\ IMEP^{-0.2}\right\}^{0.8} \tag{4.17}$$

$$c_1 = 2.28 + 0.308\left(\frac{c_u}{c_m}\right) \tag{4.18}$$

Where D is the cylinder bore, $P_{Cyl.}$ is the cylinder pressure, $T_{Cyl.}$ is the cylinder temperature, c_m is the mean piston speed, V_{TDC} is the cylinder volume where the piston is at TDC, V is the actual volume in the cylinder, and c_u is circumferential velocity.

4.3.4 NO$_x$ Formation Model

The NO$_x$ emissions represent one of the most important evaluation criteria in this study. So, the extended Zeldovich mechanism (EZM) was used for NO$_x$ prediction [85]. The model was widely used and based on the three reactions as the following:

$$O + N_2 \overset{K_1}{\longleftrightarrow} NO + N \tag{4.19}$$

$$N + O_2 \overset{K_2}{\longleftrightarrow} NO + O \tag{4.20}$$

$$N + OH \overset{K_3}{\longleftrightarrow} NO + H \tag{4.21}$$

where K_1, K_2, K_3 are the reaction rates. Equation (4.19) and (4.20) were firstly supposed by Zeldovich, while Equation (4.21) was presented by Lavoie et al. [86].

4.3.5 Methane Slip Formation Model

Methane slip represents a challenge in the dual-fuel engines because of the gaseous nature of the utilized fuel. Further, the lean mixture operation boosts the methane slip formation as more fuel is subjected to misfire. Many studies in the literature [87, 88, 89] confirmed that the major sources of the methane slip are:

- The crevice volumes between the piston and the liner, where the unburned mixture is pushed. As shown in Figure 4.11, the flame cannot propagate in those crevices and the unburned mixture is released back again during the exhaust stroke and leaves the cylinder through the exhaust valve.
- The partial burning when the combustion quality is poor or the misfiring.
- The valve overlap period, when the boost pressure enforces the fresh charge to escape through the exhaust valve to the exhaust system.

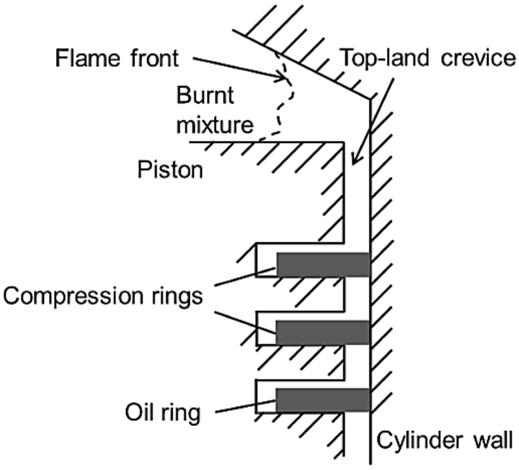

Figure 4.11: Crevice volumes in combustion chamber. Adapted from [90].

In this study the three previous sources were considered, and the sum of them will be mentioned as “Total methane slip”. The unburned methane due to the lubricating oil absorption was neglected, as the methane solubility in oil is very low in comparison with the liquid fuels [91].

The methane slip from the crevice volumes according to Lavoie[92] , was calculated as the following:

$$m_{crevice} = \frac{P_{cyl.} \cdot V_{crevice} \cdot M}{R \cdot T_{Piston}} \tag{4.22}$$

Where $m_{crevice}$ is the mass of unburned charge in the crevices, $P_{Cyl.}$ is the cylinder pressure, $V_{Crevice}$ is the total crevice volumes, M is the molecular weight of unburned charge, R is the gas constant, and T_{Piston} is the piston temperature. The model assumes that the pressure in the cylinder and inside the crevice volumes is the same. Also, the piston temperature represents the temperature in both of them.

In dual-fuel engines, partial burning can occur because of high charge dilution or too lean mixture. So, it was described with a semi-empirical correlation which was proposed by Lavoie [93] as the following:

$$F_P = C_{P1} \cdot exp\left\{-\frac{\theta_{EVO}-\theta_{90}}{[C_{P2}(\theta_{90}-\theta_0)]}\right\} \tag{4.23}$$

Where F_P is the fraction of unburned charge due to partial burning, C_{P1} is a tunable constant, θ_{EVO} is the crank angle at exhaust valve opening, θ_{90} is the crank angle at which 90% of the fuel is burned, C_{P2} is a constant depends on the equivalence ratio, and θ_0 is the crank angle at which 0% of the fuel is burned.

Regarding the methane slip from the valve overlap, it was calculated automatically during the simulation as all the chemical species are transported through the model elements during the engine cycle. For the three mentioned sources, it was assumed that no post-oxidation takes place for the unburned mixture.

4.4 Simulation Setup

Simulation was performed in AVL CRUISE-M using the filling and emptying method, in which the principles of mass and energy conversion are applied for every volume at each time step. In that way it covers the pulsation effects in the gas path. All the cam pairs in Figure 4.4 were investigated according to the test points in Figures 4.6 and 4.7 at three engine loads (50%, 75%, 100%). For every load, the engine power, lambda, and center of combustion (COC) were controlled through three PID controllers to be constant during the entire simulation process as shown in Table 4.2. The first PID controller adjusts the intake air pressure to reach the desired power and keep it constant according to the selected load.

Table 4.2: Constant parameters during simulation

Engine Load [%]	λ [−]	COC [°ATDC]	Power [kW]
50	2	5.5	210
75	2	7	320
100	2	8	436

To calculate the exhaust pressure, a turbocharger correlation is integrated by a user defined function. Hence, exhaust pressure can be calculated automatically during the simulation depending on the intake pressure. In order to keep constant lambda through the different valve timing positions, the second PID controller is used to modify the fuel rate through the SOGAV valve considering the PWM method. The correlation of the valve flowrate was provided from [68] and was implemented also in the model with the help of a user defined function. In this aspect, it worth to mention that the fuel rate is totally controlled keeping the substitution ratios constant (95% NG, 5% Diesel). The third PID controller adopts the ignition timing to hold the COC constant. The previous procedures were followed with the same manner in the experimental tests. Additionally, the conditions in Table 4.2 were applied with the all test points for every cam pair in Figure 4.4 aiming to keep equitable comparison between the different valve positions.

4.5 Summary

In this chapter, a simulation model was developed aiming to investigate the effect of the flexible valve train on the dual-fuel engine performance and emissions. The model includes two parts, the first one was established in MATLAB to predict the valve timing. Different cam profiles are included with a wide range of valve timing combinations from FCT mechanism and Multi-segment Camshaft. Then, the resulting valve lift curves were examined against piston collision and exported to the sconed part, which is a phenomenological combustion model in the AVL Cruise-M platform. The combustion model consists of different blocks representing the engine components and aims to predict the combustion characteristics using the fractal combustion principle. Additionally, it includes many sub-models to calculate the emissions formation (NO_x and UHC) and the ignition delay period. The simulation process was controlled by three PID controllers to keep constant engine power, lambda, and center of combustion (COC). Three engine loads were considered during the simulation (50%, 75%, 100%), as they represent the most common loads for marine engines.

5 Model Validation and Results Analysis

In order to use the entire model for further investigations, this section includes the model validation against experimental data. The results of the valve train model are compared with the measured valves' profiles from the test bed. In terms of the combustion model, cylinder pressure and rate of heat release are considered. Also, the results of exhaust emissions and ignition delay are compared. After that, the effect of the FCT mechanism on the engine performance and emissions are discussed and previewed. The influence of the intake and exhaust cam phasing are included also. And finally, the effect of the valve overlap positions is introduced.

5.1 Model Validation

5.1.1 Flexible Valve Train Model

For the valve train model, experimental results were obtained from the engine test bench using cam pair (1) in Figure 4.4 as it represents the standard cams and will be mentioned again as the reference case. The aim of this model is to predict the valve lift curves with the different valve timings. Figure 5.1 shows the model validation at four FCT angles representing different levels of Miller effect.

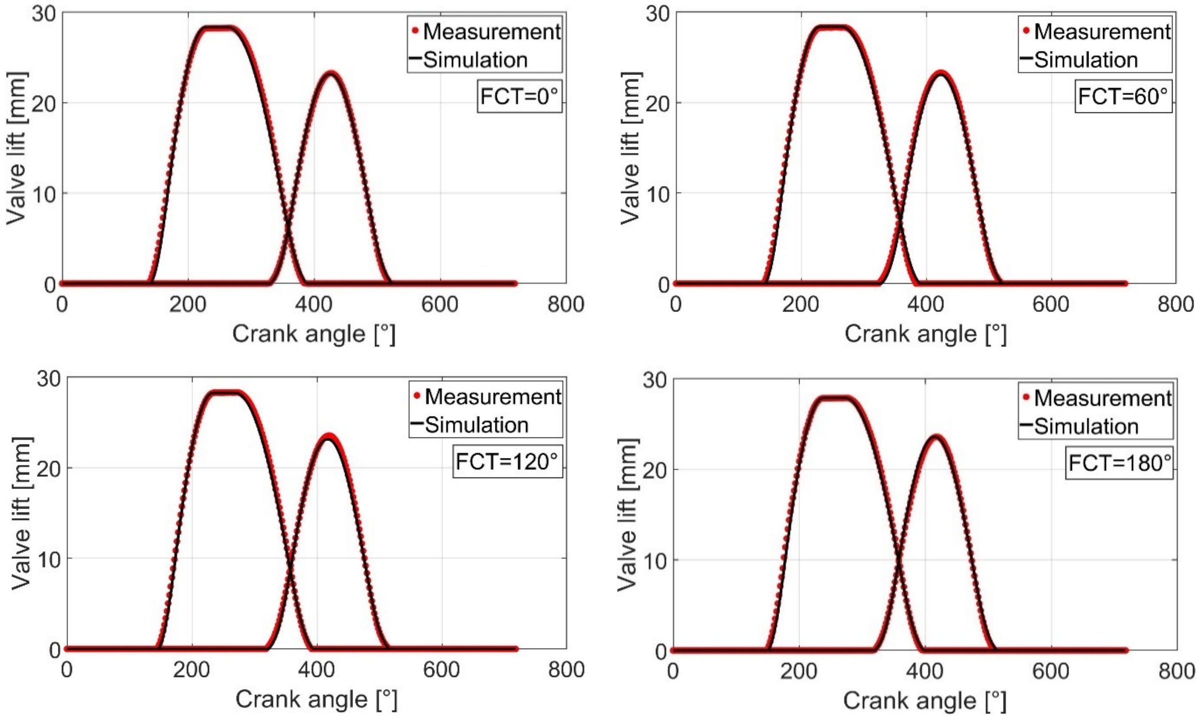

Figure 5.1: Validation of flexible valve train model.

5.1.2 Combustion Model

Combustion model was validated in terms of cylinder pressure and rate of heat release (ROHR) as shown in Figure 5.2 and 5.3 respectively. Two loads with four different FCT angles were considered while all the other conditions were kept the same.

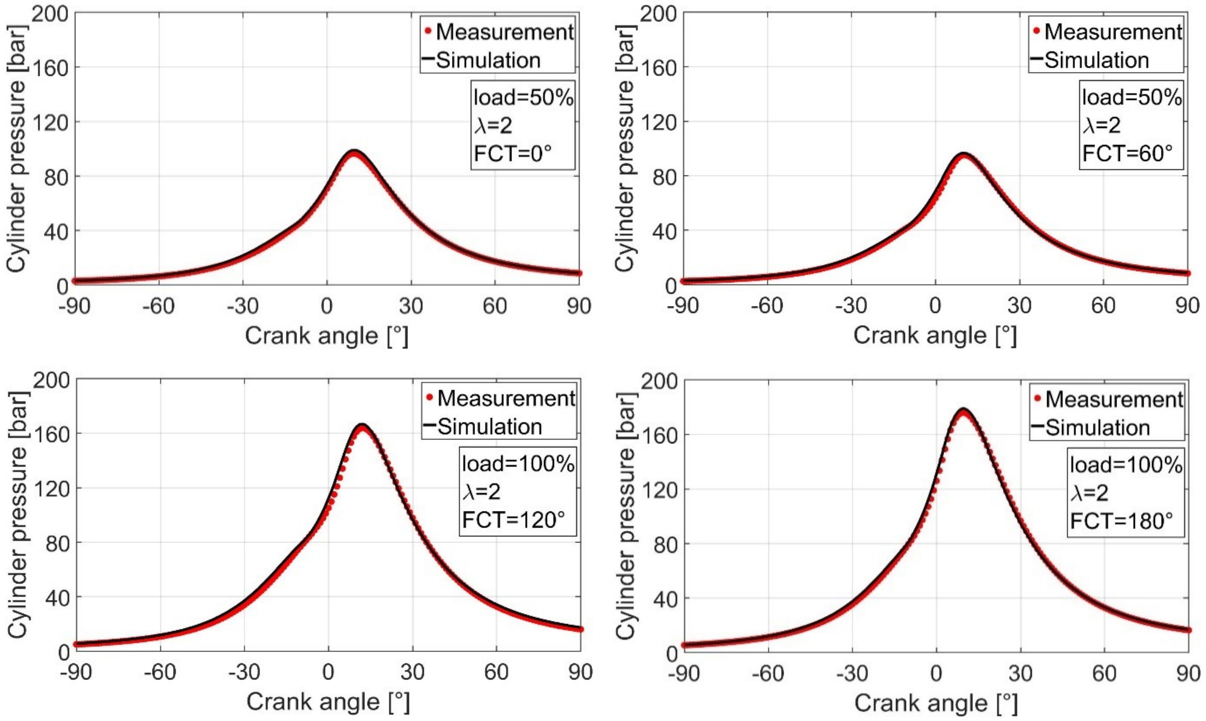

Figure 5.2: Validation of cylinder pressure.

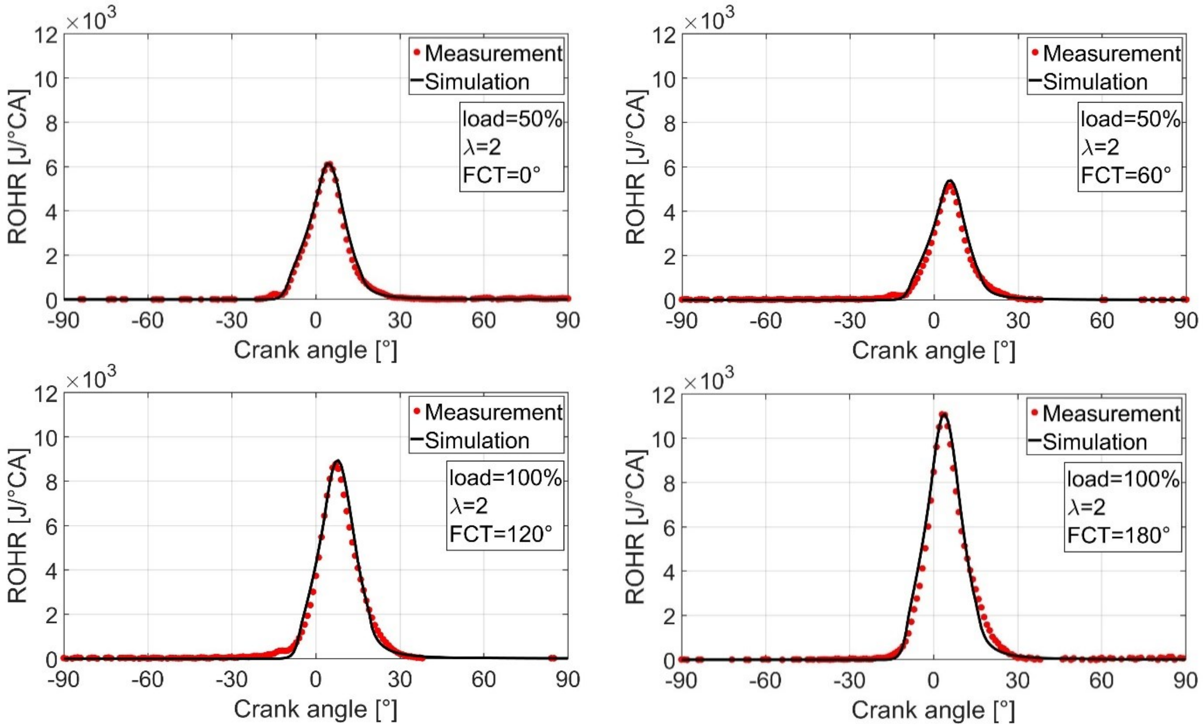

Figure 5.3: Validation of rate of heat release.

In the previous Figure, the experimental results were acquired from the test bed using cam pair (1) in Figure 4.4. The crank angle range of -90° : 90° was selected to focus on the combustion phase. From the curves, it can be concluded that the model can effectively predict the combustion parameters.

5.1.3 Emissions and Ignition Delay Models

Emissions were validated concerning the brake specific nitrogen oxides (BSNO$_x$) and the brake specific total methane slip, as the latter includes the sum of the three methane slip sources. Also, the resulted ignition delay from the simulation model was compared with the experimental one as it represents the different between the start of injection and start of combustion. The standard cam pair is considered also for this purpose and the full range of the FCT with step 10° was applied.

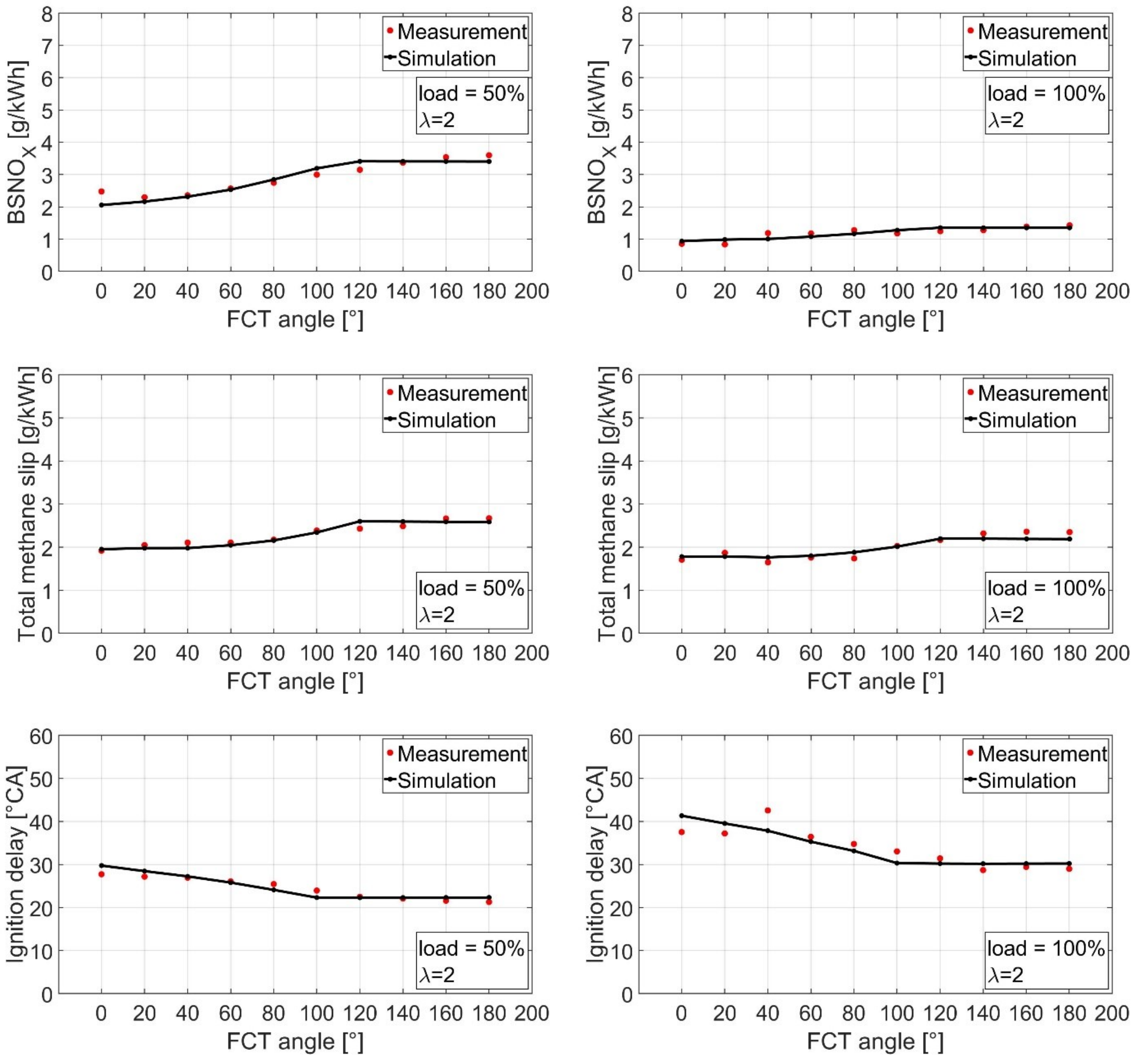

Figure 5.4: Validation of emissions and ignition delay.

5.2 Results Analysis and Discussion

After validating the simulation results with the experimental data, the model was employed to evaluate the effect of the flexible valve train strategy on the engine performance and emissions. All the cam pairs in Figure 4.4 were considered in the simulation process but only the results of cam pairs (1, 2, 7, 8) will be shown in this study, as they cover a moderate cam profiles range in comparison with the standard one. The results will show the influence of the two sub-mechanisms (FCT and Multi-segment Camshaft) using different parameters like IVO, EVC and valve overlap.

5.2.1 Effect of FCT on Engine Performance and Emissions

Figures 5.5 to 5.8 show the influence of the FCT angle on the engine characteristics using cam pairs (1, 2, 7, 8), while the intake and exhaust cam phase angle were set to the neutral values.

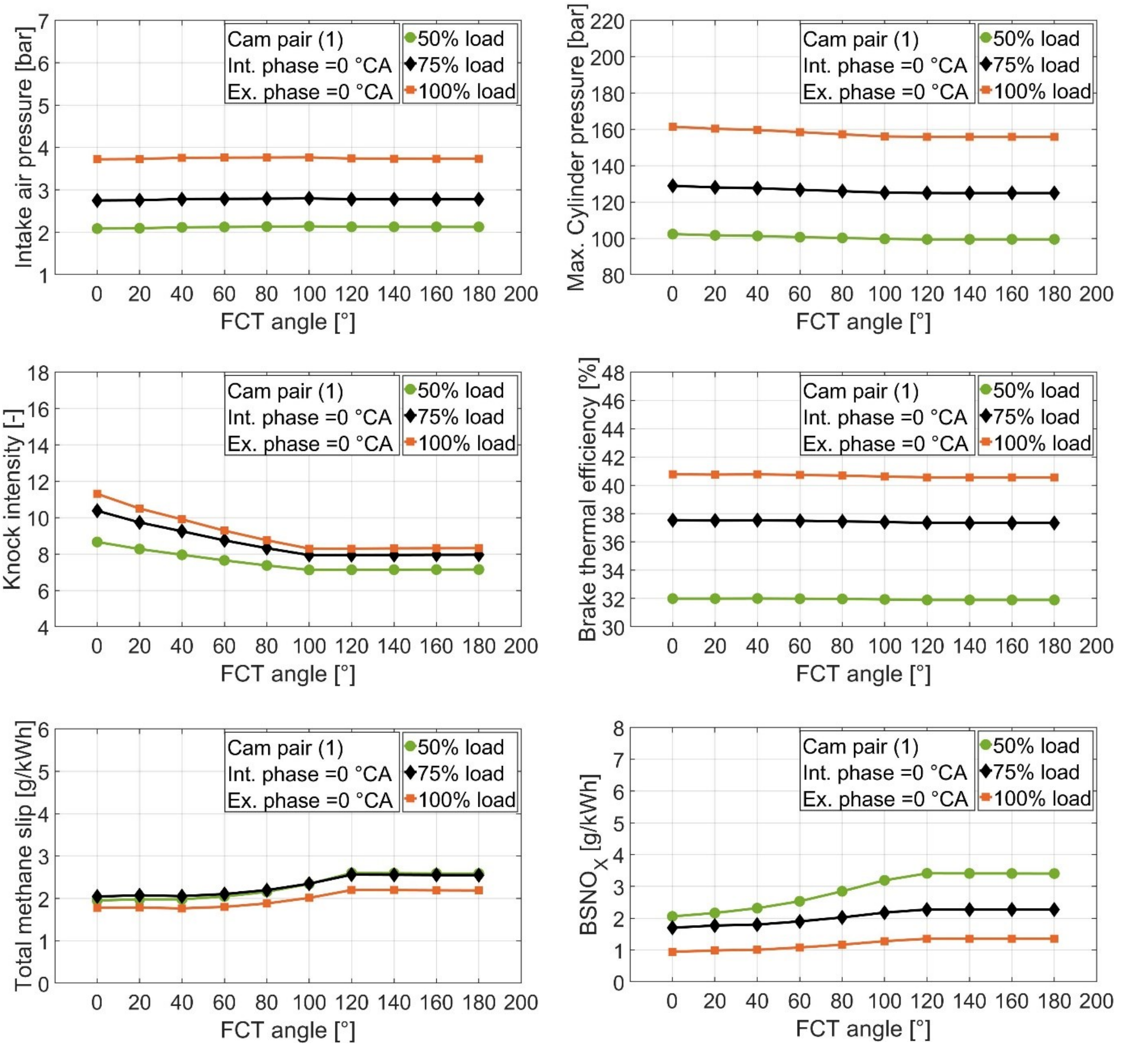

Figure 5.5: Effect of FCT with cam pair (1).

Generally, with the four cases, the trendlines of the different parameters are a little bit similar to that in Figure 3.7. It can be seen that, as the FCT angle increased the cylinder pressure is reduced with the four pairs. The reason behind that is the lower effective compression ratio with the higher FCT angles (strong Miller effect). Consequently, more charge is required to keep the same output power, which is noticeable by increasing the intake air pressure with the four pairs also. Knock intensity is decreased at the higher FCT values, likewise during the experimental tests as the FCT value had to be increased to avoid the strong knocking especially with the higher loads. Nitrogen oxides emissions show higher values with the strong Miller effect and the same tendency is noticed with the four cases. The reduction in the effective compression ratio with the higher FCT values resulted in higher in-cylinder temperature as less mass is trapped with less heat capacity, hence more nitrogen oxides are produced.

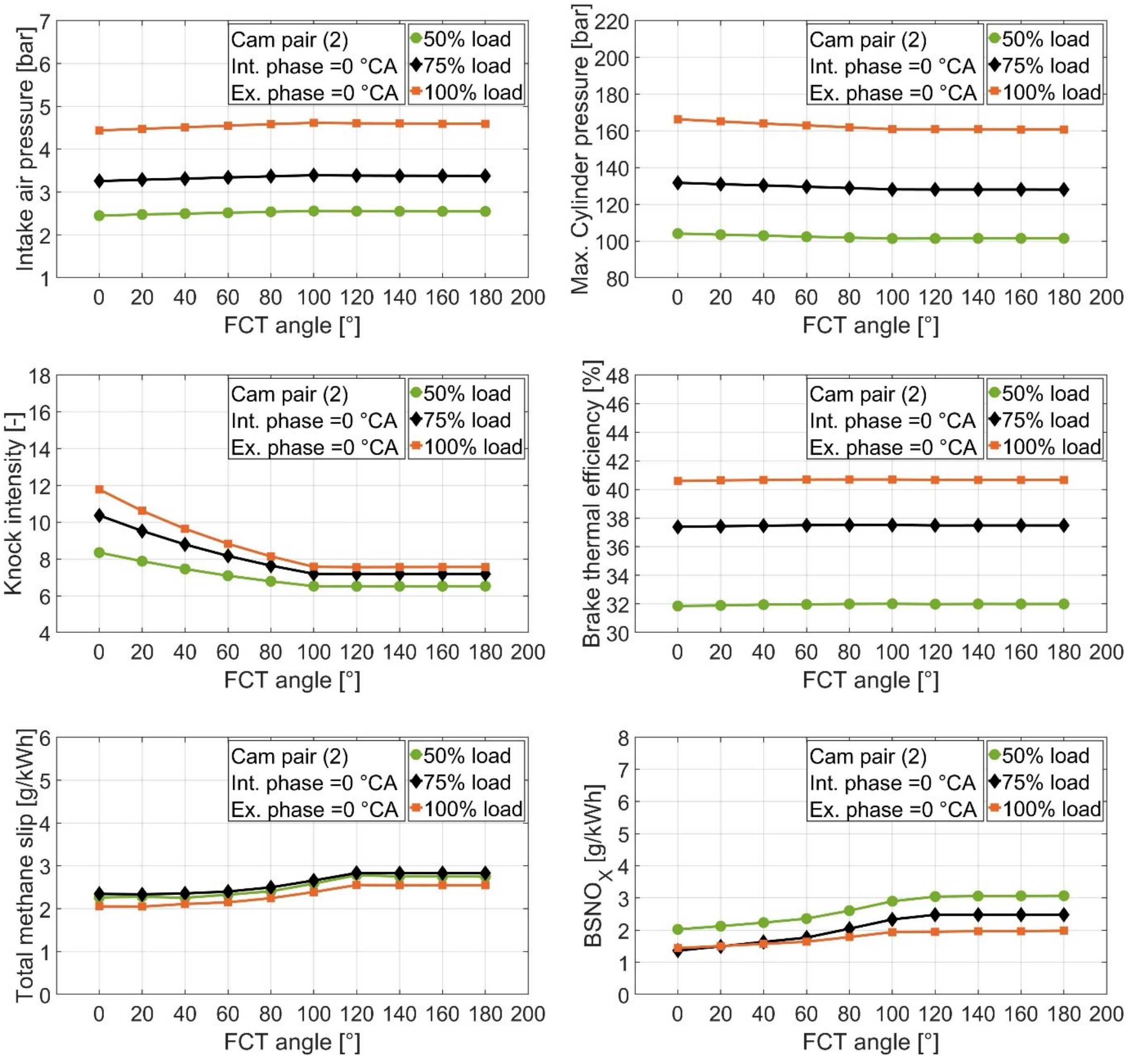

Figure 5.6: Effect of FCT with cam pair (2).

The same behavior was reported in [45] for the NO_x production with the strong Miller cycle effect. Total methane slip with cam pairs (1, 2) shows increasing trend with the higher FCT values, while no significant change is noticed with cam pairs (7, 8). The common factor between pairs (1, 2) is the late EVC in comparison with pairs (7, 8). As the EVC event is retarded, the overlap period is increased which allows more charge to escape from the exhaust valve especially in the turbocharged engines as stated also in [94]. Brake thermal efficiency does not show a clear difference between the four cases as the combustion parameters were kept fixed. By comparing the intake air pressure between the four cases, it is observed that the lower values of the three loads belong to cam pair (1). Usually, the charged air is provided through air compressors, which represent power consuming units and should be taken into account in terms of the total power consumption.

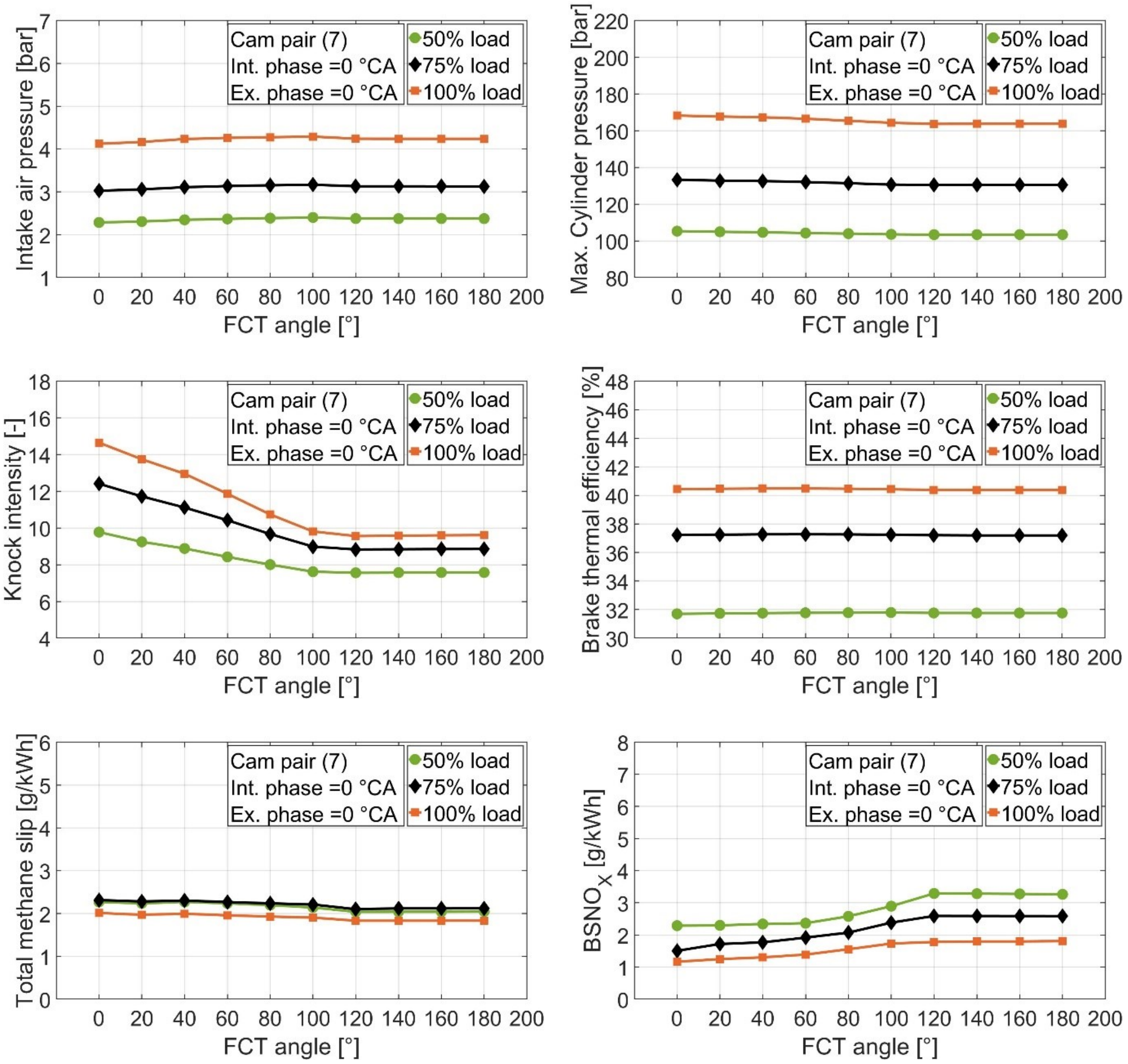

Figure 5.7: Effect of FCT with cam pair (7).

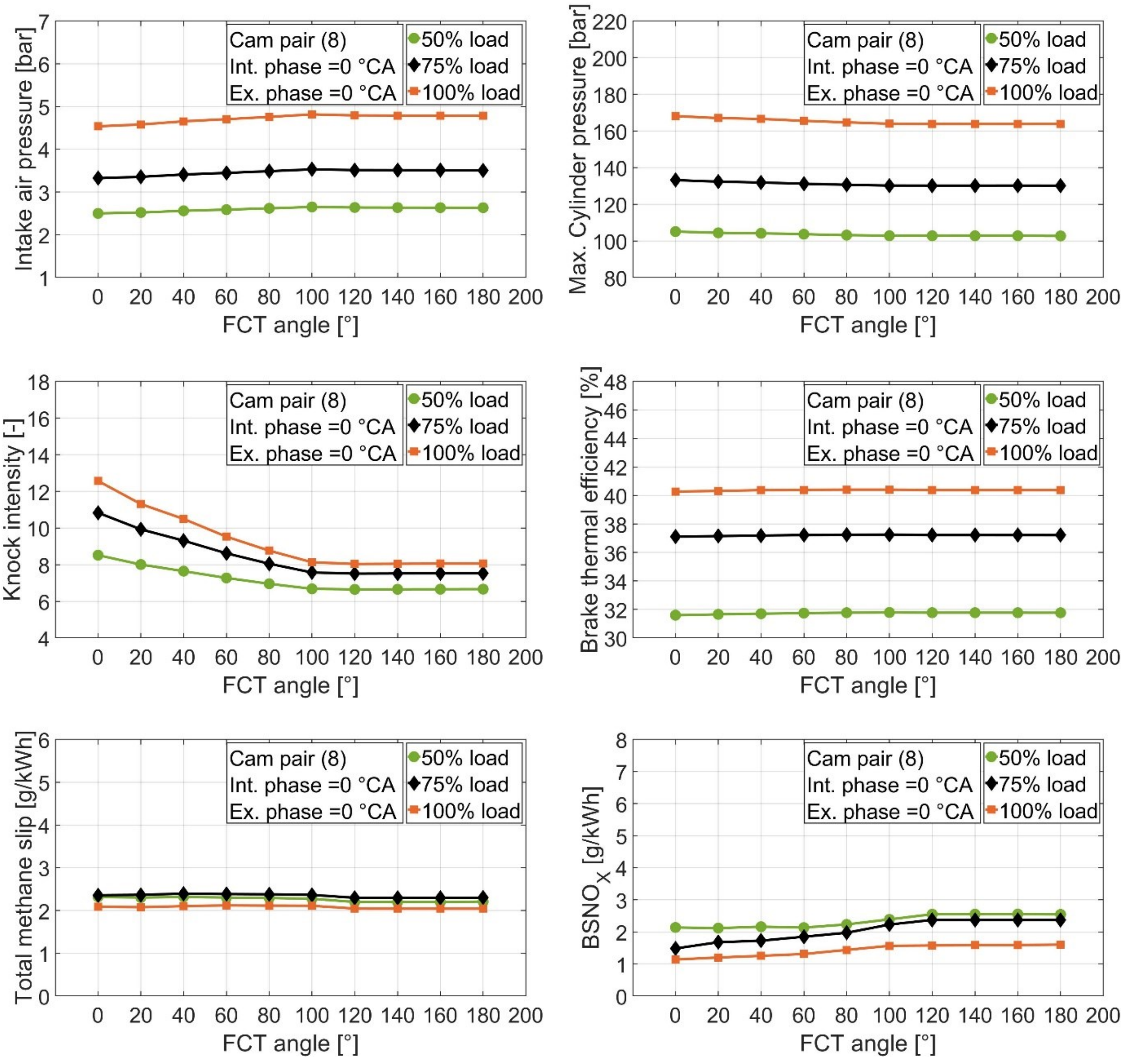

Figure 5.8: Effect of FCT with cam pair (8).

With the four cases, knock intensity shows an opposed behavior for that of the NO$_x$. Hence, it is available to maintain lower NO$_x$ emissions by reducing the FCT angles, but it comes at the expense of knock intensity. So, compromising points of FCT = 80° : 120° would bridge the gap between the two parameters as this range has a positive effect also on the total methane slip emissions.

5.2.2 Effect of Intake Valve Timing on Engine Performance and Emissions

In this section, the effect of the intake cam position on the engine characteristics is presented. The intake cam was advanced and retarded within the full range as stated in Table 4.1, while every exhaust cam was set to its neutral position (exhaust cam phase angle = 0 °CA) and the FCT mechanism was adjusted also to its neutral position (FCT = 0°).

Expressing the cam positions in terms of the phase angle values will be confusing, because every cam has a different profile than the other one. Also, it will not reflect the real opening and closing points relative to the crank angle. Thus, referring the valve events to the crank angle degrees is more reliable. Particularly in this study, the EVC and IVO in terms of the crank angle will be used to express the valves' positions, as they are preferred rather than EVO and IVC to demonstrate the valve overlap period.

Figures 5.9 to 5.12 show the influence of the IVO event on the engine performance and emissions for cam pairs (1, 2, 7, 8) respectively. With the four cases, its observed that advancing the IVO point by 40 °CA reduced the maximum cylinder pressure and required more intake air pressure to maintain the same power.

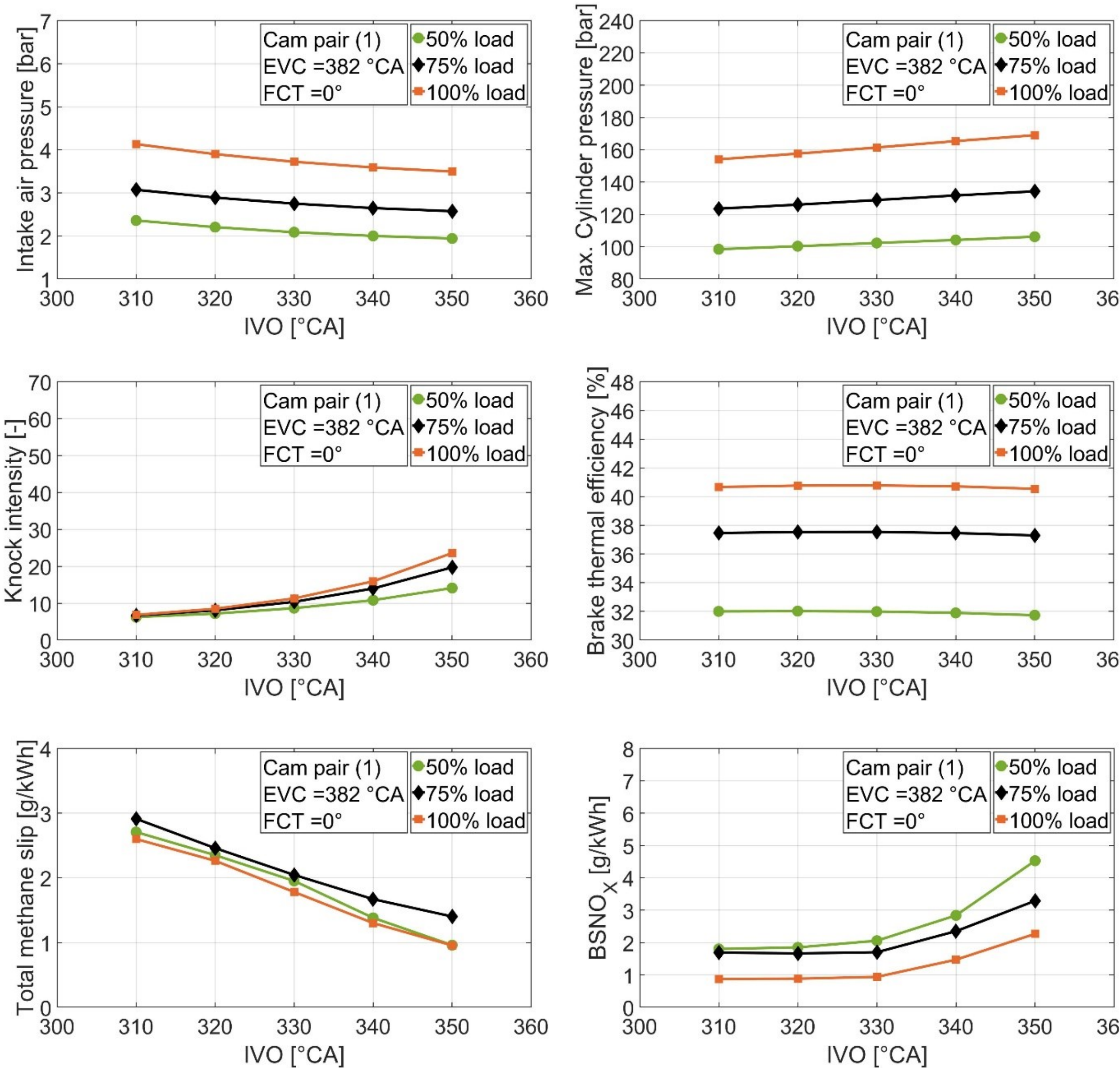

Figure 5.9: Effect of IVO with cam pair (1).

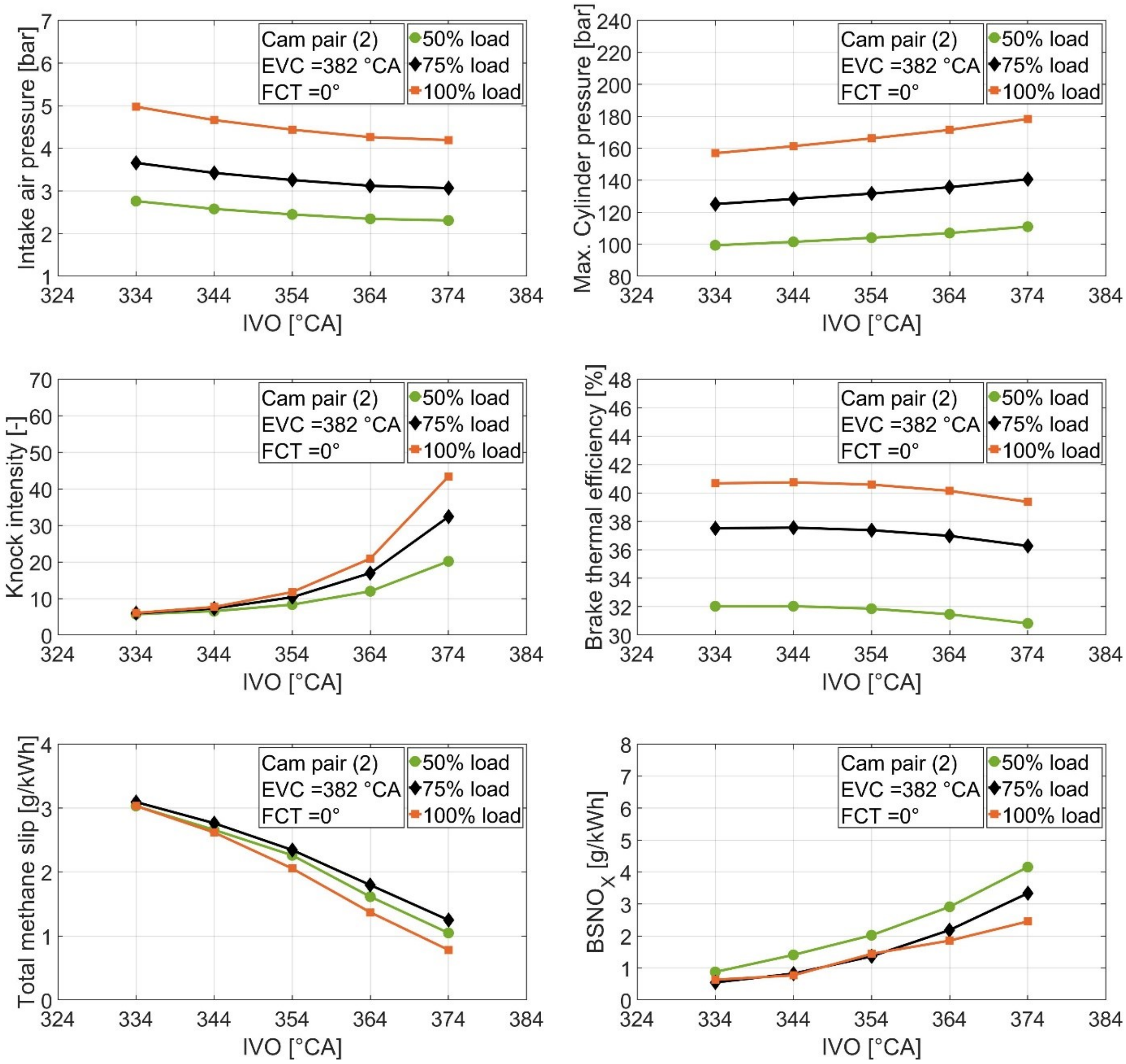

Figure 5.10: Effect of IVO with cam pair (2).

Furthermore, the knock intensity is dramatically decreased with the earlier IVO values, while the total methane slip is affected negatively. When the intake valve is opened earlier, the in-cylinder pressure is still relatively high and longer overlap is obtained. As a result, some amount of the exhaust gases are pushed through the intake valve as shown in Figure 2.10 (b). Then, during the intake stroke, the exhaust gases are recycled again into the cylinder causing a dilution effect like internal EGR. This impact is significantly reflected on the NO_x production especially with pairs (2, 7, 8). Total methane slip is increased also with advancing the IVO which supports the dilution phenomena occurrence and the low temperature combustion. The second reason for the higher methane slip with the earlier IVO, is the longer overlap period which allows the charge to escape through the exhaust port. Some researchers in the literature reported the same influence with the earlier IVO as stated in [95, 96].

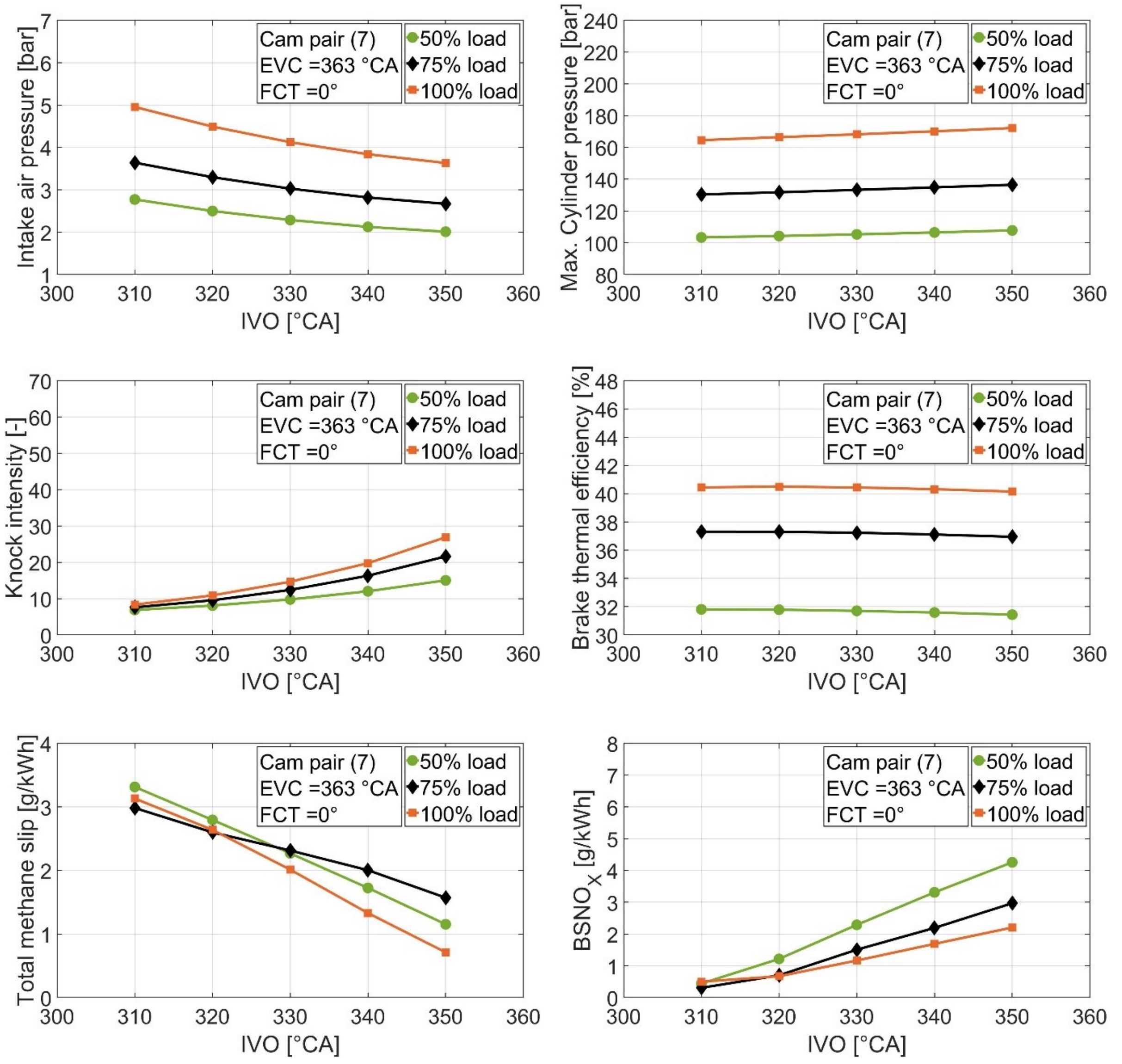

Figure 5.11: Effect of IVO with cam pair (7).

In pairs (1, 7), brake thermal efficiency does not show a noticeable change with the full IVO range, while it deteriorates at the maximum IVO retarding with pairs (2, 8). That means more fuel is consumed however the power remains the same through the four cases. This effect is more obvious by comparing the required intake air pressure through the four pairs. The smaller intake cam profile in pairs (2, 8) requires more charge than that in pairs (1, 7) to produce the same power. Hence, more intake air pressure is exerted. Total methane slip is slightly higher also with pairs (2, 8) rather than that with pairs (1, 7) which indicates more dissipated fuel. A strong trade-off between the total methane slip and the NO$_x$ is noticed with the four pairs which represents an obstacle in the valve timing tuning. The increasing in the NO$_x$ emissions is slightly sharper with pairs (2, 7, 8) than that with the standard pair.

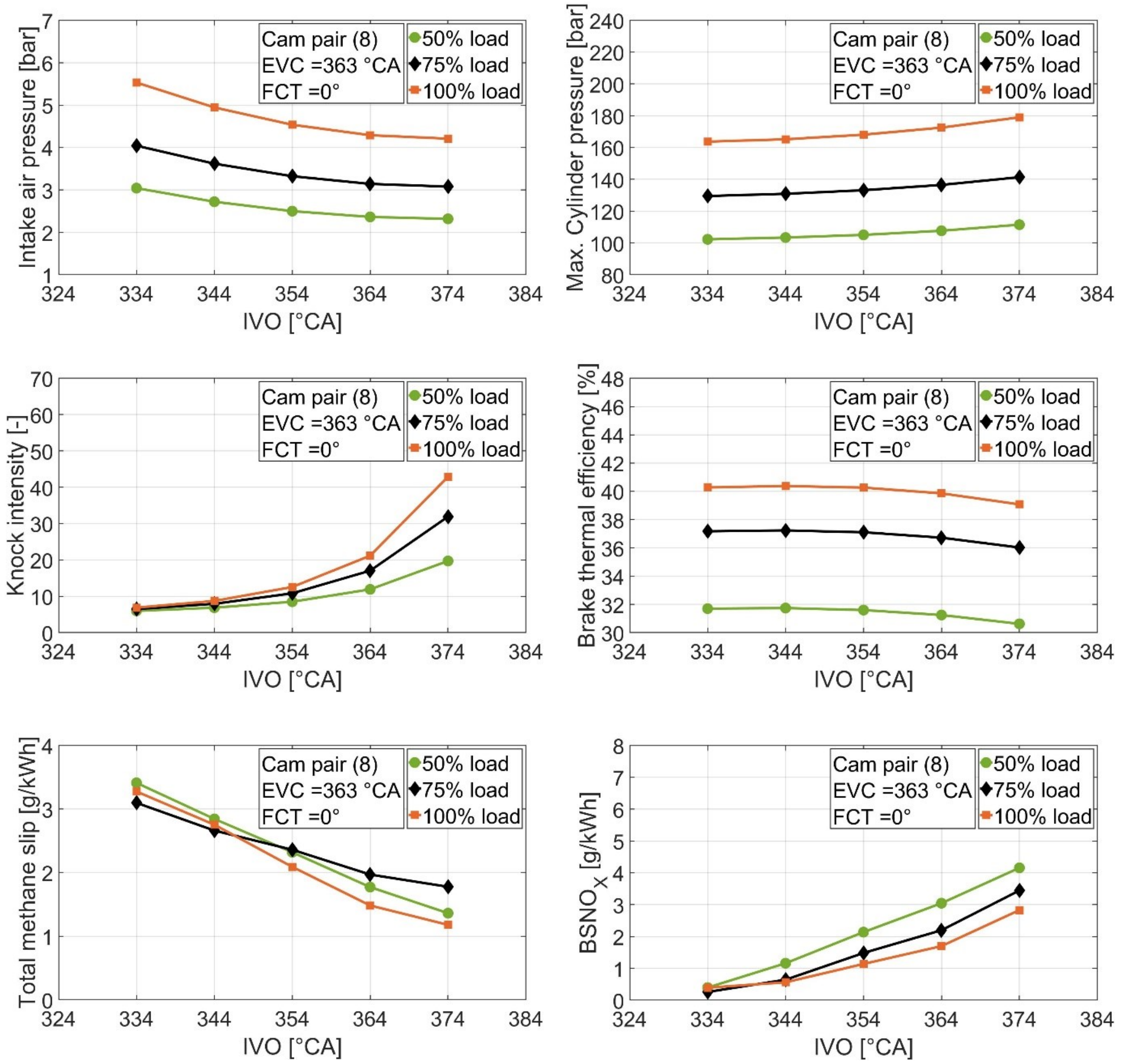

Figure 5.12: Effect of IVO with cam pair (8).

In terms of knocking intensity, cam pairs (2, 8) show higher values than cam pairs (1, 7) which is correlated with the smaller cam profile associated in pairs (2, 8).

5.2.3 Effect of Exhaust Valve Timing on Engine Performance and Emissions

This part of the results represents the opposite of the previous one, as it aims to discuss the effect of the exhaust cam position on the engine performance. The exhaust cam phase angle was tuned within the full range as indicated before in Table 4.1, while the intake cam phase angle and the FCT value were adjusted to the neutral positions (intake cam phase angle = 0 °CA and FCT = 0°).

Figures 5.13 to 5.16 show the influence of the EVC event on the engine performance and emissions for cam pairs (1, 2, 7, 8) respectively.

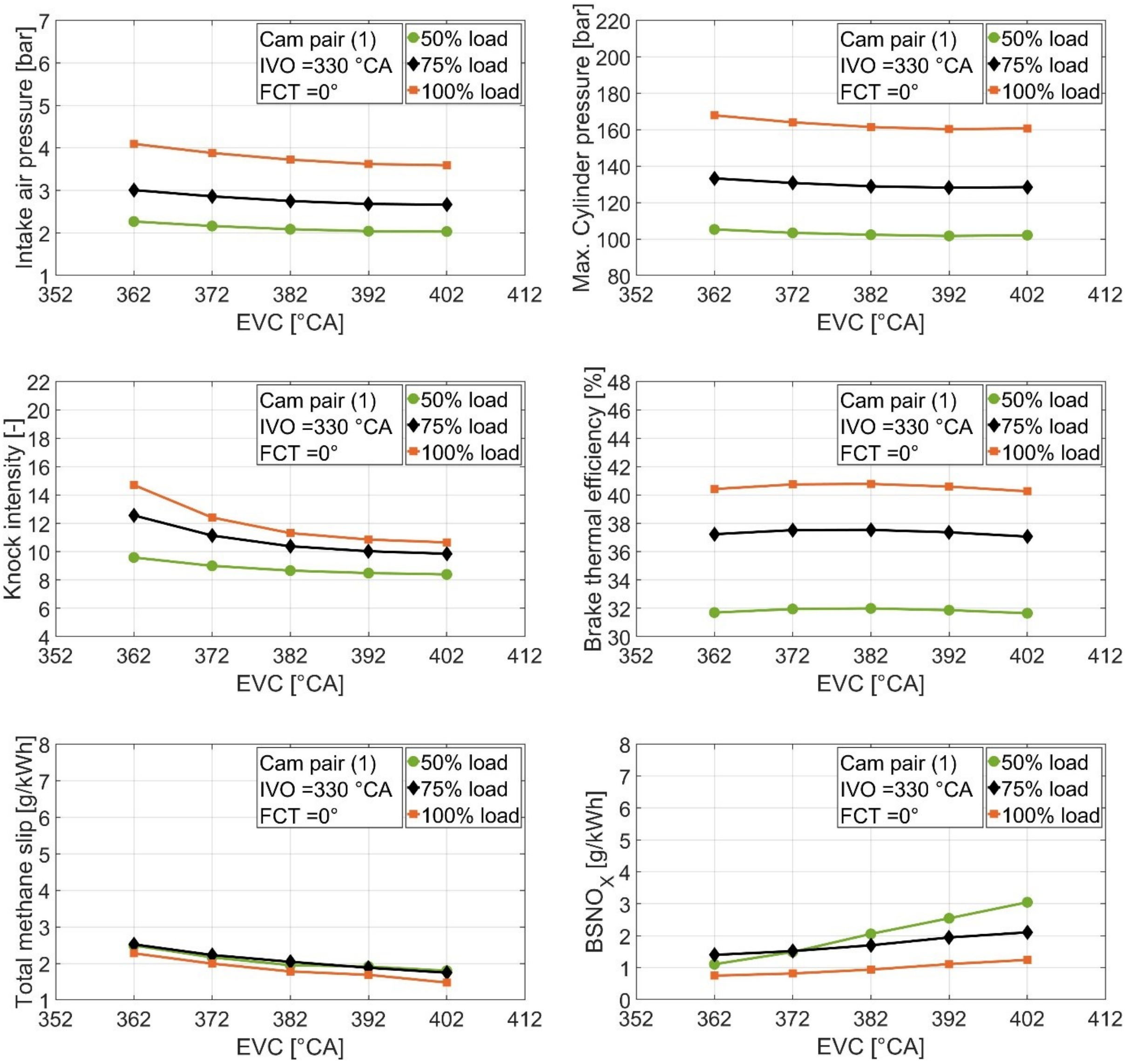

Figure 5.13: Effect of EVC with cam pair (1).

Generally with the four pairs, it appears that the trendlines are not sharp for the different parameters as they were with the intake cam tuning, which reflects less effectiveness for the exhaust cam position. As the EVC is advanced by 40 °CA, both the intake air pressure and the cylinder pressure is increased. This effect is more obvious with pairs (1, 7, 8), while it was minor with cam pair (2). Also, the knock intensity with cam pair (2) is lower than that with pairs (1, 7, 8). Brake thermal efficiency shows lower values at the excessive EVC advancing or retarding with the four pairs.

Tuning the EVC point means also that the EVO event is tuned with the same value as the cam profile is constant (in this study). Hence, advancing the EVC point causes earlier EVO which reduces the effective combustion stroke and lowers the in-cylinder pressure suddenly before

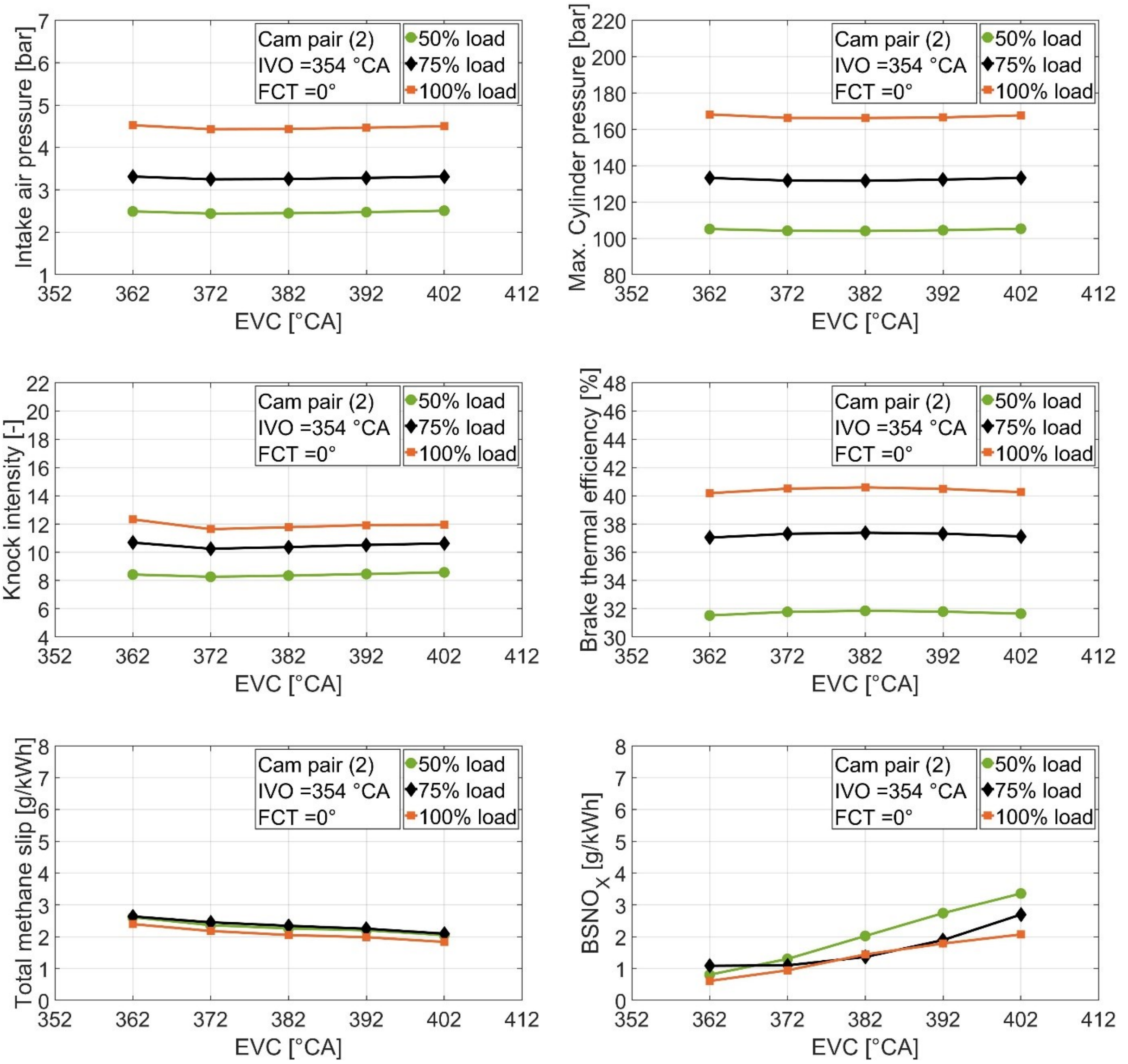

Figure 5.14: Effect of EVC with cam pair (2).

the end of combustion. The behavior of the total methane slip supports this effect as it increased by advancing the EVC with the four pairs. Furthermore, the NO_x emissions are lower with advancing the EVC which represents an indication for the lower temperature inside the combustion chamber.

The other reason for the lower NO_x with advancing the EVC and EVO, is that the exhaust gases are not effectively scavenged from the cylinder which promotes the dilution effect and reduces the in-cylinder temperature.

The higher intake air pressure with advancing the EVC is caused by the loss of the power due to the earlier EVO. Hence, more charge pressure is a mandatory to keep the power constant. With the four pairs, the moderate advancing of the EVC does not cause much loss to the brake thermal efficiency, while it affects the NO_x emissions positively.

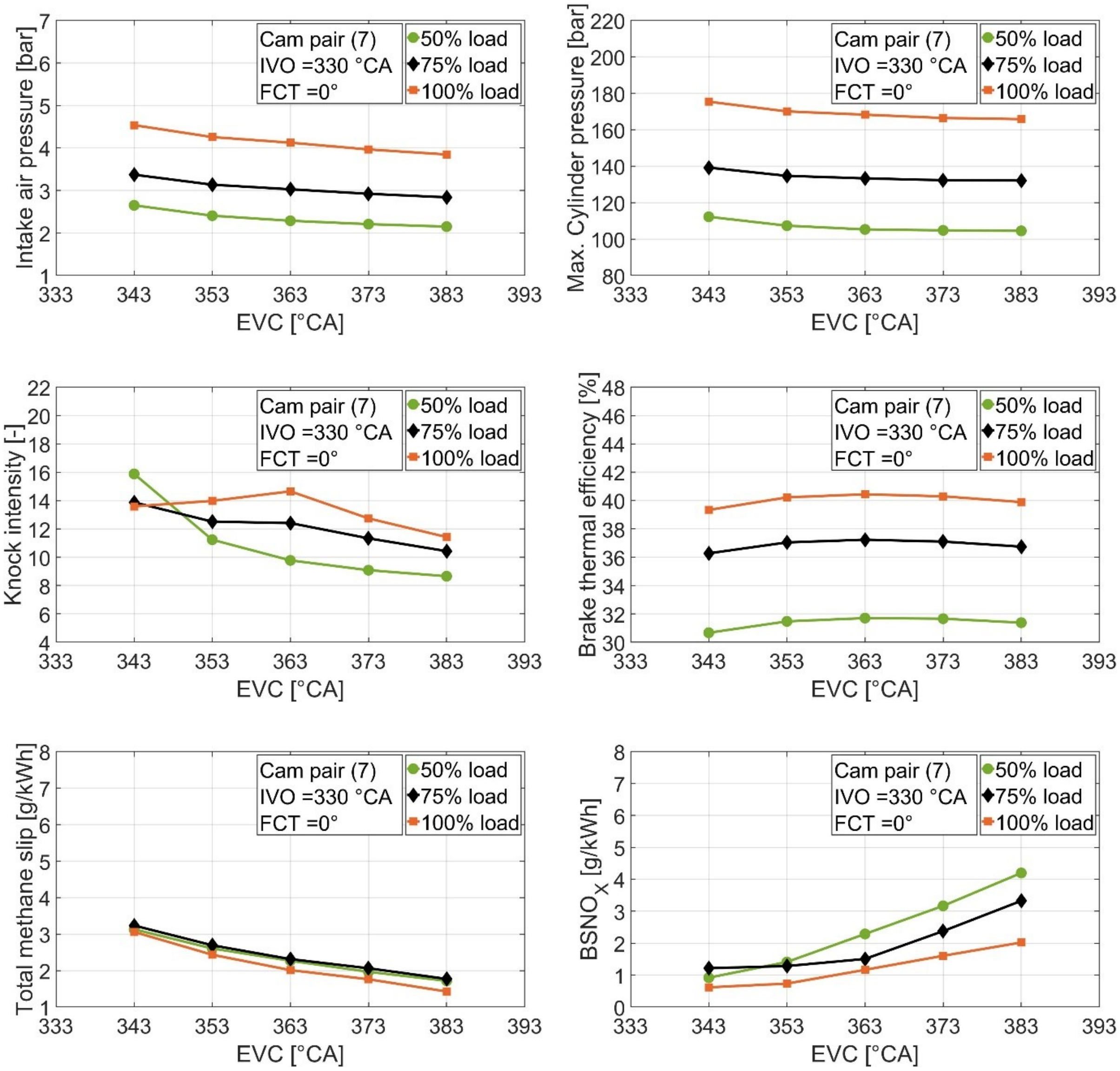

Figure 5.15: Effect of EVC with cam pair (7).

Usually for the conventional diesel engines, the EVO lies between 30 °CA: 40 °CA before BDC which assures optimal exhaust scavenging. Also, the EVC is around 10° ATDC which provides an appropriate overlap to maintain ideal exhaust scavenging with the effect of the new charge. In terms of the exhaust emissions, as the EVC is advanced, the increasing of the total methane slip and the reduction of the NO_x are more sharply and noticeable with pairs (7, 8) than those of pairs (1, 2). The common feature between pairs (7, 8) is that the exhaust cam profile has less width than that of pairs (1, 2), which promotes the effect of the valve timing.

The extreme advancing or retarding of the EVC may improve one parameter in terms of the exhaust emissions or engine performance, but on the other hand, another parameter is deteriorated. Hence, the moderate tuning is preferable as it allows to find a compromising point combining between all the advantages.

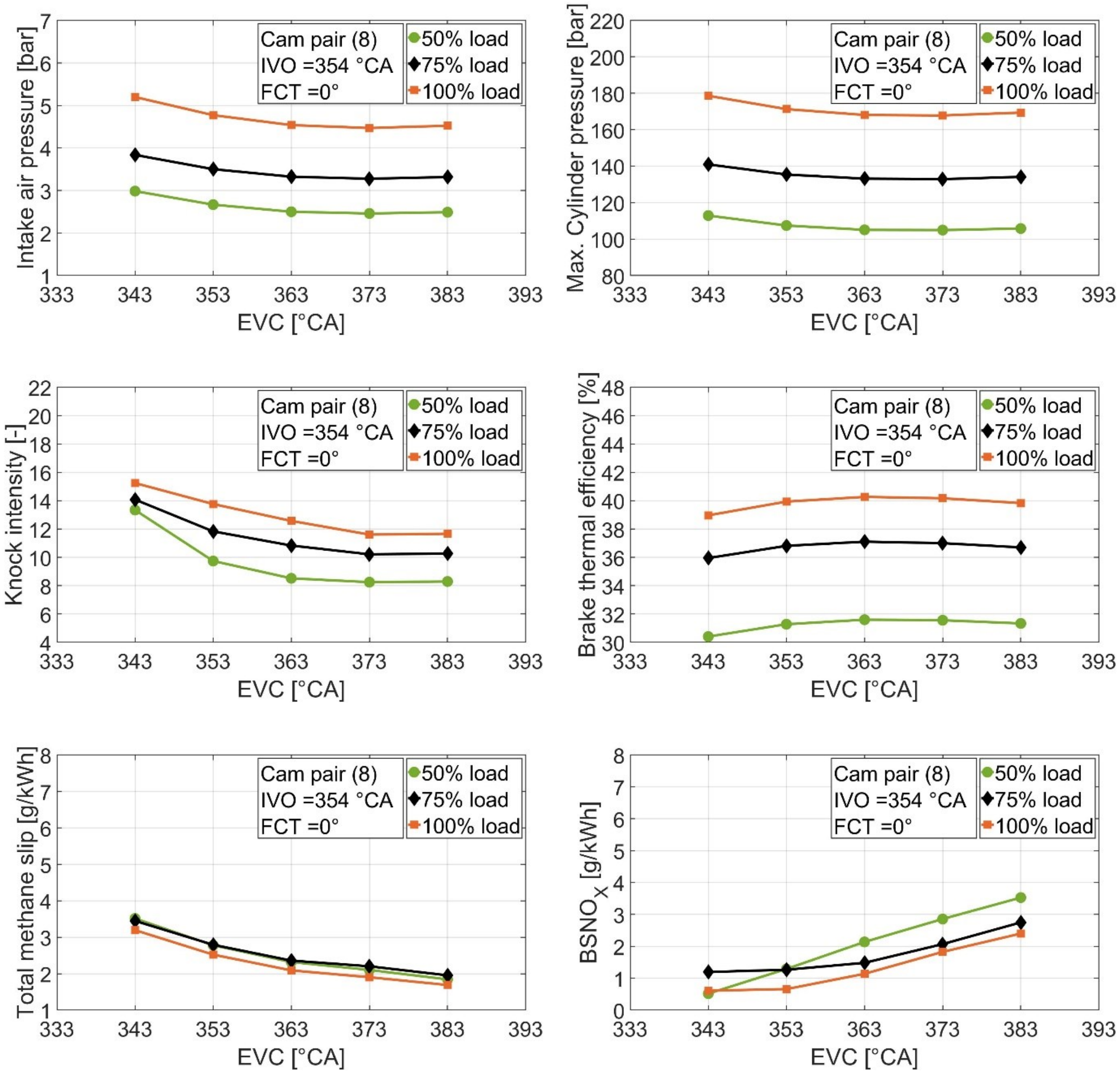

Figure 5.16: Effect of EVC with cam pair (8).

5.2.4 Effect of Valve Overlap Position on Engine Performance and Emissions

Valve overlap represents a critical parameter as it affects engine performance and emissions formation. From this point of view, this section discusses the effect of the valve overlap position, while the overlap period remains the same. This pattern was achieved by tuning the both cams together with the same value within the full range, from the maximum advancing to the maximum retarding. So, the valve overlap period stills identical, but it begins at different crank angles. Figures 5.17 to 5.20 show the influence of the valve overlap beginning on the engine characteristics for cam pairs (1, 2, 7, 8) respectively. It can be seen that, the maximum advancing and retarding of the overlap beginning is associated with more cylinder pressure in the four cases.

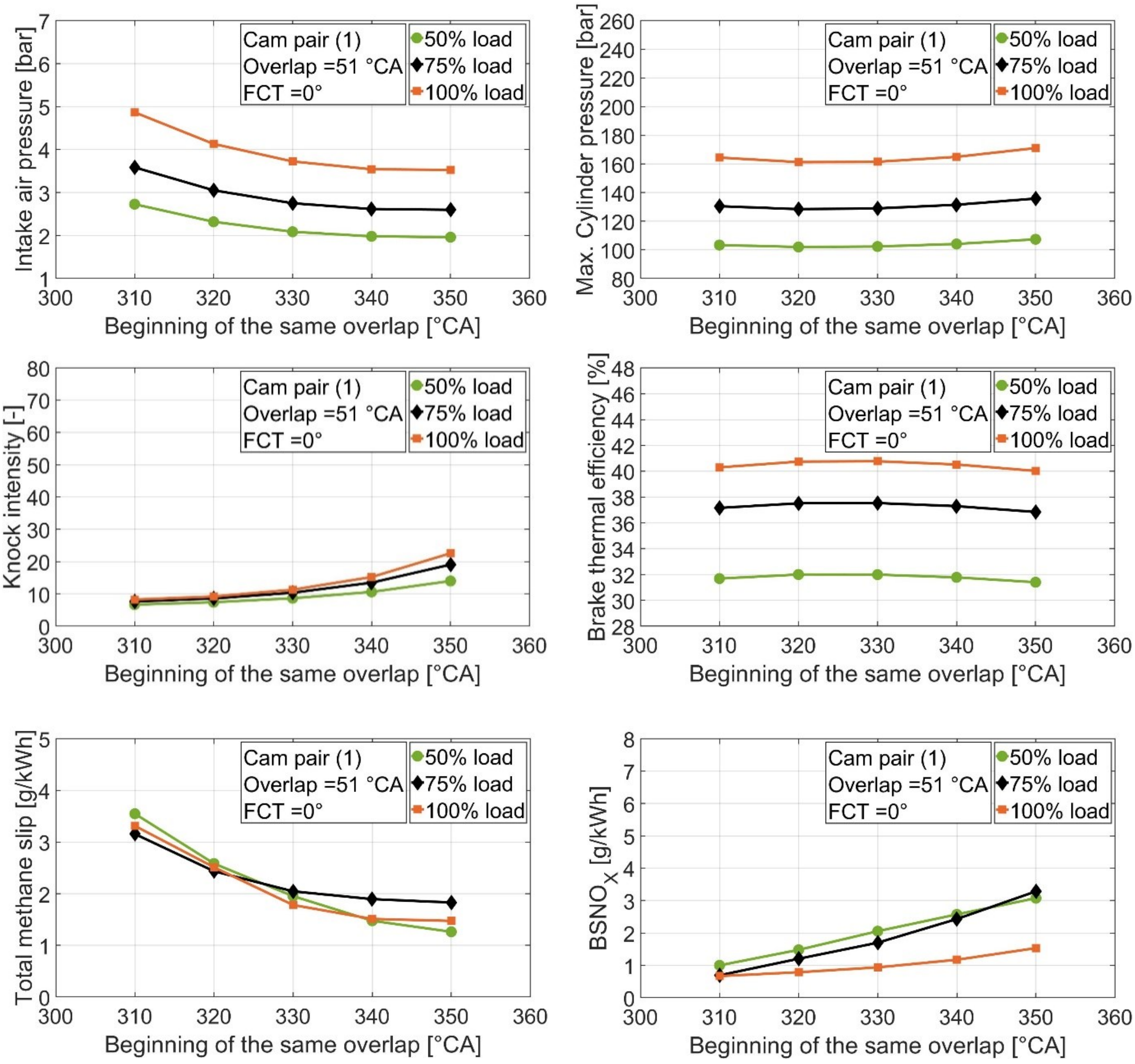

Figure 5.17: Effect of overlap position with cam pair (1).

The required intake air pressure also shows higher values as the overlap beginning is advanced for the all pairs, but the increasing rate is slightly different in cam pairs (1, 7) than that with pairs (2, 8). The same difference can be found also by comparing the knock intensity behavior in pairs (1, 7) with that in pairs (2, 8). With retarding the overlap beginning, the knock intensity is sharply increased in cam pairs (2, 8), while its growing is smoothly with pairs (1, 7). The maximum retarded valve overlap in pairs (1, 7) begins at 350 °CA, while it begins at 374 °CA with pairs (2, 8). Consequently, the relative position of the valve overlap period with respect to the TDC plays an effective role in the combustion characteristics.

The brake thermal efficiency is reduced with the extreme advancing and retarding of the overlap beginning with the four pairs.

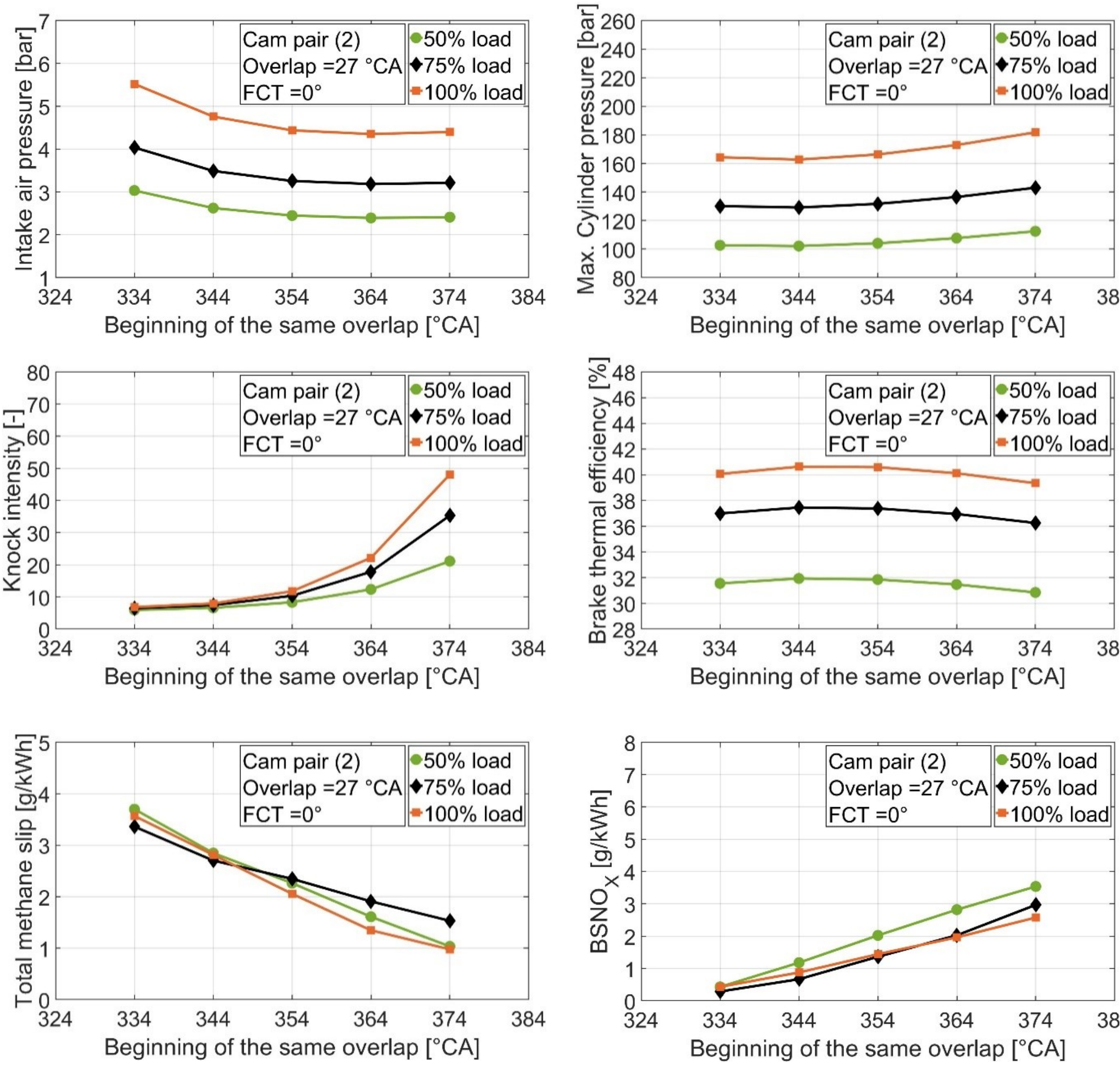

Figure 5.18: Effect of overlap position with cam pair (2).

In terms of the exhaust emissions, they show similar behavior with the four cases but with different values. Advancing the overlap beginning causes more methane slip with lower NO$_x$ production, but in cam pairs (1, 2) the values are less than those of pairs (7, 8). The amount of the valve overlap period in pairs (7, 8) is less than those of pairs (1, 2). The too short valve overlap does not maintain effective exhaust scavenging which is reflected on the NO$_x$ production.

From cam pairs (1, 2, 8) it is observed that, as the overlap period is positioned slightly around the TDC, tuning the valve timing is more feasible without rapid effects on the engine parameters. The extreme advancing or retarding of the overlap position will lead to one of the two effects which mentioned before in Figure 2.10.

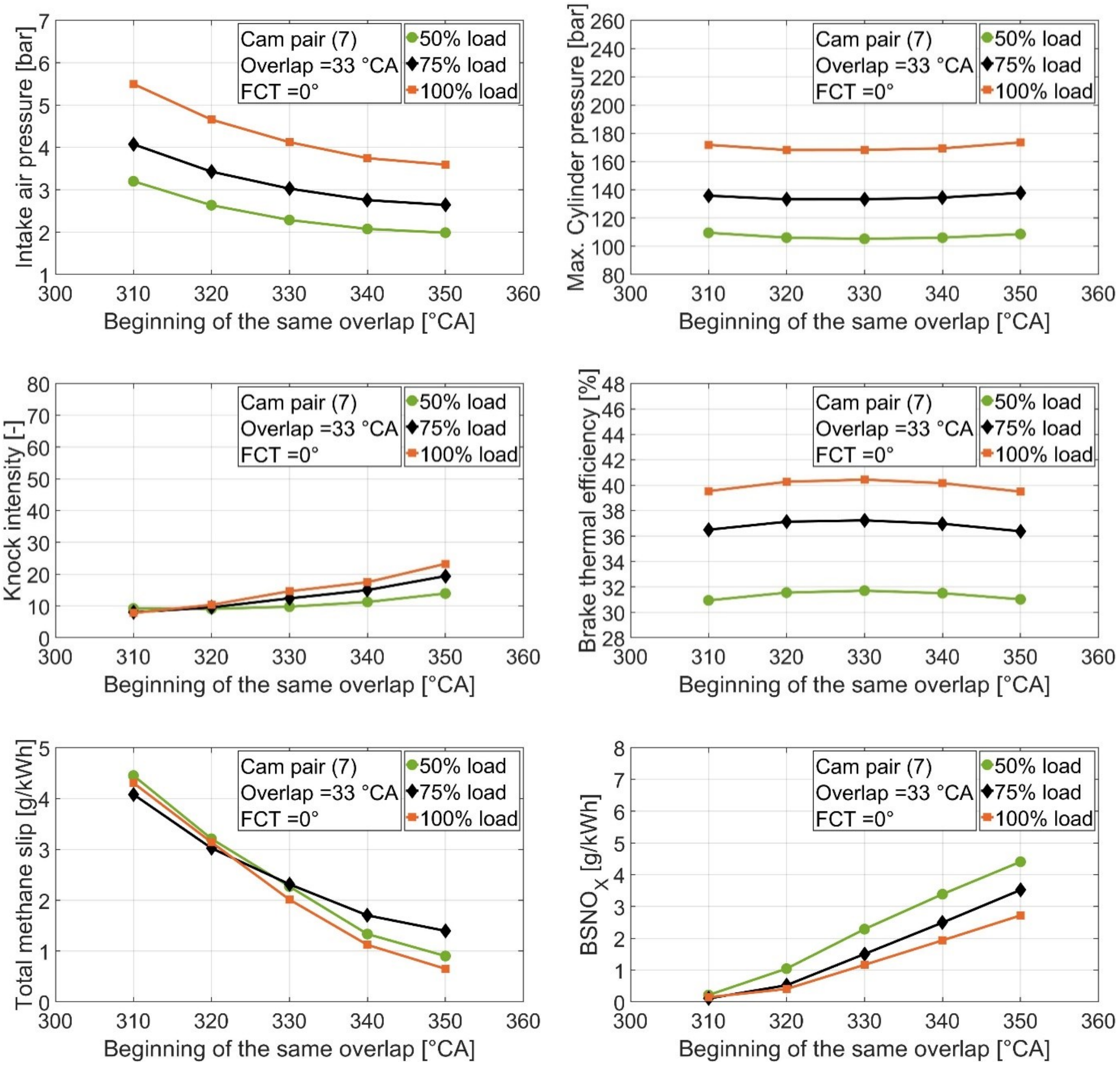

Figure 5.19: Effect of overlap position with cam pair (7).

By comparing cam pair (8) with pairs (1, 2, 7), it is noticed that the brake thermal efficiency is more affected with the overlap positions in pair (8). The reason behind that is the smallest overlap period in pair (8) in comparison with the three pairs (1, 2, 7). From this point of view, it can be concluded that the too small overlap is not recommended since it constricts the tuning range.

In terms of the overlap position for the four cases, cam pair (1) shows better values for the engine performance and emissions as it has a valve overlap of 51° CA. In the second place, cam pairs (2, 7) with valve overlap of 27 °CA and 33 °CA respectively, that is why their performance is a little bit similar. And finally, cam pair (8) with the higher exhaust emissions and more brake thermal efficacy loss as it has a valve overlap of 9 °CA.

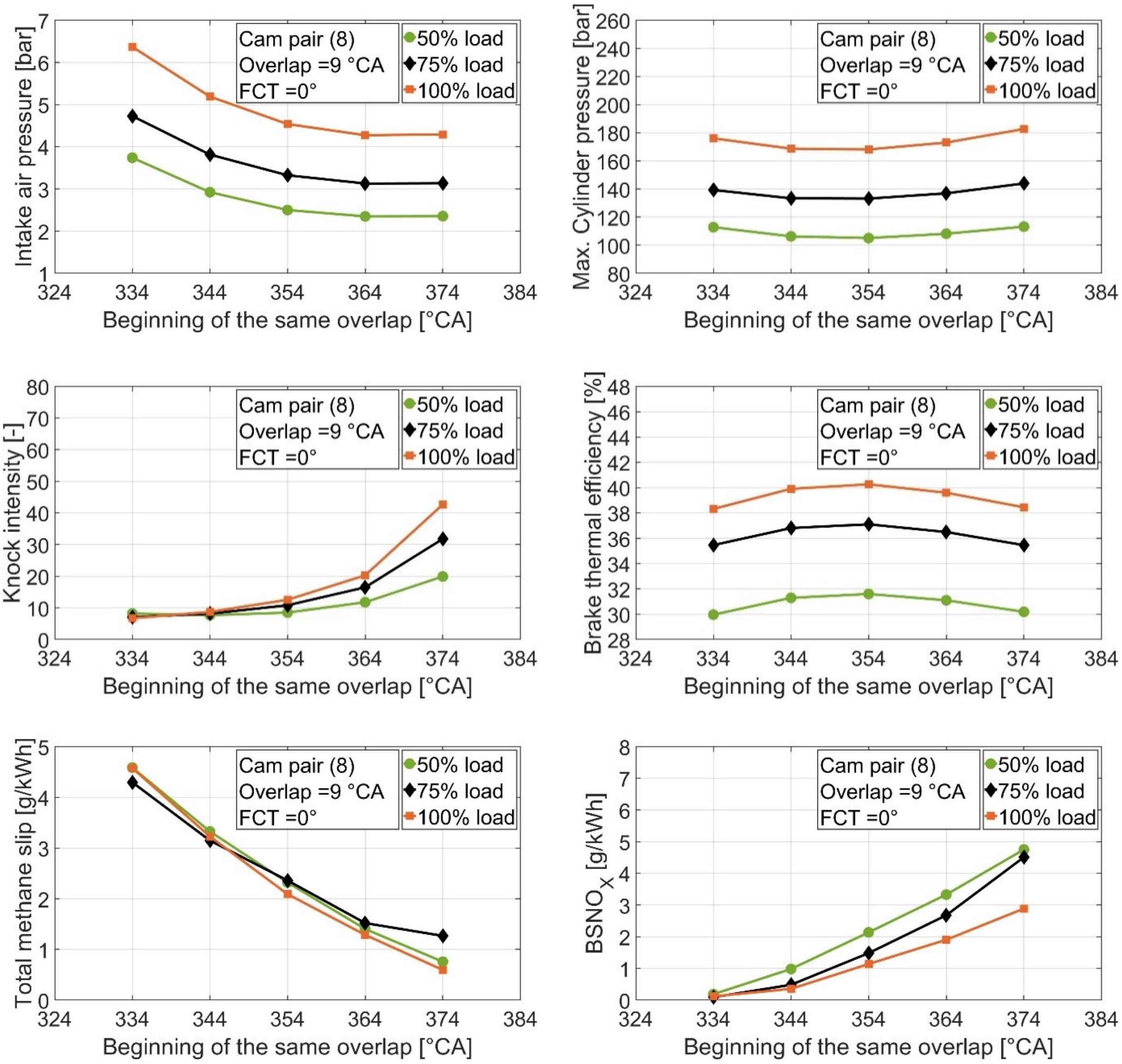

Figure 5.20: Effect of overlap position with cam pair (8).

6 Conclusion and Outlook

6.1 Conclusion

In this study, a simulation model was developed for a dual-fuel marine engine equipped with flexible valve train strategy. The model aims to optimize the engine performance and reduce its emissions by using different valve timings. Two parts are included in this model, the first one being the flexible valve train model which was developed in MATLAB. It aims to predict the different valve timings taking into account the effect of the flexible camshaft technology (FCT) and the Multi-segment Camshaft.

The second part is the phenomenological combustion model, which was developed in AVL CRUISE-M to predict the rate of heat release and the emissions formation in the engine depending on many sub-models. The resulting valve timing positions from the MATLAB model were exported to the engine combustion model in order to investigate their influence on engine performance.

After reviewing the results, it can be concluded that the flexible valve train model can effectively predict the valve timing positions as the simulation results show a very good agreement with the experimental data.

In terms of the combustion model, the results of the in-cylinder parameters and exhaust emissions match well with the experimental tests on the engine test bench. Hence, the model was used for further investigations and four cam pairs (1, 2, 7, 8) with different valve timings were discussed in this study.

Results indicated that increasing the FCT angle has a positive effect on the knock intensity at engine loads of 50%, 75% and 100% with all four cam pairs. Generally, as the FCT angle increased, more valve overlap period is attained. With cam pairs (1, 2), the higher FCT values are associated with more NO_x and total methane slip in the exhaust emissions. The reason behind that is the escaped fresh charge through the exhaust valve as the overlap period increased. On the other hand, increasing the FCT value in cam pairs (7, 8) caused more $BSNO_x$ with a slight reduction in the total methane slip. The common factor between pairs (7, 8) is the EVC event, which indicates that not only the overlap value affects the emissions formation, but also the position of the overlap relative to the crank angle. Brake thermal efficiency was not majorly affected with the different FCT values.

Using the cam phase angle possibility, the effect of the intake valve timing was investigated. The results showed that advancing IVO requires more intake air pressure to maintain the same power, which was very obvious with all four pairs. As IVO is advanced, IVC becomes earlier, which means a strong Miller effect (lower effective compression ratio). Furthermore, with advancing IVO, the overlap period is increased which allows more methane to escape out of the cylinder without participating in the combustion process. Knock intensity and $BSNO_x$ are reduced with advancing the IVO points at all investigated engine loads.

Regarding the EVC tuning, it showed a lower effect on engine performance and emissions in comparison with IVO tuning. The progressive advancing of EVC increased knock intensity with all four cam pairs. More methane slip is detected in the exhaust emissions by advancing EVC as the exhaust valve is opened before the end of combustion. The level of $BSNO_x$ is affected positively by the earlier EVC with all four pairs.

In terms of the valve overlap value and position, the results stated that a too small valve overlap affected the exhaust emissions negatively as the valve overlap helps in the scavenging process. Moderate overlap values showed better performance and had more stable range for valve tuning which allows the optimization of other parameters without sacrifices. The results showed that not only the amount of the valve overlap, but also the position of the overlap relative to TDC is significant. The best performance with lower emissions was obtained when the valve overlap position was near to the TDC.

6.2 Outlook

New combustion technologies are mandatory nowadays since more efficient engines with lower emissions are required due to climate considerations and legislation. Many combustion technologies were introduced and discussed in this study, since they still need more development in terms of combustion control. Pilot-DF combustion has more advantages in comparison with the other technologies, as two fuels are used which enhances the control of the combustion parameters. Miller cycle and flexible valve timing can be utilized effectively in pilot-DF engines to achieve ultra-low emissions with low fuel consumption. Many variable valve timing mechanisms are available depending on the engine characteristics. In this study, flexible camshaft technology (FCT) was implemented since it allows valve timing tuning during engine operation within a range of 10 °CA for the two valves together. Results showed that it can effectively reduce exhaust emissions with low knock levels especially at higher engine loads. The cam phasing mechanism is the second possibility explored in this study. It provides a wide range of cam tuning but it cannot be used during engine operation, as the engine must be stopped for some assembly and disassembly procedures. So, merging the two mechanisms together would be more practical and allows a wide range of valve timing with the different operating conditions. Also, developing the FCT mechanism to enable only one cam tuning either the intake or the exhaust will be more flexible. In terms of the combustion in the dual-fuel engines, phenomenological models are considered effective and flexible modelling approach since many sub-models can be implemented as required.

References

[1] European Environment Agency, "*Greenhouse Gas Emission Intensity of Fuels and Biofuels for Road Transport in Europe*", https://www.eea.europa.eu/ims/greenhouse-gas-emission-intensity-of, 2021.

[2] M. ALLEN, "*The Science and Policy of Cumulative and Short-Lived Climate Pollutants*", 2015.

[3] J. Lynch, M. Cain, R. Pierrehumbert, and M. Allen, "*Demonstrating GWP: A Means of Reporting Warming-equivalent Emissions that Captures the Contrasting Impacts of Short- and Longlived Climate Pollutants*", Environ Res Lett, vol. 15, no. 4, Apr 2, 2020.

[4] U.S. Environmental Protection Agency, "*Overview of Greenhouse Gases*", https://www.epa.gov/ghgemissions/overview-greenhouse-gases, 2019.

[5] Climate science, "*Greenhouse Gases: What is Warming Up our Earth?*", https://climatescience.org/advanced-greenhouse-gases, 2022.

[6] E. Shim, H. Park, and C. Bae, "*Comparisons of Advanced Combustion Technologies (HCCI, PCCI, and Dual-Fuel PCCI) on Engine Performance and Emission Characteristics in A Heavy-Duty Diesel Engine*", Fuel, vol. 262, 2020.

[7] L. Wei, and P. Geng, "*A Review on Natural Gas/Diesel Dual Fuel Combustion, Emissions and Performance*", Fuel Processing Technology, vol. 142, pp. 264-278, 2016.

[8] B. Wang, A. Yao, C. Chen, C. Yao, H. Wang, M. Liu, and Z. Li, "*Strategy of Improving Fuel Consumption and Reducing Emission at Low Load in a Diesel Methanol Dual Fuel Engine*", Fuel, vol. 254, 2019.

[9] I. May, A. Cairns, H. Zhao, V. Pedrozo, H. Wong, S. Whelan, and P. Bennicke, "*Reduction of Methane Slip Using Premixed Micro Pilot Combustion in a Heavy-Duty Natural Gas-Diesel Engine*", SAE Technical Paper 2015-01-1798, 2015.

[10] R. Reitz, and G. Duraisamy, "*Review of High Efficiency and Clean Reactivity Controlled Compression Ignition (RCCI) Combustion in Internal Combustion Engines*", Progress in Energy and Combustion Science, vol. 46, pp. 12-71, 2015.

[11] A. Paykani, A. Kakaee, P. Rahnama, and R. Reitz, "*Progress and Recent Trends in Reactivity-Controlled Compression Ignition Engines*", International Journal of Engine Research, vol. 17, no. 5, pp. 481-524, 2015.

[12] S. Turns, "*An Introduction to Combustion Concepts and Applications*", New York, NY, USA: McGraw-Hill Companies, vol. 287, 1996.

[13] Z. Ahmad, O. Kaario, C. Qiang, and M. Larmi, "*Effect of Pilot Fuel Properties on Lean Dual-Fuel Combustion and Emission Characteristics in a Heavy-Duty Engine*", Applied Energy, vol. 282, 2021.

[14] S. Kokjohn, R. Hanson, D. Splitter, and R. Reitz, "*Fuel Reactivity Controlled Compression Ignition (RCCI): A Pathway To Controlled High-Efficiency Clean Combustion*", International Journal of Engine Research, vol. 12, no. 3, pp. 209-226, 2011.

[15] J. Li, W. Yang, and D. Zhou, "*Review on the Management of RCCI Engines*", Renewable and Sustainable Energy Reviews, vol. 69, pp. 65-79, 2017.

[16] Y. Wu, and R. Reitz, "*Effects of Exhaust Gas Recirculation and Boost Pressure on Reactivity Controlled Compression Ignition Engine at High Load Operating Conditions*", Journal of Energy Resources Technology, vol. 137, no. 3, 2015.

[17] A. Dempsey, N. Walker, and R. Reitz, "*Effect of Piston Bowl Geometry on Dual Fuel Reactivity Controlled Compression Ignition (RCCI) in a Light-Duty Engine Operated with Gasoline/Diesel and Methanol/Diesel*", SAE International Journal of Engines, vol. 6, no. 1, pp. 78-100, 2013.

[18] L. Sun, Y. Liu, K. Zeng, R. Yang, and Z. Hang, "*Combustion Performance and Stability of a Dual-Fuel Diesel–Natural-Gas Engine*", Proceedings of the Institution of Mechanical Engineers, Part D: Journal of Automobile Engineering, vol. 229, no. 2, pp. 235-246, 2014.

[19] B. Yang, C. Xi, X. Wei, K. Zeng, and M. Lai, "*Parametric Investigation of Natural Gas Port Injection and Diesel Pilot Injection on the Combustion and Emissions of a Turbocharged Common Rail Dual-Fuel Engine at Low Load*", Applied Energy, vol. 143, pp. 130-137, 2015.

[20] R. Papagiannakis, and D. Hountalas, "*Experimental Investigation Concerning the Effect of Natural Gas Percentage on Performance and Emissions of a DI Dual Fuel Diesel Engine*", Applied Thermal Engineering, vol. 23, pp. 353-365, 2003.

[21] K. Cheenkachorn, C. Poompipatpong, and C. Ho, "*Performance and Emissions of a Heavy-Duty Diesel Engine Fuelled with Diesel and LNG (Liquid Natural Gas)*", Energy, vol. 53, pp. 52-57, 2013.

[22] R. Papagiannakis, and D. Hountalas, "*Combustion and Exhaust Emission Characteristics of a Dual Fuel Compression Ignition Engine Operated with Pilot Diesel Fuel and Natural Gas*", Energy Conversion and Management, vol. 45, no. 18-19, pp. 2971-2987, 2004.

[23] L. Shenghua, W. Ziyan, and R. Jiang, "*Development of Compressed Natural Gas/Diesel Dual Fuel Turbocharged Compression Ignition Engine*", Proceedings of the Institution of Mechanical Engineers, Part D: Journal of Automobile Engineering, vol. 217, no. 2, 2003.

[24] A. Ball, D. Dowson, and C. Taylor, "*Cam and Follower Design*", 15th Leeds-Lyon Symposium on Tribology, pp. pp 111-130, 1989.

[25] Y. Wang, "*Introduction to Engine Valvetrains*", SAE International, 2006.

[26] Wärtsilä, "*Gas and Multi-Fuel Power Plants*", 2014.

[27] M. t. Bus, "*MAN Engines entwickelt wartungsfreien Ventiltrieb für Industriemotoren*", 2019.

[28] Baudouin, " *6F21 User manual*", https://baudouin.com/, 2022.

[29] J. Halderman, "*Automotive Technology: Principles, Diagnosis, and Service. 3rd Edition*", Pearson Prentice Hall, 2009.

[30] R. Stone, "*Introduction to Internal Combustion Engines*", Brunel University, Macmilian LTD, 1992.

[31] R. Lewis, and R. Joyce, "*Automotive Engine Valve Recession* ", Professional Engineering Publishing Limited, 2002.

[32] W. Pulkrabek, "*Engineering Fundamentals of the Internal Combustion Engine*", Pearson Prentice Hall, 2004.

[33] J. Rodriguez, and W. Cheng, "*Potential of Negative Valve Overlap for Part-Load Efficiency Improvement in Gasoline Engines*", SAE International Journal of Engines, vol. 11, no. 6, pp. 657-668, 2018.

[34] L. Olesky, "*An Experimental Investigation of the Burn Rates of Naturally Aspirated Spark Assisted Compression Ignition Combustion in a Single Cylinder Engine with Negative Valve Overlap*", Ph.D., The University of Michigan, 2013.

[35] H. Persson, M. Agrell, J. Olsson, B. Johansson, and H. Ström, "*The Effect of Intake Temperature on HCCI Operation Using Negative Valve Overlap*", SAE Technical Paper 2004-01-0944, 2004.

[36] L. Koopmans, R. Ogink, and I. Denbratt, "*Direct Gasoline Injection in the Negative Valve Overlap of a Homogeneous Charge Compression Ignition Engine*", SAE Technical Paper 2003-01-1854, 2003.

[37] T. Guohong, W. Zhi, W. Jianxin, S. Shijin, and A. Xinliang, "*HCCI Combustion Control by Injection Strategy with Negative Valve Overlap in a GDI Engine*", SAE Technical Paper 2006-01-0415, 2006.

[38] R. Fitzgerald, R. Steeper, J. Snyder, R. Hanson, and R. Hessel, "*Determination of Cycle Temperatures and Residual Gas Fraction for HCCI Negative Valve Overlap Operation*", SAE Int. J. Engines 3(1), 2010.

[39] Z. Ahmad, O. Kaario, C. Qiang, and M. Larmi, "*Effect of Negative Valve Overlap in a Heavy-Duty Methanol-Diesel Dual-Fuel Engine: A Pathway To Improve Efficiency*", Fuel, vol. 317, 2022.

[40] H. Theißl, T. Kraxner, H. Seitz, and P. Kislinger, "*Miller Valve Timing for Future Commercial Diesel Engines*", MTZ worldwide, vol. 76, pp. 4-11, 2015.

[41] R. Balmer, "*Modern Engineering Thermodynamics*", Academic Press, 2011.

[42] E. Schutting, A. Neureiter, C. Fuchs, T. Schatzberger, M. Klell, H. Eichlseder, and T. Kammerdiener, "*Miller- und Atkinson-Zyklus am aufgeladenen Dieselmotor*", MTZ 93, No. 6, 2007.

[43] H. Hiereth, and P. Prenninger, "*Charging the Internal Combustion Engine*", Springer Vienna, 2007.

[44] Y. He, J. Liu, D. Sun, and B. Zhu, "*Development of an Aggressive Miller Cycle Engine with Extended Late Intake Valve Closing and a Two-stage Turbocharger*", Proceedings of the Institution of Mechanical Engineers, Part D: Journal of Automobile Engineering, vol. 233, no. 2, pp. 413-426, 2017.

[45] W. Guan, X. Wang, H. Zhao, and H. Liu, "*Exploring the High Load Potential of Diesel–Methanol Dual-Fuel Operation with Miller Cycle, Exhaust Gas Recirculation, and Intake Air Cooling on a Heavy-Duty Diesel Engine*", International Journal of Engine Research, vol. 22, no. 7, pp. 2318-2336, 2020.

[46] H. Gan, H. Wang, Y. Tang, and G. Wang, "*Investigation of the Miller Cycle on the Performance and Emission in a Natural Gas-Diesel Dual-Fuel Marine Engine by Using Two Zone Combustion Model*", Thermal Science, vol. 24, no. 1 Part A, pp. 259-270, 2020.

[47] S. Hires, R. Tabaczynski, and J. Novak, "*The Prediction of Ignition Delay and Combustion Intervals for a Homogeneous Charge, Spark Ignition Engine*", SAE Technical Paper 780232, 1978.

[48] M. Mikulski, R. Balakrishnan, E. Doosje, and C. Bekdemir, "*Variable Valve Actuation Strategies for Better Efficiency Load Range and Thermal Management in an RCCI Engine*", SAE Technical Paper Series, 2018.

[49] P. Wang, X. Tang, L. Shi, X. Ni, Z. Hu, and K. Deng, "*Experimental Investigation of the Influences of Miller Cycle Combined With EGR on Performance, Energy and Exergy Characteristics of a Four-Stroke Marine Regulated Two-Stage Turbocharged Diesel Engine*", Fuel, vol. 300, 2021.

[50] G. Stiesch, "*Modeling Engine Spray and Combustion Processes*", Springer Berlin, Heidelberg, 2003.

[51] F. Cernik, "*Phenomenological Combustion Modeling for Optimization of Large 2-stroke Marine Engines under both Diesel and Dual Fuel Operating Conditions*", Ph.D. Thesis, Czech Technical University, 2018.

[52] Z. Liu, and G. Karim, "*A Predictive Model for the Combustion Process in Dual Fuel Engines*", SAE Technical Paper 952435, 1995.

[53] H. Hiroyasu, and T. Kadota, "*Models for Combustion and Formation of Nitric Oxide and Soot in Direct Injection Diesel Engines*", SAE Paper 760129, 1976.

[54] S. Stoumpos, G. Theotokatos, E. Boulougouris, D. Vassalos, I. Lazakis, and G. Livanos, "*Marine Dual Fuel Engine Modelling and Parametric Investigation of Engine Settings Effect on Performance-Emissions Trade-offs*", Ocean Engineering, vol. 157, pp. 376-386, 2018.

[55] S. Xu, D. Anderson, M. Hoffman, R. Prucka, and Z. Filipi, "*A Phenomenological Combustion Analysis of a Dual-Fuel Natural-Gas Diesel Engine*", Proceedings of the Institution of Mechanical Engineers, Part D: Journal of Automobile Engineering, vol. 231, no. 1, pp. 66-83, 2016.

[56] C. Nani, R. Hutter, and K. Boulouchos, "*Spray Model Based Phenomenological Combustion Description and Experimental Validation for a Dual Fuel Engine*", SAE Technical Paper 24-0098, 2017.

[57] M. Musculus, and K. Kattke, "*Entrainment Waves in Diesel Jets*", vol. SAE Int. J. Engines 2(1):1170-1193,, 2009.

[58] C. Barro, A. Lucjan, Z. Li, P. Kyrtatos, S. Pandurangi, Y. Wright, and K. Boulouchos, "*Development and Experimental Validation of a Fast Spray Ignition Model for Diesel Engines Using Insights from CFD Spray Calculations*", SAE International Journal of Fuels and Lubricants, vol. 10, no. 2, pp. 304-317, 2017.

[59] R. Papagiannakis, D. Hountalas, and C. Rakopoulos, "*Theoretical Study of The Effects of Pilot Fuel Quantity and its Injection Timing on the Performance and Emissions of a Dual Fuel Diesel Engine*", Energy Conversion and Management, vol. 48, no. 11, pp. 2951-2961, 2007.

[60] J. B. Heywood, "*Internal Combustion Engine Fundamentals*", McGraw Hill, New York, 1988.

[61] H. Hiroyasu, T. Kadota, and M. Arai, "*Development and Use of a Spray Combustion Modeling to Predict Diesel Engine Efficiency and Pollutant Emissions*", Bulletin of JSME, vol. 26 no. 214 pp. 569-575, 1983.

[62] I. Taritas, D. Kozarac, M. Sjeric, M. Aznar, D. Vuilleumier, and R. Tatschl, "*Development and Validation of a Quasi-Dimensional Dual Fuel (Diesel – Natural Gas) Combustion Model*", SAE International Journal of Engines, vol. 10, no. 2, pp. 483-500, 2017.

[63] G. North, and D. Santavicca, "*The Fractal Nature of Premixed Turbulent Flames*", Combustion Science and Technology, vol. 72, no. 4-6, pp. 215-232, 1990.

[64] C. Abagnale, M. Cameretti, L. Simio, M. Gambino, S. Iannaccone, and R. Tuccillo, "*Numerical Simulation and Experimental Test of Dual Fuel Operated Diesel Engines*", Applied Thermal Engineering, vol. 65, no. 1-2, pp. 403-417, 2014.

[65] F. Stringer, A. Clarke, and J. Clarke, "*The Spontaneous Ignition of Hydrocarbon Fuels in a Flowing System*", SAGE Journals, vol. 184, no. 10, 1969.

[66] B. Magnussen, and B. Hjertager, "*On Mathematical Modeling of Turbulent Combustion With Special Emphasis on Soot Formation*", Symposium (International) on Combustion, Pittsburgh, pp. 719-729, 1977.

[67] MaKMed, "*M34 DF Propulsion*", https://www.makmed.fr/en/moteurs/moteurs-mak/m-34-df-propulsion/, 2022.

[68] WOODWARD, "*SOGAV 105 Top-Land Version Product Manual*", 2022.

[69] AVL List GmbH, "*AVL SESAM i60 User Manual*", https://www.avl.com/testing-solutions-for-large-engines/-/asset_publisher/gYjUpY19vEA8/content/avl-sesam-i60-ft-multi-component-exhaust-measurement-system, 2022.

[70] AVL List GmbH, "*Emission Measurement Instruments: AVL Smoke Meter*", 2018.

[71] Caterpillar Marine, "*Technologies for Reducing Black Carbon From Marine Engines*", 2016.

[72] L. Johannes, "*Operating Internal Combustion Engines*", Patent, European Patent Office, 2015.

[73] AVL, "*Motoraufbau- und Servicedokumentation 1-Zylinder Forschungsmotor 850kW*", 2015.

[74] F. Gouldin, "*An Application of Fractals to Modeling premixed turbulent falmes*", Cambustion and Flame, vol. 68, no. 3, pp. 249-266, 1987.

[75] AVL List GmbH, "*CRUISE-M user manual*", 2018.

[76] S. Yoshiyama, E. Tomita, Z. Zhang, and Y. Hamamoto, "*Measurement and Simulation of Turbulent Flame Propagation in a Spark Ignition Engine by Using Fractal Burning Model*", SAE Technical Paper 2001-01-3603, 2001.

[77] K. Suzuki, and K. Nishiwaki, "*Fractal Dimension Growth Model for SI Engine Combustion*", SAE Technical Paper 2004-01-1993, 2004.

[78] F. Bozza, and A. Gimelli, "*Validation of a Fractal Combustion Model through Flame Imaging*", SAE Technical Paper 2005-01-1120, 2005.

[79] G. Damköhler, "*Der Einfluss der Turbulenz auf die Flammengeschwindigkeit in Gasgemischen*", Z. f. Elektroch, vol. 46, no. 11, pp. 601-652, 1940.

[80] S. Poulos, and J. Heywood, "*The Effect of Chamber Geometry on Spark-Ignition Engine Combustion* ", SAE Paper 830334, 1983.

[81] F. Bozza, and A. Gimelli, "*A Comprehensive 1D Model for the Simulation of a Small-Size Two-Stroke SI Engine*", SAE Technical Paper 2004-01-0999, 2004.

[82] H. Walther, "*Erstellung eine phänomenologischen Modells zur Vorausberechnung des Brennverlaufes von Gasmotoren mit Piloteinspritzung*", Abschlussbericht FVV-Vorhaben Nr. 960. Heft 951-2012, Frankfurt am Main, 2012.

[83] H. Walther, S. Schlatter, G. wachtmeister, and K. Boulouchos, "*Combustion Models for Lean-Burn Gas Engines with Pilot Injection*", MTZ Worldwide 73(2), pp. 56-63, 2012.

[84] G. Woschni, "*Einfluß von Rußablagerungen auf den Wärmeübergang zwischen Arbeitsgas und Wand im Dieselmotor*", 3 Tagung der Arbeitsprozess des Verbrennungsmotors, Institut für Verbrennungskraftmaschinen und Thermodynamik, Graz, Austria, 1991.

[85] Y. Zeldovich, "*The Oxidation of Nitrogen in Combustion and Explosion*", Acta Physicochim URSS, 21, pp. 577-628, 1946.

[86] G. Lavoie, J. Heywood, and J. Keck, "*Experimental and Theoretical Study of Nitric Oxide Formation in Internal Combustion Engines*", Combustion Science and Technology, vol. 1, no. 4, pp. 313-326, 1970.

[87] N. Thompson, and J. Wallace, "*Effect of Engine Operating Variables and Piston and Ring Parameters on Crevice Hydrocarbon Emissions*", SAE Technical Paper 940480, 1994.

[88] T. Amano, and K. Okamoto, "*Unburned Hydrocarbons Emission Source from Engines*", SAE Technical Paper 2001-01-3528, 2001.

[89] J. Han, M. Jensen, K. Pang, J. Walther, J. Schramm, and C. Bae, "*Numerical Simulation of Methane Slip in Dual Fuel Marine Engines*", Spring and Autumn Conference of the Korean Society of Mechanical Engineers, pp. 1475-1480, 2017.

[90] P. Janas, M. Ribeiro, A. Kempf, M. Schild, and S. Kaiser, "*Penetration of the Flame Into the Top-Land Crevice-Large-Eddy Simulation and Experimental High-Speed Visualization*", SAE 2015-01-1907, 2015.

[91] P. Kristensen, B. Karll, A. Bendtsen, P. Glarborg, and K. Johansen, "*Exhaust Oxidation of Unburned Hydrocarbons from Lean-Burn Natural Gas Engines*", Combustion Science and Technology, vol. 157, no. 1, pp. 262-292, 2007.

[92] G. Lavoie, and P. Blumberg, "*A Fundamental Model for Predicting Fuel Consumption, NO_x and HC Emissions of the Conventional Spark-Ignited Engine*", Combustion Science and Technology, vol. 21, no. 5-6, pp. 225-258, 2007.

[93] G. Lavoie, A. Adamczyk, E. Kaiser, J. Cooper, and W. Rothschild, "*Engine HC Emissions Modeling: Partial Burn Effects*", Combustion Science and Technology, vol. 49, no. 1-2, pp. 99-105, 1986.

[94] S. Tavakoli, M. Jensen, E. Pedersen, and J. Schramm, "*Unburned hydrocarbon formation in a natural gas engine under sea wave load conditions*", Journal of Marine Science and Technology, vol. 26, no. 1, pp. 128-140, 2020.

[95] R. Siewert, "*How Individual Valve Timing Events Affect Exhaust Emissions*", SAE Technical Paper 710609, 1971.

[96] G. Parvate-Patil, H. Hong, and B. Gordon, "*Analysis of Variable Valve Timing Events and Their Effects on Single Cylinder Diesel Engine*", SAE International, vol. 113, no. 3, pp. 1510-1519, 2004.